TR-788: MITIGATION OF CHLORIDE-INDUCED CORROSION THROUGH CHEMISORPTION

FINAL REPORT
IHRB PROJECT TR-788

JULY 2023

SPONSORED BY
THE IOWA HIGHWAY
RESEARCH BOARD

Disclaimer Notice

The contents of this report reflect the views of the authors, who are responsible for the facts and the accuracy of the information presented herein. The opinions, findings, and conclusions expressed in this publication are those of the authors and not necessarily those of the sponsors.

The sponsors assume no liability for the contents or use of the information contained in this document. This report does not constitute a standard, specification, or regulation. The sponsors do not endorse products or manufacturers. Trademarks or manufacturers' names appear in this report only because they are considered essential to the objectives of the document.

Statement of Non-Discrimination

Federal and state laws prohibit employment and/or public accommodation discrimination on the basis of age, color, creed, disability, gender identity, national origin, pregnancy, race, religion, sex, sexual orientation or veteran’s status. If you believe you have been discriminated against, please contact the Iowa Civil Rights Commission at 800-457-4416 or Iowa Department of Transportation's affirmative action officer. If you need accommodations because of a disability to access the Iowa Department of Transportation’s services, contact the agency's affirmative action officer at 800-262-0003.

TECHNICAL REPORT DOCUMENTATION PAGE

1. Report No. IHRB Project TR-788	**2. Government Accession No.**	**3. Recipient's Catalog No.**
4. Title and Subtitle Mitigation of Chloride-induced Corrosion through Chemisorption		**5. Report Date** July 2023 **6. Performing Organization Code**
7. Author(s) Ravi Kiran Yellavajjala, Ph.D., P.E. https://orcid.org/0000-0001-8300-0767 Hizb Ullah Sajid. https://orcid.org/0000-0002-2370-8592 Sher Afgan. https://orcid.org/0000-0001-6326-2452		**8. Performing Organization Report No.**
9. Performing Organization Name and Address North Dakota State University, 1340 Administration Ave, Fargo, ND-58105		**10. Work Unit No.** **11. Contract or Grant No.**
12. Sponsoring Agency Name and Address Iowa Highway Research Board Iowa Department of Transportation 800 Lincoln Way Ames, IA 50010.		**13. Type of Report and Period Covered** 7/1/2020-6/30/2023 **14. Sponsoring Agency Code**
15. Supplementary Notes		

16. Abstract

Salt brine deicing solution contains chloride ions that can penetrate the passive layer and cause corrosion in rebars. While epoxy coatings are effective, they can be easily damaged during transportation and construction. In addition, aggressive localized corrosion is observed in damaged epoxy coated rebars. To address this issue, this project aims to mitigate chloride-induced corrosion using two methods. First, migratory corrosion inhibitors, specifically polyols, are employed as they can adsorb onto the metal surface and block the chemical reactions responsible for corrosion. Second, a biobased coating is synthesized to act as a secondary coat to the epoxy coated rebars and improve the bond with concrete. In TR-754 project, polyols have been proven effective as corrosion inhibitors and their effect on cementitious materials is investigated in this project. Cement mortar samples are exposed to 90 wet-dry cycles of a salt brine solution containing the optimal amount of polyols. Surface scaling, mass loss, compression strength changes, ion penetration and chemical changes are monitored periodically. The addition of the optimal amount of polyol corrosion inhibitor (1% w/w) to the deicing solution did not lead to further deterioration in the properties of the hardened cement mortar compared to using the salt brine alone. Another aspect of this study involves synthesizing a new soy-based coating material for repairing damaged epoxy coated rebars. The soy-based coatings are made using denatured soy protein isolate (SPI) and corn-derived sorbitol plasticizer. Subsequently, chemically inert oxide abrasives are incorporated into the SPI coatings in varying proportions to improve the mechanical properties, including abrasive resistance and lap shear strength. Potentiodynamic polarization tests and macrocell analyses have revealed significant improvements in short-term and long-term corrosion performance, with reductions of 94% and 78% respectively, compared to SPI coatings without abrasives. Furthermore, an improvement in bond strength of up to 90.41% is observed justifying the incorporation of abrasives.

17. Key Words Deicing chemicals; Reinforcing bars; Corrosion Protection; Chloride; and Anticorrosion Coatings	**18. Distribution Statement** No restrictions.		
19. Security Classif. (of this report) Unclassified	**20. Security Classif. (of this page)** Unclassified	**21. No. of Pages** 117	**22. Price**

Form DOT F 1700.7 (8-72) Reproduction of completed page authorized

Mitigation of Chloride-induced Corrosion through Chemisorption

Final Report
July 2023

Principal Investigator

Ravi Kiran Yellavajjala, Ph.D., P.E.
Associate Professor
School of Sustainable Engineering and the Built Environment
Ira A. Fulton Schools of Engineering
Arizona State University

Co-authors

Hizb Ullah Sajid[**]
Sher Afgan[*]
[**]Research Engineer
Genex Systems/ FHWA Turner-Fairbank Highway Research Center
[*]Graduate Research Assistant
Department of Civil and Environmental Engineering
North Dakota State University

Sponsored by

the Iowa Highway Research Board
(IHRB Project TR-788)

A Report from

Damage in Materials and Structures Laboratory
School of Sustainable Engineering and the Built Environment
Room #174, ISTB5, 550 E Orange St.,
Tempe, AZ 85281
Phone: 480-965-2790
Fax: 480-965-0557

Table of Contents

List of Figures

List of Tables

Acknowledgment

The Principal Investigator (PI) extends heartfelt gratitude to the Iowa Highway Research Board (IHRB) for their generous sponsorship of this research endeavor. The PI would also like to express sincere appreciation to the Technical Advisory Committee (TAC) members, namely Chris Brakke, Todd Hanson, Jeff De Vries, Wade Weiss, Ahmad Abu-Hawash, and Brian Moore, for their valuable comments and suggestions throughout the project. Their enthusiasm for this project and suggestions provided during the TAC meetings have contributed to the successful completion of the project.

The PI is immensely grateful to Ms. Vanessa Goetz for her unwavering support during the execution of this project. Special recognition is also extended to Ms. Jan Lofberg and Ms. Jackie Benson from NDSU Civil Engineering for their outstanding administration of the grant. The PI extends his heart-felt thanks to Prof. Mijia Yang for managing this project at NDSU since January of 2023.

The authors wish to acknowledge the invaluable assistance provided by the laboratory staff at the Research Park, NDSU. Furthermore, the authors express their deep appreciation to the Polymers and Coatings Department for their technical guidance in this regard. Their support was instrumental in carrying out the corrosion tests.

Lastly, the authors would like to thank the Civil, Construction and Environmental Engineering and North Dakota State University for graciously providing the necessary laboratory facilities to conduct the experiments.

1 Chloride-induced Corrosion in Rebars

1.1 Introduction

Iowa DoT used more than 7 million gallons of salt brine to conduct snow and ice control in 2018 utilizing a full fleet of 879 snowplows that have the potential to deice more than 10,000 lane-miles (source: Iowa DoT winter operations). Although salt brine is economical and efficient, it has two negative consequences on transportation infrastructure: 1) chloride-ion induced corrosion in bridge decks and concrete pavements, and 2) corrosion of vehicles and snowplows. Chloride-ions penetrate the passive layer on the reinforcement and react with iron and water to form corrosion products that have 2-3 times more volume when compared to intact steel. The high-volume corrosion products result in high internal stresses leading to cracks parallel to reinforcement and delamination of concrete. In addition to this, the rebars lose their load-carrying capacity due to the loss of cross-sectional area. The corrosion of reinforcement in the bridge decks and concrete pavements makes them dysfunctional, requiring frequent repairs or replacement, resulting in road closures and traffic congestion. Americans lost 6.9 billion hours (42 hours per capita) and 3.1 billion gallons of fuel due to traffic delays resulting in a cumulative loss of $160 billion in 2014 alone [1]. According to a report published by Midwest Economic Policy Institute [2], the cost of road repair and maintenance in colder urban regions can be significantly more than the national average due to stringent design standards, complicated intersections, and complex work zones. Hence, minimizing road repair and maintenance is important to Iowa's economy. On the other hand, the salt brine causes significant corrosion damage to passenger vehicles and snowplows. In 2018, Iowa DoT shortened the lifecycle of its snowplow fleet from 17 years to 12 years to save repair costs. An optimal replacement cycle of six to seven years is recommended based on a study conducted on ten years' worth of maintenance records. Corrosion and high wear and tear are among the main reasons for this short life span of snowplows. Moreover, according to a new AAA (American Automobile Association) survey, the U.S. drivers paid an estimated $3 billion per year (share of Iowa ~$30 million per year) for fixing corrosion-related damages to the passenger vehicles due to deicing salts. The overarching goal of this study is to optimize the synthesis and application parameters for the newly developed polyol-salt brine deicer, and abrasives impregnated organic coating to minimize the corrosion damage in embedded rebars, snowplows, and passenger vehicles while improving the bond between coated rebars and the concrete.

1.2 Rebar corrosion in pavements and bridge decks

Bare steel embedded in fresh concrete reacts with available moisture and oxygen to form an insoluble, passive protective layer composing of oxides and hydroxides which is around 17 to 50 μm thick. This passive layer protects the steel by minimizing the dissolution of metal ions in concrete pore water (very low rate of anodic reactions), restricting the corrosion loss to less than 0.1 mm/year [3]. According to ACI222-2001 [4], the corrosion rates could be at least 1000 times higher in the absence of the passive layer. Moreover, concrete surrounding the reinforced steel offers physical protection to the passive layer. In addition to this, the high pH value (between 9.5 and 13) of hardened concrete blocks most of the non-aggressive net-negative charged anions further protecting the steel. Notwithstanding this, the integrity and functionality of the passive protective layer is compromised due to the carbonation of concrete and chloride ion attack. Carbonation is a process in which the calcium hydroxide in the concrete reacts with carbon dioxide dissolved in the water trapped in the pores of concrete, also known as pore water resulting in the

formation of calcium carbonate decreasing the pH of concrete pore water from ~12.0 to ~8.5. According to the Pourbaix diagram for iron [5] which provides the possible phases of an aqueous electrochemical system, iron is passive only when the pH values of pore water is above 9.5. Hence, carbonation deteriorates the passive protective layer initiating the corrosion of reinforced steel. However, carbonation is a very slow process and progresses at a rate of about 0.04 inches per year in high-quality low porosity concrete. Moreover, the calcium carbonate formed as a result of carbonation blocks a certain percentage of concrete pores preventing further deterioration.

On the other hand, the chloride-induced corrosion due to the application of salt brine is extremely invasive and rapid when compared to carbonation [6] and have multiple paths to attacking the embedded rebars. Firstly, due to the hygroscopic nature of the deicing salts, they absorb moisture from the air, and hence the corrosion reactions proceed even at relatively lower humidity levels. Secondly, the presence of chloride ions increases the conductivity of water and hence results in faster corrosion rates. Thirdly, chloride ions can deteriorate the protective oxide layer that might be present on the surface of the steel. More alarmingly, the chloride ions are regenerated at the end of the corrosion reactions leading to more corrosion. Hence, few applications of salt brine deicer every year will leave behind a perennial source of chloride ions that can progressively corrode the embedded rebars, snowplows, and passenger vehicles.

1.3 Strategies for mitigating corrosion damage in rebars

1.3.1 Corrosion resistant materials

Employing corrosion-resistant materials is a strategy that can mitigate corrosion damage in rebars. Stainless steel rebars [7] and stainless steel clad rebars [8] are typically employed in environments with high corrosive potential and where maintaining structural integrity is paramount. Alloying elements such as nickel lends these rebars their corrosion resistance [9]. However, compared to carbon steel, stainless steel's high cost, limits its widespread use in practice. Rebars made from glass fiber reinforced polymer (GFRP) [10, 14, 15], carbon fiber reinforced polymer (CFRP) [13], and basalt fiber reinforced polymer (BFRP) [17, 18] are chemically inert and exhibit high resistance to various corrosive environments. Among these non-metallic materials, CFRP offers the highest strength, GFRP is the least expensive and lightest, and BFRP offers a balance between GFRP and CFRP in terms of both strength and cost. However, while these fiber-reinforced polymers are resistant to corrosion, they present drawbacks. Their bond with concrete is weak, they exhibit less stiffness than steel, and they are relatively more expensive than steel [10, 13, 17, 18].

1.3.2 Corrosion inhibiting admixtures and migratory inhibitors

The most commonly used admixed and migratory corrosion inhibitors include nitrites (e.g., calcium nitrite, sodium nitrite, and potassium nitrite), alkanolamines (e.g., diethanolamine, dimethylpropanolamine, monoethanolamine, dimethylethanolamine, triethanolamine, and methyldiethanolamine), amines (e.g., methylamine, dimethylamine, ethylamine, propylamine, cyclohexylamine, triethylentetramine, and hexamethylentetramine), carboxylic acids (e.g., sodium gluconate, D-Saccharic acid, monopotassium salt, calcium α-D eptagluconate, phthalic acid, monopotassium salt, lactic acid, maleic acid, suberic acid, adipic acid, and sodium benzoate), sodium monofluoro phosphate, nitrates, benzoates, zinc and magnesium salts, and chromates [16–21]. In addition to these corrosion inhibitors, several proprietary blends of different corrosion

inhibitors are used in concrete that includes Darex Corrosion Inhibitor (DCI® and DCI®-S from GCP Applied Technologies Inc.), POSTRITE® (from GCP Applied Technologies Inc.), MCI® 2000 (from Cortec), Ferrogard® 901 and 903 (from Sika), Catexol 1000 CI (from Axim Concrete Technologies) and Rheocrete® 222^{+} (from BASF). These commercial corrosion inhibitors are based on alkanolamines, amines, and their salts with organic and inorganic acids [17, 22–24]. Moreover, oil/water emulsions have also been utilized as corrosion inhibitors for concrete in the past. Recently, eco-friendly and natural corrosion inhibitors have been proposed for usage in reinforced concrete [24–26]. The above-discussed corrosion inhibitors act as anodic, cathodic, or mixed inhibitors. Some of these corrosion inhibitors act as pore blockers [27, 28] and thus restrict the deleterious ingress species (e.g., chlorides) in concrete, whereas others displace the chloride ion and form a protective film on the rebar surface. The efficiency of both admixed and migrating corrosion inhibitors depend on their dosage [19, 26, 29]. At sufficiently high dosage, nitrite (e.g., calcium nitrite) and other corrosion inhibitors are quite effective. However, a reduction in their dosage is linked with an increase in corrosion rate and appearance of cracks in concrete. Therefore, it is necessary to maintain a certain dosage of corrosion inhibitors in concrete to ensure desirable levels of corrosion inhibition.

While the increase in the dosage of corrosion inhibitors ensure sustained and higher corrosion inhibition efficiency, the higher dosage is observed to have a negative impact on the properties of fresh and hardened concrete (e.g., setting time, compressive strength, etc.) in the case of some corrosion inhibitors [19, 29]. Schutter and Luo [30] investigated the influence of four different types of corrosion-inhibiting admixtures on properties of normal strength concrete that utilized ordinary Portland cement (OPC) and blast furnace slag cement. They observed a decrease in both early age and long-term compressive strength of concrete regardless of the cement type. The usage of amino- and ester-based aqueous solution corrosion inhibitor resulted in about a 14% decrease in the 28 days compressive strength of OPC-based concrete. Overall, a 7.5–20.5% decrease in compressive strength of concrete was noticed. A similar observation of a 10-20% reduction in the compressive strength was noticed in several other investigations that utilized amino and ester-based organic inhibitors in concrete [31–33]. Schutter and Luo [30] also used a blend of amino alcohols and organic and inorganic inhibitors and noticed a 10.5% and 16.5% decrease in the 28-days compressive strength of concrete specimens corresponding to OPC and blast furnace slag cement, respectively. Similarly, Heren and Ölmez [34] observed a reduction in compressive strength of cement paste when ethanolamine corrosion inhibitors (monoethanolamine, diethanolamine, and triethanolamine) are used at 1% (wt.% of cement) dosage. The authors observed a reduction of 2%, 21%, and 26% in the 90-day compressive strength of cement paste corresponding to monoethanolamine, diethanolamine, and triethanolamine, respectively [34]. Saraswathy and Song [20] studied the impact of various anodic, cathodic, and mixed-type corrosion inhibitors on the properties of concrete, namely sodium nitrite, zinc oxide, mixed inhibitor ($NaNO_2$+ZnO), monoethanolamine, diethanolamine, and triethanolamine. The authors used three types of dosages that include 1%, 2%, and 3% by weight of OPC. The dosage rate of 1% resulted in 6-24% decrease in the compressive strength of concrete specimens. On the

other hand, a high dosage rate of 3% resulted in 12-39% decrease in the compressive strength of concrete specimens. This included a decrease of 12.25%, 13.52%, 17.09%, 30.36%, 35.71%, and 39.54%, corresponding to sodium nitrite, zinc oxide, monoethanolamine, triethanolamine, diethanolamine, and mixed inhibitor, respectively. Interestingly, the authors observed an increase in the compressive strength in most corrosion inhibitors when using a dosage of 2% by weight of OPC. An earlier review conducted by Hansson et al. noted that sodium nitrite, sodium benzoate, potassium chromate, and an organic corrosion inhibitor (mixture of amines and esters in a water medium) reduced the compressive strength of concrete [28]. For certain corrosion inhibitors (e.g., calcium nitrite and a proprietary migrating corrosion inhibitor), some researchers reported around 15% increase in the compressive strength of concrete [30, 33]**.** Some conflicting results are also documented in the literature wherein some researchers reported up to a 20% increase in the compressive strength of concrete when aminoalcohol-based corrosion inhibitors are used [31, 33] whereas other researchers observed an increase in the compressive strength for a similar class of corrosion inhibitors [19, 26, 30, 35]. Furthermore, the negative impact of deicers on cementitious materials with and without corrosion inhibitors are well-documented in the literature [36–38].

1.3.3 Rebar coatings

Coating of rebars is a common approach to mitigate corrosion damage in rebars. Both organic and metallic coatings have been used for this purpose. Epoxy coatings [39] are very popularly used and are reported to be very effective in combating corrosion damage in bridge decks and concrete pavements [29–31]. These coatings are around 100-300 μm thick, [43] forming an impenetrable barrier between the aggressive chloride environment and the rebar, protecting it from corrosion damage. Galvanizing or coating the rebars with zinc that acts as a sacrificial anode is another technique to protect the rebar from corrosion [44]. Galvanizing followed by an epoxy coating of rebars is also discussed in the literature for better protection but is rarely employed due to the cost [45]. Cement polymer composite (CPC) coating is an alternative coating approach that involves coating the rebar with a rapid-setting primer followed by a coat of cement polymer [46]. Epoxy coatings are susceptible to damage during transportation requiring special handling. Corrosion of damaged epoxy coatings will lead to severe localized deterioration of metal, leading to catastrophic outcomes necessitating the use of secondary coats.

1.4 Research gaps

The following major research gaps were identified based on the literature review:

1) *Influence of Migratory Corrosion Inhibitors on Concrete Durability:* A majority of corrosion inhibitors tend to decrease the compressive strength of concrete, whereas some corrosion inhibitors can increase the compressive strength of concrete, depending on their pore-blocking ability, chemical interaction with the cement hydration products, corrosion inhibitor dosage, age of concrete, mode of application (admixed or migrating), and type of cement. Therefore, when investigating the efficacy of new corrosion inhibitors, it is important to evaluate their impact on the strength and durability properties of concrete.
2) *Damaged Epoxy Coated Rebars*: the epoxy coating could get damaged during transportation and operation. Accelerated and localized erosion of metal was reported in

the vicinity of damaged epoxy coatings in the past. With this, a coating material that can be painted in-situ and can efficiently seal the damaged epoxy regions should be developed.

3) *Enhance the Bond with Concrete*: usually coatings reduce the bond with concrete. Ideally, coatings that do not reduce the bond and instead improve the bond are more desirable and should be developed.

1.5 Technical Objectives

The overarching goal of this project is to mitigate rebar corrosion by employing sustainable and renewable materials. This goal is accomplished by fulfilling the following technical objectives:

1) To conduct a detailed literature review of existing body of research that targeted understanding the chemical and physical deterioration in concrete caused by migratory corrosion inhibitors.
2) To quantify the deterioration mechanisms in cementitious materials exposed to polyol corrosion inhibitors.
3) To synthesize and characterize the corrosion and mechanical performance of a biobased coating material.
4) To improve the bond performance of a secondary biobased coating with concrete by incorporating abrasives.

1.6 Organization of the report

A detailed discussion of various experimental methods and a critical summary of physical and chemical deterioration mechanisms in concrete exposed to deicers is provided in Chapter-2. This review findings were utilized in Chapter-3 to devise a detailed experimental program that aimed at quantifying the long-term effect of utilizing polyols as corrosion inhibitors in salt brine deicers. A novel synthesis process for producing coatings from soy-protein isolate is described in Chapter-4 along with characterization techniques and results supporting the use of the new material as a secondary coating for rebars. The improvement of this coating by incorporating inert oxides is discussed in Chapter-5. The important findings of this project and recommendations for future studies are summarized in Chapter-6.

1.7 Research products from the project

This project resulted in four journal articles and five conference talks/ posters. Here are the references to the published articles:

1.7.1 Journal articles

1) Afgan S. [#], **Ravi Yellavajjala**[c], Qi X., and Bajwa D.S., (2023). "Enhancement of Corrosion Resistance and Bond Strength in Rebars Employing Abrasives-Infused Soy-Protein Isolate Coatings", submitted to the Construction and Building Materials.

2) Sajid H.U. [#], **Ravi Yellavajjala**[c] and Bajwa D.S., (2022). "Soy-protein and Corn-derived Polyol based Coatings for Corrosion Mitigation in Reinforced Concrete", Construction and Building Materials, V 319, P. 126056, DoI: https://doi.org/10.1016/j.conbuildmat.2021.126056.

3) Sajid H.U.[#], Jalal A.[#], **Ravi Yellavajjala**[c], Md. Abdullah-Al-Rahim[#] (2022). "A Survey on the Effects of Deicing Materials on Properties of Cement-based Materials", Construction and Building Materials, V 319, P. 126062, DoI: https://doi.org/10.1016/j.conbuildmat.2021.126062.

4) Sajid H.U.[#], **Ravi Yellavajjala**[c], and Bajwa D.S., (2021). "Effect of agro-derived corrosion inhibitors on the properties of Portland cement mortar", Construction and Building Materials 310 (2021): 125236, DoI: https://doi.org/10.1016/j.conbuildmat.2021.125236.

1.7.2 Conference presentations and posters

1) Afgan S.[#*], and **Ravi Yellavajjala**[c]. (2023) "Employing Biobased Coatings for In-situ Repair of Damaged Epoxy Coated Rebars in Concrete Pavements", 2023 IRF Global "Road to Tomorrow" (R2T) Conference, Phoenix, AZ.

2) Afgan S.[#*], and **Ravi Yellavajjala**[c]. (2023) "Sustainable Biobased Coatings for In-situ Repair of Damaged Coated Rebars", Engineering Mechanics Institute Conference, Georgia Institute of Technology, Georgia, Atlanta.

3) **Ravi Yellavajjala**[*c] and Sajid HS[#]. (2022) "Agro-derived Inhibitors for Mitigating Chloride-induced Corrosion", Mid-Continent Transportation Research Symposium, Ames, Iowa.

4) Sajid H.U.[#*], and **Ravi Yellavajjala**[c] (2021). "Employing Polyols for Increasing Ice Melting Capacity and Decreasing Freezing Point of Salt Brine Deicer", 19th International Conference on Cold Region Engineering, virtual conference.

5) Sajid H.U.[#*] and **Ravi Yellavajjala**[c] (2021). "Bio-based Additives for Mitigating Chloride-induced Corrosion in Transportation Infrastructure", Engineering Mechanics Institute Conference – 2021, Virtual Conference.

2 A Survey on the Effects of Deicing Materials on Properties of Cement-based Materials

2.1 Introduction to the effects of deicers on concrete

In the past decade, many studies have been conducted that explored the effects of incorporating supplementary cementitious materials on deicers-induced deterioration in concrete and the effects of deicing solutions, deicer blends, and agro-based deicers on the strength and integrity of the concrete. The objective of this chapter is to discuss the effects of the recently developed laboratory-scale deicing formulations as well as the conventional deicing solutions on important properties of concrete that include scaling, mass loss, and compressive strength. Moreover, it also aims to discuss the performance of concrete incorporating supplementary cementitious materials and alternative mix design when subjected to different deicing solutions. In essence, this chapter provides a comprehensive state-of-the-art review of the recent developments in the deicing-induced deterioration in concrete for both conventional and new deicing solutions.

2.2 Deicers-induced Deterioration Mechanisms in Concrete

Deicer-induced deterioration in concrete is commonly exacerbated by different physical processes and chemical interactions between deicers and cement paste and deicers and aggregates. These deteriorations are manifested in the form of scaling damage, loss of compressive strength, mass change, expansion, and spalling. This section summarizes each of these physical deterioration mechanisms and discusses important factors that contribute to physical deterioration in concrete. Furthermore, it discusses the chemical interactions that occur between 1) deicers and cement hydration products and 2) deicers and aggregates.

2.2.1 Physical Deterioration

2.2.1.1 Scaling

Scaling is the superficial damage (flaking or peeling) of the top surface of the concrete, which is initiated when the concrete is exposed to deicing chemical or freeze-thaw conditions. In addition to deicing chemical exposure, scaling can also result from insufficient curing and performing finishing operations while the bleed water is on the surface. The scaling can start as small patches, and it can extend to other areas. Several mechanisms of the scaling of concrete have been proposed in the literature to explain the deicing salt-induced scaling in concrete, and it is suggested to be similar to the scaling mechanism that is observed due to frost damage. Specifically, three different theories have been proposed to explain the scaling phenomena that include the hydraulic pressure theory, osmotic pressure theory, and glue-spalling theory.

Hydraulic pressure theory was one of the earliest proposed mechanisms which is based on the hydraulic pressure due to ice formation [47]. When concrete experiences freezing temperatures, the water in the voids solidifies. As the ice occupies around 9% higher volume compared to water and the volume change of cement paste is negligible, the capillary pores inside the concrete give the required extra room to the ice to some extent creating hydraulic pressure

inside the concrete. A schematic of this mechanism is depicted in Figure 2-1. As observed in Figure 2-1 (c), an escalation of hydraulic pressure causes scaling in the surface and result in the break-away of surface particles. If the temperature increases again, the ice becomes water and releases the hydraulic pressure. The process repeats, and more surface concrete particles are affected by scaling. Later, Powers [48] introduced an osmotic pressure mechanism for salt scaling. According to the osmotic pressure theory, ions from the deicers get concentrated in the pores over time. Once water molecules start to freeze in the pores, salt ions do not occupy the frozen pore area, and hence a differential salt concentration is formed. Due to this differential concentration, water molecules of lower salt concentration areas get diffused to higher salt concentration areas. This diffusion creates osmotic pressure in the higher concentrated surface area of the concrete which causes tensile stresses, a buildup of internal pressure, and mechanical damage in capillary voids and eventually leads to scaling. Apart from hydraulic and osmotic pressure theories, glue-spalling is another theory that was proposed by Valenza II and Scherer [49]. According to the glue-spalling theory, as the deicer melts the snow, the water forms a brine solution with the salt in deicers. Later, the temperature might drop again that will cause the ice to form again, and this ice penetrates into the pores of the concrete, thus adhering to concrete-like glue. With the subsequent fall in temperature, the ice begins to shrink (up to five times more than the concrete layer) which causes the underlying concrete to shrink together initiating cracks and scaling. Scaling can also result from salt crystallization. When the deicers are applied, the concentration of salt ions on the surface gets higher than that in the pores. Salt begins precipitating in the pores and thus forms crystals. The growth of crystals produce mechanical stresses within the pores which cause scaling in the long run [50].

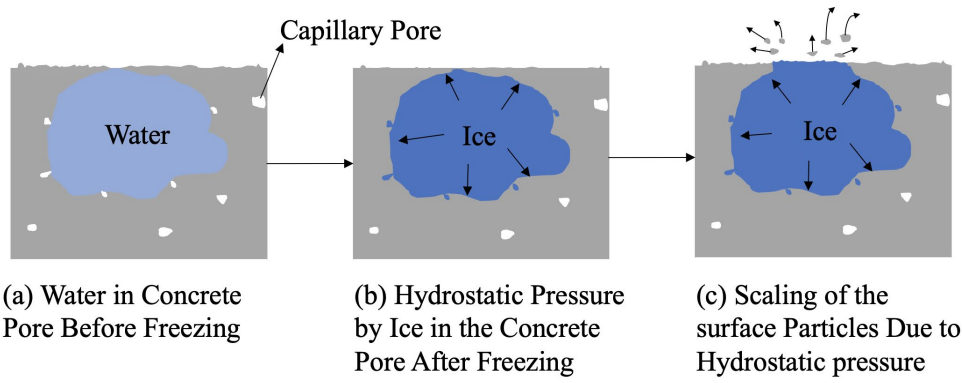

Figure 2-1: Mechanism of scaling due to hydrostatic pressure. (a) water in the concrete pore before freezing; (b) hydrostatic pressure by ice in the concrete pores after freezing where the capillary pores leave space to the increased ice volume (c) scaling of the surface particle due to hydrostatic pressure.

2.2.1.2 Mass Change

Mass change is also a common physical characteristic of the concrete exposed to a deicer solution. Portland cement-based material (concrete) can experience either mass loss or mass gain upon exposure to deicing chemicals. The mass loss could occur due to surface scaling. At the same

time, mass gain is also possible due to salt crystallization and water absorption. Different deicers show different mass change characteristics throughout deicing exposure time. Typically, about 0.5-2.0%, mass change has been observed in concrete when it is exposed to common chloride and acetate-based deicing chemicals for an extended duration.

2.2.1.3 Expansion

Concrete and cement mortar can exhibit expansion upon exposure to deicing chemicals for an extended period. This expansion depends on various parameters of the experiment. Several deicers demonstrate different types of expansion characteristics. The deicing chemicals-induced expansion in concrete is commonly observed to be a function of the water to cement ratio, the concentration of deicing salts in the deicing solution, and the calcium-magnesium ratio of the deicers.

2.2.1.4 Spalling

In addition to scaling, deicing chemicals can also result in spalling of concrete, which refers to the breaking away of concrete surfaces. Spalling often extends to the top layer of the reinforcing bars and is commonly caused by the deicers-induced corrosion of rebars. Moreover, the factors that contribute to scaling are also observed to be responsible for spalling.

2.2.2 Chemical Deterioration

The chemical deterioration mechanism is different for different deicers based on their chemical compositions. Deicers may cause damaging effects to concrete by causing reactions with cement paste and aggregates. The chemical interactions between deicers and concrete (cement paste or aggregates) can be linked with some of the physical deteriorations. In the following sections, the chemical deterioration mechanisms in concrete are discussed for the commonly available deicers.

2.2.2.1 Reaction Between Cement Paste and Deicers

Ions in the deicers can react with the cement paste. For example, chloride ions in sodium chloride, calcium chloride, and other chloride-based deicers can cause calcium hydroxide leaching [37, 51, 52]. Calcium hydroxide can occupy more than 20 percent of the total volume of cement paste. Calcium hydroxide leaching can cause a significant deterioration in concrete and adversely affect the strength and durability of concrete. $CaCl_2$ based deicers can cause slow but severe deterioration in concrete. Calcium hydroxide in cement paste can react with $CaCl_2$ to form calcium oxychloride [53, 54].

$$3\ Ca(OH)_2 + CaCl_2 + 12\ H_2O \rightarrow 3\ CaO{\cdot}CaCl_2{\cdot}15\ H_2O$$

$MgCl_2$ can stem from Mg-based deicers, which can react with calcium hydroxide to form $CaCl_2$.

$$MgCl_2 + Ca(OH)_2 \rightarrow Mg(OH)_2 + CaCl_2$$

Calcium oxychloride can cause immense hydraulic pressures in concrete, which can lead to severe cracking. Sutter et al. [54] found radial cracking in the cylinders that were exposed to $CaCl_2$ and $MgCl_2$ solutions. In another study, affected areas of the cement paste were found to be more porous

[55], and nearly no calcium hydroxide was found in that area. Besides, oxychloride formation also affects the strength and durability of the concrete.

Magnesium ions in $MgCl_2$ and other Mg-based deicers can react with C-S-H in cement paste and create M-S-H [51, 53, 56].

$$MgCl_2 + C\text{-}S\text{-}H \rightarrow M\text{-}S\text{-}H + CaCl_2$$

M-S-H is a non-cementitious product that is not associated with the strength of the cement. C-S-H is a significant contributor to the strength of concrete; thus, magnesium ions can reduce the compressive strength of the concrete [51, 56–58]. Moreover, magnesium ions can form brucite ($Mg(OH)_2$ crystal) that causes crystal growth pressure in concrete, which can cause concrete to expand and lose strength [51, 56, 58, 59]. The complex salt formation, e.g., brucite and calcium oxychloride, depends largely on the concentrations of the solution. Calcium oxychloride formation occurs at a temperature between 0°C to 50°C [60]**.** Deicers-induced chemical deterioration in concrete becomes a key factor when deicers are used in higher concentrations [55].

2.2.2.2 Reaction Between Aggregates and Deicers

The two most common aggregate cement reactions are the alkali-silica reaction (ASR) and alkali-carbonate (ACR) reaction. Deicers can accelerate ASR in concrete with reactive aggregates [52, 61–63]. Deicers provide extra alkali to the pore solution, which forms N(K)-S-H gel. This gel swells as it attracts water from the cement paste. When absorbing pressure, this gel can cause internal pressure which can lead to expansion and cracking of the aggregate and cement paste.

$CaCl_2$ and $MgCl_2$ do not have any impact on ASR. From several studies, it is indicated that NaCl primarily causes the instigation of the ASR process [64–67]. The increase in pH in the pore solution is the potential cause of ASR. NaOH is formed by the reaction between NaCl and $Ca(OH)_2$. Chloride ions in deicing salts can accelerate ASR [68].

$$2NaCl + Ca(OH)_2 \rightarrow CaCl_2 + 2NaOH$$

Dolomite ($CaMg(CO_3)_2$) aggregate can react with alkalis in cement paste, referred to as Alkali-Carbonate Reaction (ACR). Dolomite aggregate reacts with OH- anion in the cement paste and creates Mg^{2+} and CO_3^{2-} cations [38]. CO_3^{2-} cations form $CaCO_3$ and OH- by reacting with the portlandite, while brucite is formed from the precipitation of Mg^{2+} ions [38]. This formation of brucite and $CaCO_3$ crystals can cause crystal growth in the concrete, which eventually causes expansion and cracking in the cement paste [69].

2.3 Experimental Techniques for Characterizing Physical and Chemical Deterioration

This section describes the experimental techniques and specimen preparation procedures that have been adopted in the literature for investigating the deicers-induced physical and chemical deterioration in cement-based materials. Specifically, the mix design and materials that are used in the preparation of concrete specimens, the experimental procedures for simulating the concrete deicing exposure, and the laboratory tests that are used for quantifying the deicer-induced deterioration in concrete are discussed in this section.

2.3.1 Materials Selection and Mix Design

The deicer-induced deterioration has been investigated for both ordinary Portland cement (OPC) concrete and concrete mixes that use supplementary cementitious materials. Many of the earlier studies focused on understanding the performance of air-entrained and non-air-entrained OPC and high-strength concrete when subjected to conventional chloride-based deicers. Recent research efforts have been dedicated to understanding the role of unconventional concrete mix design and supplementary cementitious materials in mitigating or accelerating the harmful effects of conventional deicers on concrete. Specifically, extensive investigations have been conducted to understand the deicers-induced deteriorations in concrete mixes wherein the cement is partially replaced by fly ash [59, 70, 71] blast furnace slag [59, 70, 72] and modified forms of blast furnace slag [70]. In most of the literature on the deicers' impact on concrete, a water-cement ratio of 0.35-0.5 is adopted. Moreover, a variety of admixtures are used in the concrete specimens used in the literature to simulate the concreting in cold regions or to improve the properties of concrete. Similarly, concrete specimens with and without air entrainment are used and their performance in deicing exposure tests is compared. For this purpose, a wide variety of commercially available entraining agents are utilizes in different studies to achieve the desired air content in the hardened concrete specimens [37, 72–74].

2.3.2 Deicer Selection

For field applications, deicers are selected based on their effectiveness during the freezing temperatures, cost, availability, and ease of application on the pavement surface. The effectiveness of deicers in melting ice and snow is defined by their effective temperature, which is the lowest temperature where a deicer can be practically used for ice melting, anti-icing, and other applications [75]. In highway deicing and anti-icing operations, chloride-based deicers are most commonly used due to their lower cost and ample availability [76]. Among the chloride-based deicers, NaCl is most commonly employed in the highways. The effective temperature for NaCl is 15°F [77]. Below this temperature, it cannot melt the snow, thereby making it inappropriate during extremely low freezing temperatures. However, it is often mixed with other deicers and corrosion inhibitors to make it applicable to a wide range of areas. Changing the concentration of NaCl deicers and mixing it with other deicers and additives is knowns to reduce the freezing point of NaCl solution and hence making them more effective in snow melting at temperatures below 15°F [78–80]. While NaCl does not cause serious deterioration in concrete, it is widely observed to corrode steel [76, 81] and is known to adversely affect the environment and aquatic life [81]. On the other hand, calcium chloride is also a chloride-based deicer that is effective at temperatures as low as -25° F, which makes it suitable for cool winter areas. It is relatively harmless to the environment. However, it causes significant deterioration in concrete [37, 53] and is more expensive as compared to sodium chloride [82]. Magnesium chloride is another chloride-based deicer that works at a relatively low temperature (-10°F) and it is widely used for deicing on highways and parking lots [81]. However, it is also observed to be corrosive, cause severe deterioration in concrete, and may cause pollution to the environment [83, 84]. Calcium magnesium acetate (CMA) deicer is less corrosive when compared to chloride-based deicers [85].

It is also biodegradable, which makes it environmentally friendly to some extent. However, CMA is not as cost-effective as chloride-based deicers. Moreover, its application is limited to moderately cold temperatures. Potassium acetate is another acetate-based deicer that works at a very low temperature (-15°F) [86]. Like CMA, it is a less corrosive and more environmentally friendly option. Hence, it is mostly employed in airport runways. In addition to the aforementioned deicers, potassium formate, calcium formate, and urea are also used as deicers in different applications [38].

Selecting deicers is an integral part of the experimental schemes adopted in the literature. Different deicers have different characteristics and lead to varying rates of deterioration in concrete. To this end, the most commonly tested deicers include chloride-based deicers (NaCl, $CaCl_2$, and $MgCl_2$), acetate-based (e.g. CMA), and formate-based deicers. Additionally, agro-based and other propriety deicing chemicals have also been investigated for their deterioration impact in cement-based materials. Some researchers also added certain corrosion inhibitors to the deicing solutions while investigating the influence of deicing chemicals on concrete. The above-mentioned deicing solutions have been used in the deicing exposure experiments in concentrations that mostly ranged from 3% to 30%. Moreover, some studies used mixed deicers wherein NaCl and another chloride-based deicer are mixed in 50-50 or other ratios. As sodium chloride is the most commonly used deicer, it is used as a deicer in almost every study. Additionally, calcium chloride and magnesium chloride are also used in many experiments related to deicers, as they show the most severe deteriorations in concrete. Furthermore, several new deicing chemicals have been investigated in recent studies.

2.3.3 Deicer Exposure Methods

To investigate the physical and chemical deterioration of concrete due to deicer, it is essential to select the appropriate deicer exposure method. To this end, three deicer exposure techniques are commonly adopted in the experimental schemes that include continuous soaking, freeze-thaw exposure, and wet-dry exposure of deicing solutions. Each of these deicing exposure techniques is discussed in the subsequent sections.

2.3.3.1 Continuous Soaking

Continuous soaking of concrete samples in the deicer solution is a standard experimental technique for characterizing physical and chemical deterioration in concrete. The continuous soaking exposure method has been used in different studies [53, 58, 61, 85]. During the continuous soaking exposure method, the samples are immersed in a deicer solution or water solution for a certain period. This soaking period may vary in different experimental protocols depending upon the concentration of deicer solution or experimental goal. There is no standard temperature that is followed by the researchers. The temperature could be room temperature or temperature as low as 4°C. At the end of the soaking period, samples are taken off from the solution and different physical and chemical tests are conducted. This method does not show the frost effect or temperature-change effect of the deicer solution.

2.3.3.2 Freeze-Thaw Exposure

The freeze-thaw (F-T) test is used to elucidate the physical and chemical characteristics of concrete exposed to deicers. F-T test simulates the freeze-thaw scenario that most highways experience during the winter season in colder regions. During subzero temperatures, the water trapped in the concrete pores freezes. When the temperature rises, the ice in the concrete melts which is followed by freezing once the temperature drops to subzero level again. Roadways experience several such cycles during every winter season. Ice has around 9% more volume when compared to water and this extra volume exerts hydraulic pressure in pores in the absence of adequate pore space, which eventually leads to cracks and deterioration in concrete. F-T exposure tests mimic this process in the laboratory and are hence used to study the physical and chemical deterioration of concrete. During F-T exposure tests, the samples are submerged in a deicer solution in a container and are subjected to F-T cycles. A typical F-T cycle consists of a 'freezing' interval and a 'thawing' interval. During freezing intervals, the containers wherein concrete samples are fully submerged in the deicing solution are placed in a freezer and stored at freezing temperatures (i.e., -10 to -22° C) for a certain time period. This is followed by a thawing interval during which the containers are taken out of the freezer and are placed at room temperature for thawing. The selection of the freezing and thawing period is dependent on the experimental procedure. One of the standard practices for the freeze-thaw test is to use a cycle time of 24 hours. The freezing interval varies between 12-18 hours, and the thawing interval varies between 6-12 hours. A high concentration of deicer is usually used in F-T tests due to their lower freezing point and the ability to get the required deterioration quickly. Some researchers adopted a longer cycle time using a less concentrated deicer solution. The cycle time can vary from two days to even one month. The physical and chemical deterioration in concrete is tracked at a specific number of F-T exposure cycles by conducting different laboratory tests.

2.3.3.3 Wet-Dry Exposure

Another widely used deicing exposure method is Wet-Dry (W-D) exposure test. Here, the samples are soaked in the deicing solution for a certain period (referred to as the 'Wet' period). This is followed by a 'Dry' period during which the samples are taken off from the solution and placed in an open space for drying. It is a common practice to keep the temperature around 0-4°C during the wet period and room temperature (20°-25° C) during the dry period. This wetting and drying continues for a certain number of cycles. The length of a cycle depends on the parameters of the experiments. After a specific number of W-D exposure cycles, samples are subjected to different physical and chemical tests to evaluate the deicer-induced deterioration.

2.3.4 Deicer-induced Deterioration Tests

2.3.4.1 Visual Evaluation, Scaling, and Scaling Rating

Visual evaluation is a qualitative test wherein the specimens are visually examined for physical deterioration from the deicer exposure. Visual examination of concrete, mortar, or cement paste specimens is carried out at the beginning of F-T and W-D exposure tests and after a specific number of F-T or W-D exposure cycles. To this end, specimens are visually monitored and

photographed and any change in the physical appearance of the specimen surface is noted. Physical deterioration is usually in the form of cosmetic cracks on the surface, surface scaling, and spalling. From visual evaluation, the extent of scaling in the specimens is identified. Moreover, a scaling rating is usually assigned to the specimens based on the visually observed scaling damage. The scaling rating ranges from 0 (no scaling damage) to 5 (severe scaling damage) [37].

2.3.4.2 Mass Change Evaluation

The change in the mass of the specimens is another parameter that is commonly used in literature to track deicer-induced deterioration in the concrete, mortar, or cement paste specimens. The increase in the mass of the specimen usually indicates the accumulation, precipitation, and crystallization of deicing salts in the pores, which can lead to pressure buildup in the pores and eventual cracking. On the other hand, the decrease in the mass of the specimen usually indicates scaling and the break-off of aggregates or hydration products, which is once again indicative of deicer-induced physical deterioration in the specimens. The mass change in the specimens is commonly evaluated after a specific number of F-T or W-D exposure cycles and at the end of F-T or W-D exposure tests.

2.3.4.3 Expansion Measurement

Determining volumetric expansion in the specimens is another method of evaluating deterioration in the specimens as a result of exposure to deicing solutions. For this purpose, the length, width, and height of the samples are recorded at the beginning, after a specific number of exposure cycles, and at the end of the F-T or W-D test. Usually, the visual evaluation, mass change evaluation, and expansion measurement are conducted after similar but a specific number of F-T or W-D exposure cycles, and these parameters are compared with the measurements recorded at the beginning of F-T and W-D tests for determining the deicer-induced physical deterioration.

2.3.4.4 Strength Evaluation

Strength is one of the most important parameters that indicate the extent of deterioration in the concrete, mortar, or cement as a result of exposure to deicing solutions. Compressive strength, split tensile strength, and flexural strength are the three strength parameters that can be used to evaluate the deicer-induced deterioration in concrete. Owing to its practical importance, most researchers have focused on determining the compressive strength of concrete, mortar, or cement paste specimens whereas only a few studies determined the flexural and split tensile strength of concrete specimens after deicer exposure tests. Compressive strength tests are conducted at the beginning of F-T or W-D continuous soaking testing and after a specific number of F-T or W-D exposure cycles using ASTM C39 and AASHTO T22 specifications. Moreover, non-destructive testing techniques are also used to evaluate the compressive strength of the concrete specimens [87].

2.3.4.5 Dynamic Modulus of Elasticity Evaluation

The dynamic modulus of elasticity is another durability parameter that can be used to determine the extent of deicer-induced deterioration in the concrete. The dynamic modulus of

elasticity of concrete specimens after exposure to deicing solutions is usually determined using non-destructive testing such as resonance frequency test, impulse excitation test, and sonic resonance test [87, 88].

2.3.4.6 Chemical Composition and Surface Characterization

Chemical composition analysis and surface characterization tests are commonly employed to evaluate the chemical interactions between the deicing chemicals, cement hydration products, and aggregates. Specifically, chemical composition analysis and surface characterization tests indicate the harmful or beneficial products that are formed as a result of chemical interactions between the deicing chemicals, cement hydration products, cementitious materials, and aggregates. Moreover, surface characterization techniques are also used to elucidate the presence of microcracks in the specimens as a result of exposure to the deicing solutions. In essence, these tests quantify the deicer-induced chemical deterioration in cement-based materials. The most common chemical composition analysis tests include X-ray Diffraction (XRD) and Energy Dispersive X-Ray (EDX) analysis whereas optical microscopy and Scanning Electron Microscopy (SEM) are frequently used for the characterization of surface and microcracks and morphological analysis. XRD and EDX analysis yield the crystalline compounds and elemental composition of the products formed due to chemical interaction between the deicing solution and cement hydration products. For performing XRD analysis, powder samples are obtained from surface layers at various depths. For SEM analysis, a section is cut from the concrete sample which is further polished and prepared for examining the presence of microcracks and any products. XRD, SEM, and EDX analyses are usually performed after a specific number of F-T or W-D exposure cycles.

2.3.4.7 Ion Penetration Test

The ion penetration test is commonly used to determine the extent of deicing chemical ions penetration in the concrete, mortar, or cement paste specimens after exposure to deicing chemicals. The ion penetration test gives a quantitative account of the presence of deicing chemical ions (such as chloride ion, sodium ion, and magnesium ion, etc.) at certain depths in the specimen. This information is very important since the presence and concentration of these ions have a direct impact on the extent of concrete deterioration due to the formation of expansive products and the rate of corrosion in rebars. The commonly available laboratory tests for determining the ion penetration in concrete include salt ponding test (AASHTO T259), bulk diffusion test (Nordtest NTBuild 443), Rapid Chloride Permeability Test, (AASHTO T277 and ASTM C1202), total chloride content test (ASTM C1152), electrical migration techniques, rapid migration test (CTH Test), resistivity techniques, pressure penetration techniques, indirect measurement techniques, and sorptivity analysis. Among these methods, ASTM C1152, AASHTO T259, AASHTO T277, and ASTM C1202 test methods are commonly adopted in the literature.

2.4 A Critical Review of Previous Literature

Numerous studies have been performed by different researchers to elucidate the deicer-induced physical and chemical deterioration in concrete. While many characterization tests are performed to evaluate the deicer-induced deterioration in concrete, this review article focuses only

on the most important properties of concrete that are vital for ensuring the serviceability of concrete structures and this section summarizes the most common deicer-induced concrete deterioration parameters that include scaling damage, scaling rating, mass change, and compressive strength that have been reported in the literature for different types of concrete mixes and deicing chemicals. Moreover, the results are discussed for both F-T and W-D exposure tests.

2.4.1 Scaling Research

Many researchers characterized scaling as an indicator of deicer-induced physical deterioration in concrete in their studies [89, 90]. Scaling tests and scaling rating assignments are conducted using visual evaluation procedures discussed in Section 3.4.1. The scaling damage results obtained from the literature corresponding to W-D and F-T exposure tests are summarized in Table 2-1. Moreover, the measurement of scaling damage in terms of five scaling ratings as per ASTM C 672-98 under F-T and W-D exposure cycles is provided in Figure 2-2 and Figure 2-3, respectively. The severity of each of these scaling ratings is described in Table 2-2. As observed in Table 2-1, Figure 2-2, and Figure 2-3, the scaling damage has been investigated for a variety of deicing chemicals using different deicing exposure conditions (F-T or W-D), cement types, usage of admixtures, and supplementary cementitious materials (e.g., fly ash and blast furnace slag), different water-cement ratios and aggregate types. Sahin et al. [91] conducted comprehensive investigations on the effect of NaCl deicer on concrete durability by incorporating different cement content, curing conditions, air entrainment percentage, and water to cement ratio. The normal concrete with no air-entraining agent was observed to deteriorate more quickly after exposure to NaCl deicing solution as compared to air-entrained concrete specimens. The addition of 0.1% air entrainment considerably enhanced the scaling resistance of concrete. Similarly, air curing was observed to be more effective as compared to water curing. In addition, the increase in cement amount decreased the permeability that in turn led to lower chloride ion penetration and low surface peeling [37, 91]. Matalka and Parviz [92] investigated the effect of $CaCl_2$ deicer on OPC concrete and alkali aluminosilicate cement concrete with and without air entrainment. The authors observed that normal concrete incurs minor deterioration as early as 4 F-T cycles while the addition of an air-entraining agent significantly enhanced the scaling resistance and only minor scaling was observed after 6 F-T cycles. This scaling damage in the specimens can be attributed to the pressure developed by the formation of crystals of Friedel's salt and ettringite [93]. The degradation is also attributed to the leaching of Calcium ions (Ca^{+2}) from the C-S-H structure [52, 94]. The use of alkali aluminosilicate cement reduced the scaling resistance. However, the inclusion of air-entraining agents increased the scaling resistance. The reduction in scaling resistance in the presence of alkali aluminosilicate cement is attributed to the presence of Cl^- and H^+ ions [95]. Similarly, alkali aluminosilicate cement concrete pores are rich in sodium that causes the formation of sodium chloride that disturbs the hydrates in the alkali aluminosilicates due to the low basicity of void solution [51, 52]. But the introduction of air entrainment provides the extra space for crystals to grow to reduce the pressure on the pore structure [49]. Similarly, the pozzolanic reaction of fly ash also contributes to counter the detrimental effect of calcium chloride deicing solution [96]. Santagata and Collepardi [72] investigated the effect of CMA deicer on limestone Portland

and slag-based cement concrete and paste. The decay process started after 3 months of continuous soaking exposure. Overall, limestone-based cement composition revealed high scaling deterioration, but the usage of laboratory-made CMA reduced the degradation process by half due to lack of impurities. The slag-based cement lowered the leaching of calcium hydroxide of cement.

The effects of W-D exposure cycles of deicing solutions on the scaling damage of cement mortar and concrete specimens in terms of scaling ratings are presented in Figure 2-3. Figure 2-3 depicts the same overall trend of scaling damage in cement-based materials as that observed in the case of F-T tests (see Figure 2-2). However, the extent of scaling damage in the case of W-D tests is relatively less as compared to F-T tests which can be attributed to the lack of subzero temperatures during W-D tests. As observed in Figure 2-3, at a high number of W-D cycles, NaCl deicing solution resulted in slight to moderate scaling in concrete [88]. Wang et al. [37] study concluded that in the case of $CaCl_2$ the use of corrosion inhibitors reduced the scaling rate by half. Similarly, the investigations conducted by Drawin et al. [88] revealed that reducing the concentration of $CaCl_2$ significantly reduced the scaling. In addition, the inclusion of fly ash decreases the permeability and thereby reduces the scaling deterioration [96]. Likewise, $MgCl_2$ also showed the same trend wherein low concentration and partial addition of fly ash significantly eradicated the tread of scaling. The use of CMA is observed to be detrimental both at low and high concentrations [85]. In contrast, the utilization of potassium acetate resulted in a slight or slight to moderate amount of scaling whereas agriculture-based acetate had constant scaling due to the presence of micropores [37]. The potassium acetate expands lesser during the alkali-silica reaction due to the small diameter of the hydration product. Secondly, the potassium was only found on the surface and no deep penetration was observed which avoided the reaction with cement hydration products [37, 97].

From the existing studies, deicer-induced scaling in concrete is dependent on several parameters that include cement type, aggregate types, w/c ratio, type and concentration of a deicing chemical, presence of admixtures, and exposure conditions. Considering all these parameters, a review of the existing literature suggests that all conventional chloride-based deicers (NaCl, $CaCl_2$, and $MgCl_2$) inflicted scaling damaged in concrete mainly due to decalcification of cement paste and as well as osmotic and hydraulic pressure created by the formation of expansive oxychloride products and crystallization of these salts. A comparative review suggested that $MgCl_2$ and $CaCl_2$ caused significantly higher scaling damage as compared to NaCl. Chemical and morphological investigations (e.g., SEM and XRD) conducted in various research studies confirmed the formation of several new products in concrete specimens that are exposed to these deicing chemicals. The formation of calcium oxychloride in the case of $CaCl_2$ and the formation of brucite and M-S-H in the case of $MgCl_2$ are observed to contribute to scaling damage, deterioration, and loss of strength in concrete. Other deicers like CMA, Ca-acetate, Mg-acetate, etc. showed moderate scaling damage in concrete. Also, as far as the exposure mechanisms are concerned, the samples exposed to F-T exposure showed more deteriorations as compared to W-D or continuous soaking exposure which is primarily attributed to the frost action in the case of F-T exposure. Air-entraining agents were used by several researchers to investigate the improvement of the scaling resistance of

concrete and a positive impact on scaling resistance was observed. Thus, it is recommended to use an air-entraining agent in the concrete mix. In some studies, corrosion inhibitors were used. The results showed the deicers to have a better performance in presence of certain corrosion inhibitors. But there is a lack of studies in this regard to reach a definite conclusion.

Table 2-1: Studies focused on scaling damages on concrete due to deicer exposure.

Ref.	Deicer used	Exposure method	Parameters	Findings
[98]	$CaCl_2$	-	Concrete (field)	-Damage in concrete linked with the chemical reaction between calcium chloride and cement paste, and mechanical stress developed by load and F-T cycles.
[99]	NaCl	W-D	Concrete w/c: 0.3, 0.26, 0.2	-No significant deterioration was found after 150 cycles. -W/c ratio, air void spacing factor, and length of curing did not have any impact on HPC specimens exposed to deicers.
[73]	$CaCl_2$	Soaking	Concrete (OPC, OPC with 15% SF, OPC with 30% FA	-Concrete specimens with or without air-entrained agents showed severe damage when exposed to $CaCl_2$. -This damaging effect is attributed to the formation of oxychloride products.
[85]	NaCl, CMA	Soaking	Mortar w/c =0.45,0.6 time- 22 months	-Ca/Mg molar ratio had significant effects on the mortar. -Higher Mg ion concentration is linked with increased deterioration in specimens. -NaCl did not cause significant scaling in specimens.
[58]	NaCl, $CaCl_2$, $MgCl_2$	W-D, F-T	Concrete w/c =0.45, 0.6 time: 22 months conc: 0.75,3(M)	-$CaCl_2$, $MgCl_2$, Mg-acetate, and Mg-nitrate caused significant scaling in the specimen as compared to NaCl. -Brucite formation was assumed to be the potential reason behind the deterioration.
[100]	NaCl with six CIs	Soaking	Concrete slab	-Formation of calcium phosphates, magnesium phosphates, gypsum, and other precipitates resulted in scaling damage.
[72]	CMA (25 wt%)	Soaking	Concrete (Type I, Type II, Portland clinker with 20% limestone and 40% BFS	-The deterioration of the concrete appeared to be slightly greater in the case of immersion in solutions manufactured using a commercial CMA-based deicer product rather than employing pure calcium and magnesium acetates.
[101]	NaCl, Na-formate, K-acetate, Urea	F-T	Aggregate, Concrete (field)	-Disintegration observed in aggregates exposed to F-T cycles. The limestone aggregate was found to have a higher resistance to disintegration as compared to quartzite. -Scaling damages observed in asphalt concrete samples, particularly in the case of urea.
[102]	NaCl	Soaking	Concrete (laboratory, field)	-Scaling due to formation of chloroaluminate crystals cement paste and in the air voids near the surface. -pH decreased near the surface is attributed to anisotropic expansion and tension cracks near the surface.

[53]	NaCl, $CaCl_2$, $MgCl_2$	Soaking	Mortar w/c: 0.45, 0.5, 0.6 time (d): 7, 14, 28, 56, 84, 112	-$MgCl_2$ and $CaCl_2$ showed initial deterioration after days and severe deterioration after 84 days. -No significant deterioration observed in the case of NaCl. -Deterioration is attributed to the formation of brucite and calcium oxychloride, in the case of $MgCl_2$ and $CaCl_2$.
[37]	NaCl, $CaCl_2$ (with CI), KAc, agro-deicer	W-D, F-T	Cement paste Concrete w/c =0.4 time (d): 60 (1 day cycle)	-$CaCl_2$ exhibited the highest scaling (under both W-D and F-T conditions) which is linked with salt crystallization and precipitation and leaching of cement hydration products. -KAc and agro deicer showed limited deterioration. -F-T exposure resulted in higher scaling damage as compared to W-D exposure.
[103]	KAc, NaAc, NaCl	Soaking	Concrete (low-alkali cement, high-alkali cement)	-KAc and NaAc caused ASR in the specimens containing reactive aggregates. -Extensive scaling is observed in all cases. Surface cracking was more serious in the case of KAc.
[88]	NaCl, $CaCl_2$, $MgCl_2$, CMA (6.04M & 1.06M)	W-D	Concrete w/c =0.4 time: 70 weeks (1-week cycle)	-At 6.04 molal ion concentration, $CaCl_2$, $MgCl_2$, and CMA cause significant changes in concrete. -At 1.06 molal ion concentration, all deicers exhibited relatively lower scaling damage. -Among all the used deicers, NaCl appeared to have a lower negative impact on concrete in any concentrations.
[38]	NaCl, $MgCl_2$, CMA, K-formate, K-acetate	F-T	Concrete time: until significant deterioration (1-day cycle)	- CMA solid deicer and $MgCl_2$ liquid deicer were observed to be less deleterious to concrete. -NaCl-based deicer (IceSlicerTM), and KAc-based deicer (CF7TM) caused higher deterioration in concrete.
[104]	NaCl (3 wt%)	F-T	Concrete (OPC, blast-furnace & limestone OPC)	-Severe scaling in F-T exposure regardless of air-entrainer. -Scaling is affected by the air-entrainer, second finishing treatment, cement content, w/c ratio, and curing conditions.
[105]	NaCl, $CaCl_2$, $MgCl_2$ (3,30wt%)	W-D	Mortar w/c =0.5 time 124 weeks (4 weeks cycle)	-With the increase in concentration, severe scaling is observed in the specimens exposed to $CaCl_2$. -The specimens exposed to $MgCl_2$ had less damage, and no damage was observed in the case of NaCl.
[106]	$MgCl_2$, $CaCl_2$, NaCl	Soaking	Concrete Time (d): 338	From the results, it appeared that Mg^{2+} cation has a more detrimental effect on concrete as compared to Ca^{2+} cation.
[67]	K-acetate, K-formate	Soaking	Cement paste Concrete	-Scaling and microcracks observed in the specimens. -ESEM/EDS study confirmed the formation of ASR gel.
[96]	NaCl, $CaCl_2$, $MgCl_2$	Soaking, W-T, F-T	Concrete (Type I, Type I + 20% FA time (d): 336 (1-day cycle)	-$CaCl_2$ showed the highest scaling damage among all the deicers. Specimens exposed to $CaCl_2$ had a 15% reduction in RDME after 154 cycles. For $MgCl_2$, the same amount of reduction was found after 300 cycles. -Specimens with fly ash showed better results in all the tests.

[59]	NaCl, $CaCl_2$, $MgCl_2$ (5.5M)	F-T	Concrete (Type I, Type I+FA, Type I BF, Type I+FA+BF Time (d): 350 (1 day cycle)	-$CaCl_2$ resulted in higher scaling than $MgCl_2$ and NaCl. -The deterioration is attributed to the formation of brucite and magnesium silicate hydrate. -Formation of calcium hydride is observed to increase the concrete porosity and thus result in high deicer penetration in the concrete matrix.
[107]	NaCl, K-acetate	W-D, F-T	Concrete (field and laboratory) w/c: 0.4 (laboratory)	-Interfacial transition zone (ITZ) attack was observed. -EDS results suggested leaching of Ca from cement paste. -Scaling damage due to formation of precipitates as well as crystallization-induced volume expansion.
[108]	NaCl, $CaCl_2$, $MgCl_2$, CMA	F-T	Concrete (field) Concentration: 0.75M	-Ca-acetate was less detrimental, and Mg-acetate was more detrimental. -The authors recommended using CMA with a high Ca:Mg ratio.
[92]	$CaCl_2$ (4 wt%)	F-T	Concrete (OPC, AAC)	-The concrete prepared with AAC showed lower deicing salt scaling resistance when compared to OPC concrete. -Air-entraining agents improved the deicer scaling resistance of AAC concrete specimens.

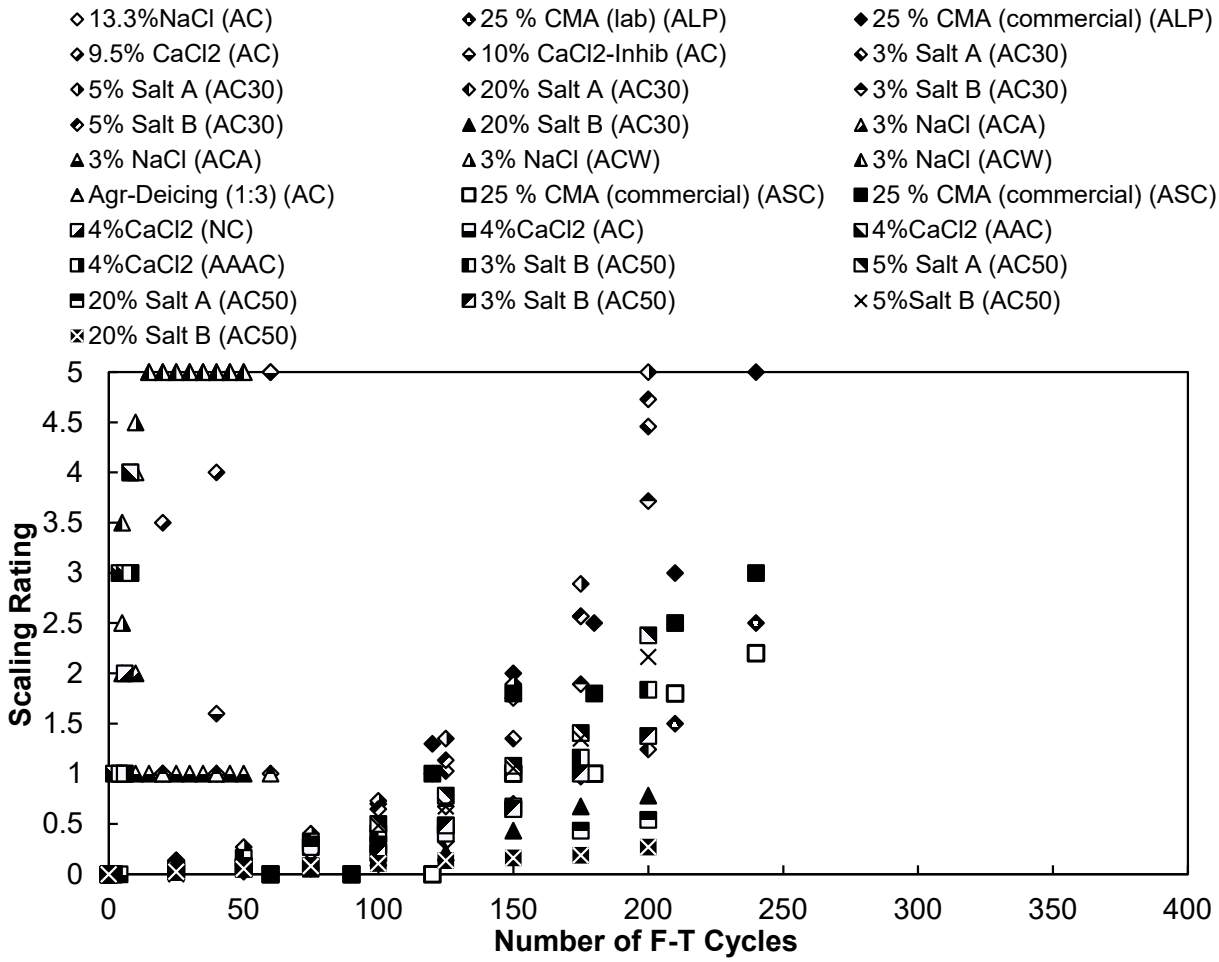

Figure 2-2: The variation of scaling rating with the number of F-T cycles for different studies [37, 38, 53, 72, 91, 92, 109].

Table 2-2: Scaling rating description.

Scaling Rating	Condition
0	No
1	Slight
2	Slight to Moderate
3	Moderate
4	Moderate to severe
5	Severe

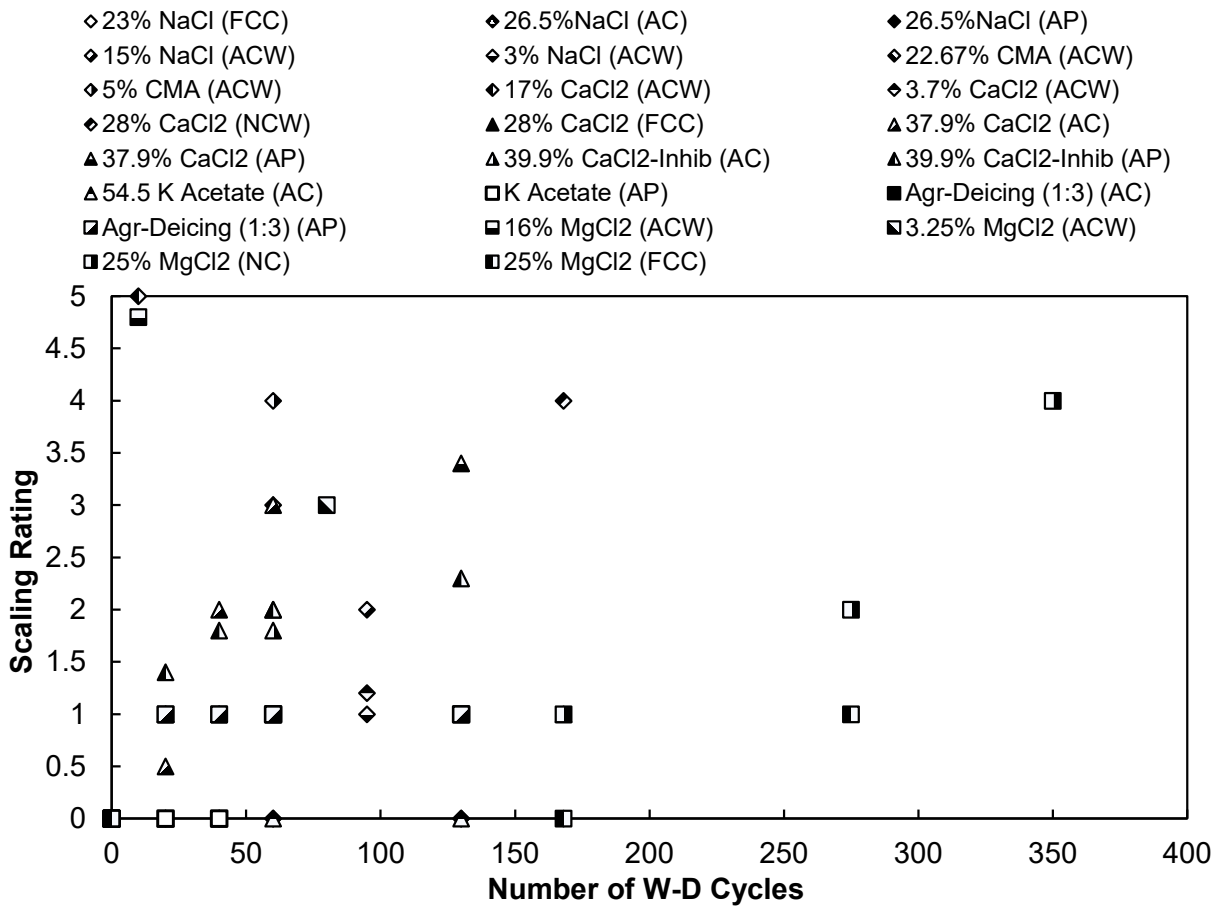

Figure 2-3: The variation of scaling rating with the number of W-D cycles for different studies [37, 53, 72, 96, 110].

2.4.2 Compressive Strength

Compressive strength is an important indicator of the deterioration of concrete. When exposed to deicers, concrete shows a noticeable change in compressive strength. The change in compressive strength depends on several factors like deicer type, deicer exposure method, cycle time, w/c ratio, etc. Several researchers used compressive strength as the primary indicator of deicer-induced deterioration in concrete. In one of the earlier studies, Peterson [53] investigated the effect of CMA solutions with different Ca/Mg ratios and w/c ratios on the properties of concrete and adopted 22 months of continuous soaking of samples in the deicing solutions. The reduction in the compressive strength was observed to be higher in the case of CMA as compared to NaCl. Peterson [53] found that the compressive strength of concrete decreases with the increase in the concentrations of deicing solutions. When considering the Ca/Mg ratios during these experiments, Peterson [53] did not find any significant difference in the samples immersed in CMA solutions in similar conditions. Peterson [53] also measured flexural strength for the samples with different immersion parameters, w/c ratios, and Ca/Mg ratios. The results followed the same pattern as the results in compressive strength. In a later study, Santagata et al. [72] used both laboratory-made CMA and commercially bought CMA with the same Ca/Mg in their experiments. For comparison,

they also immersed the samples in water. All the samples immersed in water showed an increase in compressive strength during the 8-month study period. Samples immersed in CMA solutions showed an increase in compressive strength in the first 2-3 months period, no change for in the next 2-3 months, and a rapid deterioration in the subsequent months. The authors also observed a higher deterioration in the compressive strength corresponding to commercial-CMA deicer when compared to the laboratory-made CMA. Santagata et al. [72] used two different concrete mixes (OPC Type II with limestone and OPC type III with slag) in their experiments. Wang et al. [37] conducted both W-D and F-T tests on cement paste and concrete samples and observed an increase in the compressive strength for the first 20-40 cycles which was attributed to the cement hydration. The samples immersed in distilled water and NaCl gained strength over the W-D and F-T cycles. While NaCl did not cause major deterioration in paste and concrete, the samples immersed in $CaCl_2$ suffered major deterioration. Strength loss was delayed when the inhibitor was used with $CaCl_2$. But eventually, it impacted negatively when the deterioration started. In another recent study, Shi et al. [81] compared the compressive strengths of two different concrete mixes subjected to NaCl, $CaCl_2$, and $MgCl_2$ deicers for 330-347 days. The bridge mix showed a better compressive strength compared to the pavement mix. The researchers used inhibitors to deicers to improve the corrosion resistance of the concrete, and it also resulted in a better compressive strength in the experiments. The researchers also indicated the positive role of Ca^{2+} compared to Mg^{2+}, as inhibited $CaCl_2$ showed a better compressive strength when compared to $MgCl_2$. Cutler et al. [110]subjected Portland cement pervious concrete (PCPC) to F-T cycles of distilled water, NaCl, $CaCl_2$, and CMA solutions. All the samples exposed to different deicing solutions experienced strength loss over the time of 54 cycles. Samples exposed to $CaCl_2$ had the highest strength loss among the deicing solutions. Jain et al. [96] used Type I OPC and Type I OPC with 20% fly ash concrete exposed to W-D and F-T cycles in distilled water, NaCl, $MgCl_2$, and $CaCl_2$. The researchers found that the samples subjected to $CaCl_2$ deicer had more negative impacts when compared to $MgCl_2$. Kim et al. [111] investigated the influence of waste glass sludge (WGS) on improving the F-T resistance of concrete. The concrete samples with WGS showed better compressive strength compared to the concrete with fly ash which was attributed to the high packing density and higher pozzolanic reactivity of WGS when compared to fly ash. Ning et al. [107] investigated the impact of NaCl and KAc deicers on field and laboratory-made concrete samples and observed considerable reduction in the compressive strength after 15 F-T and W-D exposure cycles for both NaCl and KAc. Verian and Behnood [70] conducted W-D and F-T tests on concrete samples prepared using different percentage mixtures of Portland cement, fly ash, and slag cement. Overall, the samples immersed in $CaCl_2$ showed the highest strength loss (up to 19.61%) among the deicers investigated, which was attributed to the formation of calcium oxychloride. Among all the deicers, NaCl showed less strength loss in the samples. The authors further inferred that samples prepared using dolomite aggregates showed better results compared to air-cooled blast furnace slag (ACBFS). The statistical analysis also suggested that F-T cycles resulted in higher deterioration in concrete when compared to W-D cycles.

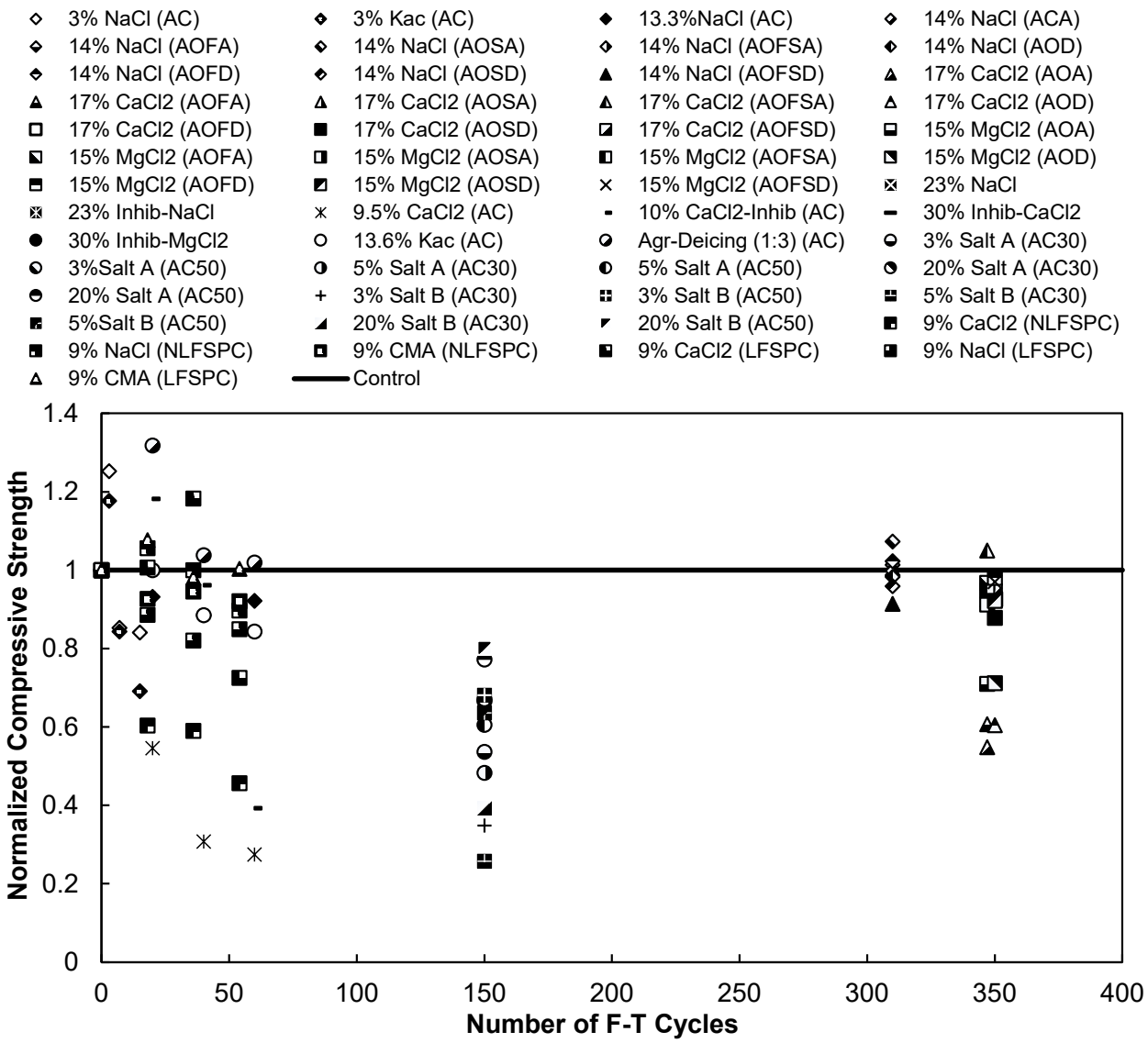

Figure 2-4: Change in concrete compressive strength under F-T cycles in deicing solution [37, 38, 59, 109, 110].

Figure 2-4 summarizes the normalized compressive strength of concrete obtained from the literature corresponding to F-T tests. The compressive strengths obtained from the literature are normalized by dividing each compressive strength with the compressive strength of control specimens to enable a comparison between different deicers. The horizontal straight line represents the reference line while the data points above that line had an increase in strength, and the data points below the reference line had a reduction in the compressive strength due to the deicing salts exposure. As observed in Figure 2-4, in most of the deicer F-T exposure tests, a reduction in the compressive strength of concrete occurs whereas an increase in the compressive strength is observed in some cases. For most of the deicing combinations, the compressive strength is observed to decrease by 30% when subjected to more than 50 F-T exposure cycles. However, for some deicers (for instance Salt B: 70% NaCl + 25% $MgCl_2$ + 5% $CaCl_2$), the compressive strength

of air-entrained concrete decreased by more than 50%. The NaCl deicing solutions reduce the compressive strength of concrete by 8% unless the modification in the concrete mix ingredients is adopted. Moreover, the addition of an air-entrainment agent limits the compressive strength reduction to only 2-8% [37, 59, 108]. In contrast, the inclusion of fly ash and air-cooled blast furnace slag (ACBFS) increased the strength up to 7% [37, 59, 70, 111] even at 310 F-T cycles. The fly ash and ACBFS reduce porosity that decreases the penetration of chloride ions and hence ensures the completion of hydration processes to gain strength. In the case of calcium chloride, the reduction is more significant, especially at higher F-T cycles. This decline may go up to 73% [37, 70] which is mainly attributed to the formation of expansive calcium oxychloride [112]. Similarly, the reaction of calcium chloride with elements involved in the hydration process of cement results in calcium hydroxide and monosulfate that raise the porosity near the surface and thus reduces the concrete durability [37, 70]. This detrimental effect can be resolved by the addition of air-entraining agents, fly ash, and slag. Similarly, the addition of corrosion inhibitors and latex modified fiber reinforced concrete initially increase the strength by up to 18% but decreased the strength at later stages [70, 111]. On average, magnesium chloride performed better but showed no enhancement even upon the addition of air-entraining agents, slag, and fly ash. Potassium acetate initially exhibited a 17% decrease in compressive strength in the presence of air-entraining agent and low concentration but eventually resulted in up to 30% reduction in compressive strength in continuous F-T cycles [107]. The SEM images revealed the formation of rod-shaped precipitate crystals that caused the expansion in concrete that led to an increase in permeability and reduction in compressive strength [107]. The limited results that are available for agricultural deicing products exhibited better compressive strength results even at higher F-T cycles, in some cases.

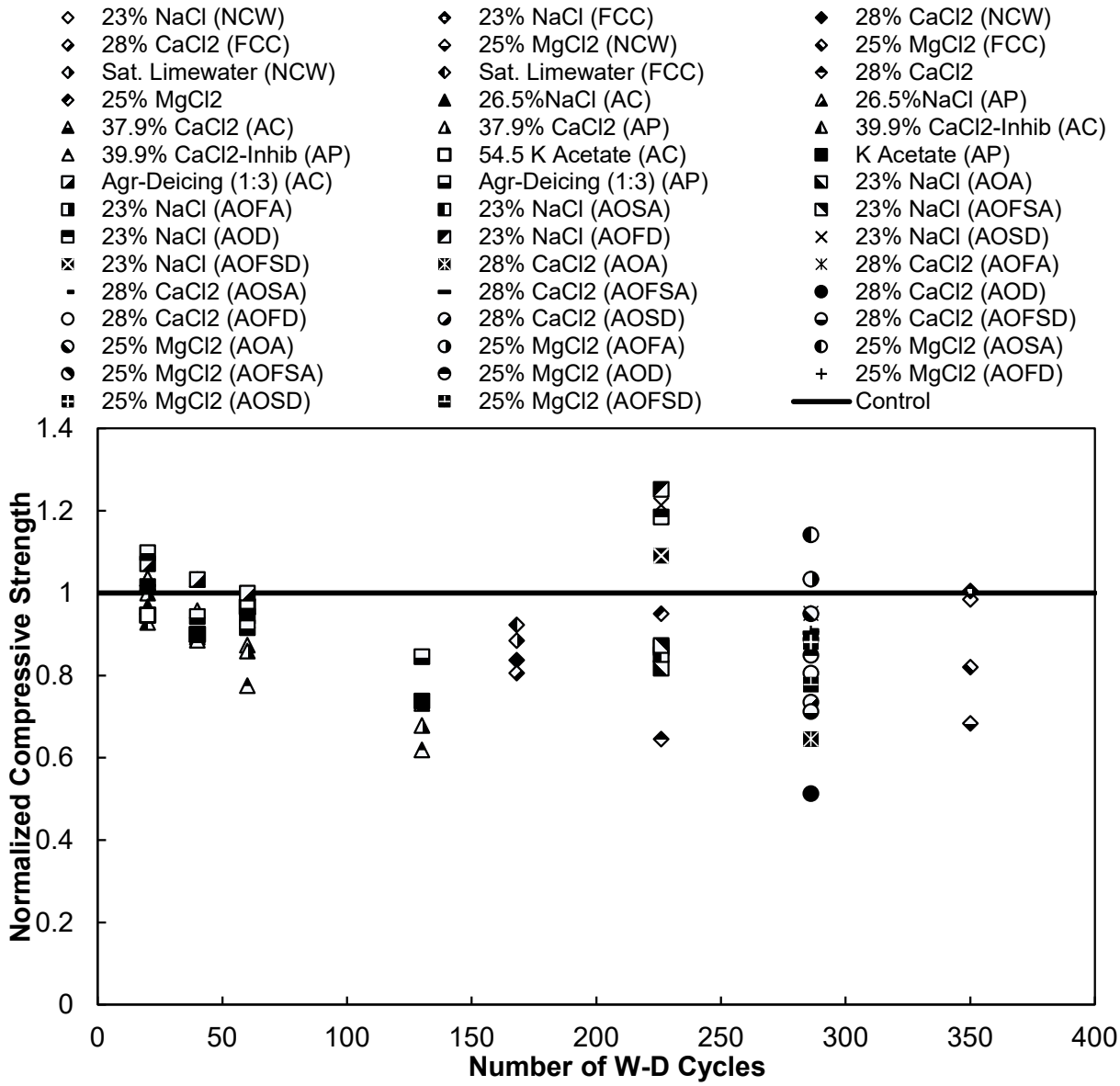

Figure 2-5: Concrete compressive strength trends observed under W-D cycles in deicing solution [37, 38, 59, 107, 110, 113].

Figure 2-5 illustrates the compressive strength trends observed in concrete when subjected to W-D cycles of different deicing chemicals. When compared to F-T exposure, relatively less variation in concrete compressive strength is observed in the case of W-D exposure cycles. Still, the majority of the deicing solutions are observed to decrease the compressive strength of concrete. Initially, NaCl showed no influence and even resulted in an improvement of up to 20% in compressive strength due to continuity of hydration process [37, 59, 96]. The comparative penetration of chloride ions is observed to be less in the case of NaCl [57]. However, the formation of chloroaluminate [70] and small precipitates of halite causes a reduction in the mechanical strength of concrete. The addition of fly ash as a partial replacement of cement marginally increased the compressive strength [96]. In contrast, the introduction of dolomite aggregate

resulted in up to 21% higher compressive strength in the presence of fly ash and slag, respectively. The reduction in compressive strength is observed to be more pronounced in the case of calcium chloride [37]. Initially, the strength reduction is minute but after two months of W-D cycles, the compressive strength decreased dramatically by up to 45%. It was found that $CaCl_2$ solution reacts with constituents of concrete to produce calcium aluminum chloride sulfate hydrate (Ca-Al-Cl-S hydrate). In addition, leaching of CH and ettringite exacerbate the deterioration process. The use of corrosion inhibitors in calcium chloride deicing solutions stabilizes the strength reduction during early W-D exposure cycles. The partial replacement of cement by fly ash or slag imparted better results. Similarly, magnesium chloride showed more stabilized behavior with simple improvement in concrete permeability, which results in substantial enhancement in compressive strength. In some cases, the addition of fly ash and slag increased strength by 3% and 14%, respectively [59]. Some of the researchers tried the saturated limewater that was found to be efficient only with fly ash concrete [96]. The potassium acetate exposure to concrete with air entrainment results in a minor reduction in compressive strength (5%) after 2 months of W-D cycles. Unlike chloride-based deicing solution, the potassium acetate has CH and no ettringite, but the economic factor hinders its application [37]. The agriculture-based deicing solutions lead to a relatively lower reduction in compressive strength which can be possibly attributed to limited penetration and absence of cement leaching [37].

Based on existing research, it can be inferred that in most of the cases, concrete gained compressive strength during early exposure periods irrespective of deicers and concrete mix used, due to cement hydration. However, the compressive strength is observed to decrease at higher W-D cycles. Among chloride-based deicers, NaCl showed a relatively lower reduction in compressive strength, whereas $CaCl_2$ and $MgCl_2$ lead to major deterioration in concrete compressive strength during W-D and F-T exposure cycles. Many of the studies indicated that $CaCl_2$ had the most detrimental effects on concrete, mainly due to the formation of calcium oxychloride. $MgCl_2$ also has some detrimental effects on concrete due to the formation of brucite and M-S-H.

2.4.3 Mass Change

Mass change is another sign of concrete deterioration, and many researchers used it as an indicator of deicer-induced concrete deterioration in their investigations. Peterson [53] in his experiments investigated the mass loss effect on concrete samples exposed to CMA solutions and observed that samples with higher w/c had more mass loss than the samples with lower w/c. It was further noticed that samples exposed to 20°C had more mass loss than the samples exposed to 5°C. Santagata et al. [72] found a similar pattern in the mass loss data as that observed in the case of compressive strength. The samples immersed in CMA solutions had mass gain for the first 3 months, which was followed by a significant mass loss. Wang et al. [37] observed that samples immersed in NaCl and water solution gained mass during the W-D period. For other deicers like $CaCl_2$, K-acetate, they found mass gain over the period which was attributed to the hydration of cement. Since a 7-day curing time was adopted, the cement hydration continued when the samples were immersed in deicer solutions, and it continued until the saturation period. The authors also assumed that the salt precipitation might be responsible for the mass gain on those samples whereas

mass loss was attributed to the peeling of materials from the surface and increased surface area due to the formation of cracks. Contrary to previous studies, a significant amount of mass loss was found for NaCl in the study conducted by Shi et al. [81]. Along with NaCl, K-acetate, Na-acetate also caused a significant amount of mass loss in concrete samples (up to 6%). The authors suggested that these deicing agents changed the chemical composition of the pore solution and created stress in the concrete. Also, Na^+ and K^+ cations increased the saltiness of the pore solution and increased the solubility of the cement hydrates. Moreover, only little mass gain/loss was observed in the case of CMA and $MgCl_2$. Cutler et al. [110] also found mass loss in the samples exposed to deicing solutions. The samples exposed to $CaCl_2$ experienced the highest mass loss while samples exposed to CMA had the least mass loss. Jain et al. [96] found mass gain in the samples exposed to W-D and F-T cycles immersed in NaCl and $MgCl_2$. The authors assumed that the mass gain was attributed to the concretion (compaction) of microstructure as well as water absorption in the microcracks. For $CaCl_2$, Type I samples had a mass loss, but cement mixed with fly ash gained mass during the W-D and F-T cycles. Ning et al. [107] found significant mass loss in the samples exposed to NaCl and KAc deicers compared to water. For NaCl exposure, the samples exhibited up to 6% loss in mass.

Figure 2-6 illustrates the mass change trends observed in concrete after exposure to F-T cycles in deicing solution. Initially, most of the data points lie near to the original mass but later on mostly drops due to the involvement of the scaling that causes the surface particles to break away and thereby induces a reduction in mass. As observed in Figure 2-6, for most of the deicing solutions, the mass loss/gain is around 2%. However, in some cases (for instance Salt A: 80% NaCl + 20% $CaCl_2$ and Salt B: 70% NaCl + 25% $MgCl_2$ + 5% $CaCl_2$), the increase in mass can be as high as 15%. When concrete specimens are subjected to $CaCl_2$ deicing solution F-T cycles, up to a 5% decrease in the mass can occur which is mainly attributed to scaling [37]. However, the inclusion of fly ash in concrete is observed to lead to mass gain because the deterioration is restricted to micro-level cracks that invite the water to penetrate [96]. No significant mass loss is noticed in the case of concrete samples that are subjected to $MgCl_2$ which is linked with the restriction of deicer ingress once a permeable layer of brucite ($Mg(OH)_2$) is formed [56]. Similarly, potassium acetate solution is observed to increase the mass because of mass gain due to water absorption and the creation of crystals [37]. In contrast, some studies found dilute potassium acetate may cause a small reduction in mass due to surface scaling [107]. Wu et al. [109] tried to investigate the combination of commonly used deicing chemicals at different concentrations and concretes of two different strengths. The combination of sodium chloride and calcium chloride showed a high level of mass loss at low concentration and a high number of F-T cycles, besides lowering the compressive strength of concrete (see Salt-A in Figure 2-6 and Figure 2-4). A similar trend was also observed when chlorides of sodium, magnesium, and calcium were mixed (Salt B). The severity was comparably low due to the involvement of magnesium chloride. The dilute salt solution may partially freeze at very low temperature therefore glue-spall theory involves and large thermal expansion coefficients difference between ice and concrete leads to tensile pressure and

subsequent scaling [49]. Similarly, high-strength concrete exhibited high resistance to the pressure created by crystals of salt and Friedel'salt [114].

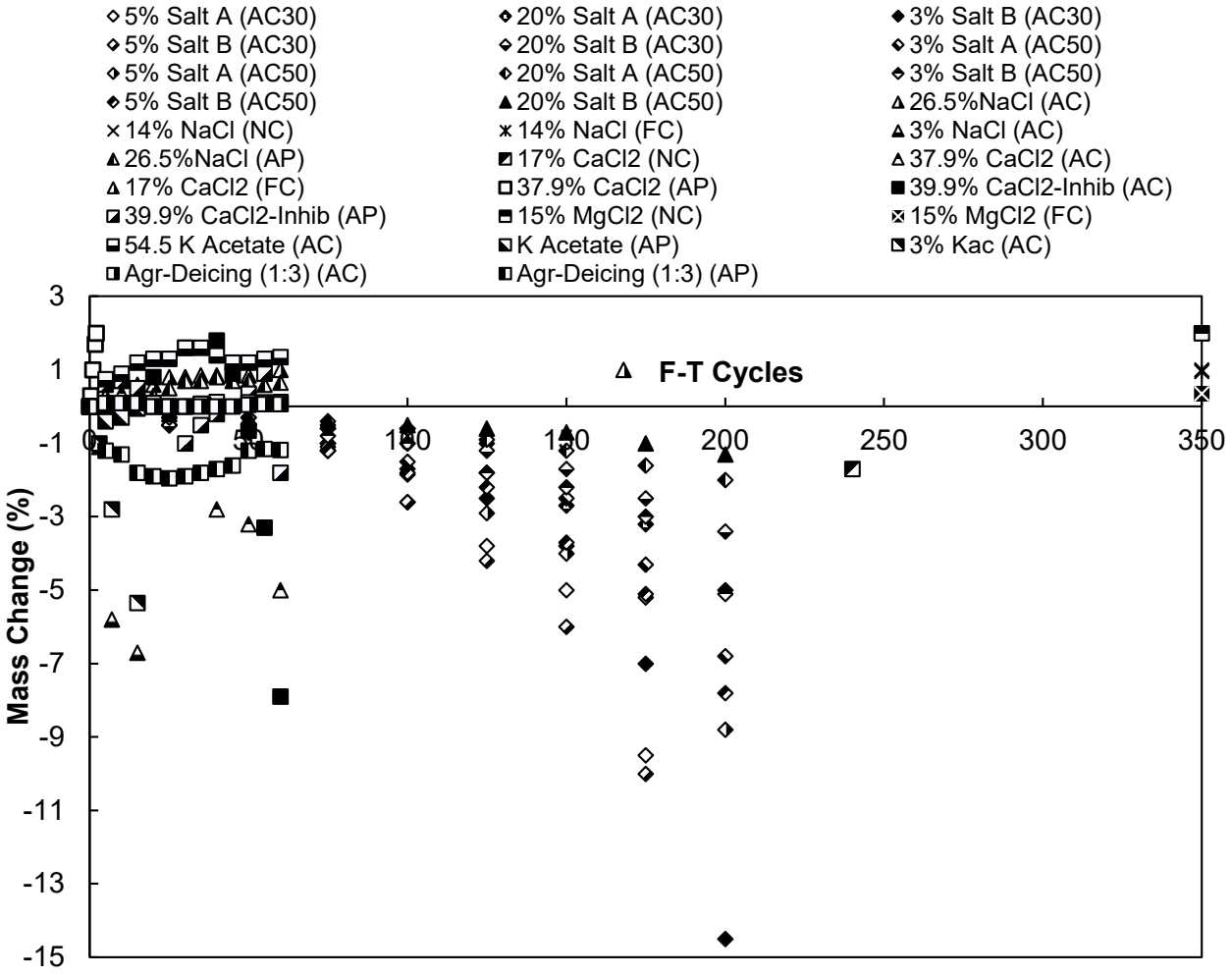

Figure 2-6: Mass variation with the increase in F-T cycles [37, 96, 107, 109].

Figure 2-7 summarizes the effect of the deicing solution on mass change in concrete under W-D cycles on concrete. Unlike F-T exposure cycles, limited studies were found that select the W-D cycles to check the effect of deicing chemicals on mass changes in concrete. When normal air-entrained concrete was exposed to NaCl deicer, its mass remained approximately constant [37]. Similarly, $CaCl_2$ also presented the same trend. The addition of corrosion inhibitor and fly ash was also found significant to reduce the concrete mass reduction [37]. Similarly, magnesium chloride also showed no reduction in mass due to limited scaling in W-D exposure. Finally, the agri-based deicing solution led to around a 2% mass change in concrete.

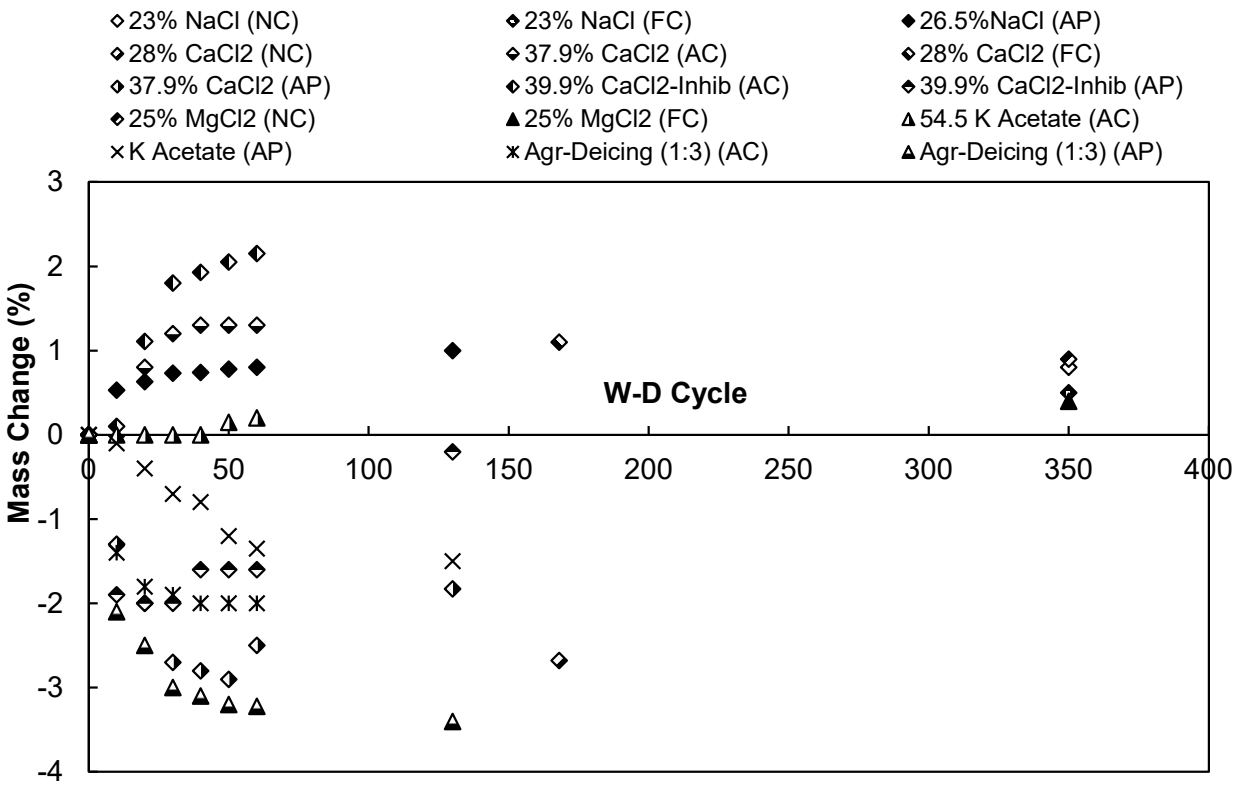

Figure 2-7: Mass variation with the increase in W-D cycles [37, 96, 107, 109].

From the existing studies, mixed results are observed for the mass loss. The samples exposed to NaCl had both mass loss and mass gain in several studies. This variation happened mainly because of the difference in the experimental setup and other factors. Salt crystallization and water absorption caused the samples to gain mass, while there could be other factors like solubility and sample handling that caused the mass loss. Without considering these, the samples seemed to gain mass during the immersion period. In most of the studies, the samples gained mass in the first few months for all the deicing solutions. For the deicers like $CaCl_2$, $MgCl_2$ the samples tend to lose mass after a certain period. This mainly happens due to the scaling and peeling of materials from the samples. From the existing studies, no clear conclusion can be reached for mass loss or mass gain. But both the mass loss and mass gain could have a negative impact on the concrete.

2.5 Literature Review Findings

The most important conclusions observed in the literature on the influence of the deicing chemicals on the properties of cement-based materials are summarized below.

1. It has been observed that the type of deicing solution, the concentration of the deicer, the type of concrete, and the handling of the experimental procedure are among the major factors that dictate the influence of deicing chemicals on the physical and chemical properties of concrete.

2. The chemical interaction of the deicing solution with cementitious hydration products leads to different products that result in physical deterioration in the form of scaling and loss of compressive strength.
3. The most studied deicing solutions were chlorides of sodium, calcium, and magnesium, and acetates of magnesium and calcium. Similarly, continuous soaking, W-D, and F-T cycles with modification were used to study the effect of the deicing solutions on concrete. Modifications were made mainly by varying the number and duration of the cycles of freezing or wetting or thawing or drying. It has been found that F-T cycles are truly representative and serve as an adequate methodology for obtaining representative conclusions. Initially, concrete behaves normally under the influence of deicing solutions but later starts deterioration due to ion penetration that chemically reacts with cement hydration products.
4. Scaling is observed to be the most common indication of deterioration in concrete. Scaling occurs either due to pressure exerted by precipitates like Friedel's salt and ettringite in the case of sodium chloride deicing solution or when the products are expansive, creating stresses in the pores of the concrete. For instance, the formation of calcium oxychloride due to the calcium chloride-based deicer. Similarly, the leaching of calcium ions due to the C-S-H structure and production of non-cementitious products like the M-S-H chain also contributes to structural degradation.
5. Among the commonly available deicing agents, magnesium chloride was found relatively better due to the formation of brucite ($Mg(OH)_2$) at the surface of the concrete that can control the chloride ion penetration. However, the application of $MgCl_2$ is linked with the formation of M-S-H that results in a deterioration in concrete compressive strength.
6. The Agricultural derived deicing formulations are observed to perform better, but further investigations about their long-term performance are needed.
7. The most common remedy for mitigating the deicers-induced deterioration in concrete is to alter the microstructure and porosity of concrete. The approach is to decrease the size and volume of voids in concrete and thus provide an obstacle to the penetration of detrimental deicing chemical ions. Researchers tried air entrainment, partial replacement of cement by a finer binding agent, and the use of different sources of aggregates. The air-entrainment and inclusion of fly ash or slag-type cement improved the freeze-thaw resistance of concrete, but the penetration of deleterious ions may still continue due to high porosity. Similarly, the ACBFS and dolomite type aggregates also enhanced the durability of concrete against the aggressive action of the deicing chemicals.

3 Effect of agro-derived corrosion inhibitors on the properties of Portland cement mortar

3.1 Introduction to influence of agri-derived deicers

A majority of corrosion inhibitors tend to decrease the compressive strength of concrete, whereas some corrosion inhibitors can increase the compressive strength of concrete, depending on their pore-blocking ability, chemical interaction with the cement hydration products, corrosion inhibitor dosage, age of concrete, mode of application (admixed or migrating), and type of cement. Therefore, when investigating the efficacy of new corrosion inhibitors, it is important to evaluate their impact on the strength and durability properties of concrete. Our previous study demonstrated the corrosion inhibition performance of three corn-derived polyol corrosion inhibitors, namely sorbitol, mannitol, and maltitol, in NaCl brine solution. A 0.5-3.0% wt. addition of these polyols in 23% wt. NaCl deicing solution reduced the corrosion rates by up to 92%. The addition of 1.0% wt. polyol in the NaCl deicer resulted in at least 80-85% reduction in corrosion rates. The polyol molecules acted as mixed corrosion inhibitors and protected the steel from corrosion via physisorption on the steel surface [76]. This chapter aims to evaluate the impact of these corn-derived polyol corrosion inhibitors on the properties of OPC-based mortar. Specifically, we aimed to investigate the effect of three types of polyol corrosion inhibitors, namely sorbitol, mannitol, and maltitol that are previously observed to considerably reduce the corrosivity of traditional NaCl deicer [76]. Important properties of OPC mortar specimens (such as scaling, mass change, compressive strength, and chemical composition) are determined when OPC mortar specimens are exposed to traditional NaCl deicing solution containing 1.0% wt. polyol corrosion inhibitors.

3.2 Experimental Procedure

This section discusses the preparation of OPC mortar specimens and deicing solutions that contain the optimum amount of polyol corrosion inhibitors. The deicer/corrosion inhibitor exposure tests and physical and chemical characterization tests that are conducted to track any physical or chemical deterioration in the Portland cement mortar specimens are discussed. Moreover, the changes observed in the compressive strength and mass of specimens as well as the scaling ratings of the specimens, are discussed in this section.

3.2.1 Test Specimens

For this study, Portland cement mortar specimens are prepared using ASTM specifications [115]. To this end, a total of 105 cement mortar cubes (specimen size: 5 × 5 × 5 cm) are prepared using Type I ordinary Portland cement and a water-cement ratio of 0.485. All test specimens are cured in water for 28 days before exposure to deicing solutions.

3.2.2 Corrosion Inhibitors Included Deicers Exposure Conditions

The field deicing solution exposure conditions are simulated by subjecting the cement mortar specimens to wetting-drying cycles. The specimens are exposed to the deicing solution with the optimal amount of corrosion inhibitors in the wetting cycle and are left indoors for the drying

cycle. To this end, four types of deicing solutions are prepared. Exposure to the distilled water in the wetting cycle is also studied herein for comparison purposes. Furthermore, 23% NaCl deicing solution without corrosion inhibitors is used as the reference deicing solution. The polyol-based deicing solutions are prepared by adding 1.0 wt.% polyol corrosion inhibitor (sorbitol or maltitol or mannitol) in the 23% NaCl deicing solution. The dosage of the corrosion inhibiting molecules in the NaCl-based deicing solution is adopted from our previous study [76], wherein 1.0 wt% of corrosion inhibitors is observed to be ideal corrosion inhibitor concentration for reducing the corrosivity of traditional NaCl deicing solution by up to 80-85%.

To simulate the exposure of the cement-based materials to the deicers, the cement mortar samples are subjected to wet-dry cycles for 90 days wherein cement mortar samples are completely immersed in the polyol-based deicing solution for 15±1 hours at 0 °C (wet period) and then dried for 9±1 hours at room temperature (25°C, dry period). As illustrated in Figure 3-1, each wet-dry (W-D) exposure cycle took approximately 24 hours to complete. The deicing solutions in the containers are changed after every 20 W-D exposure cycles.

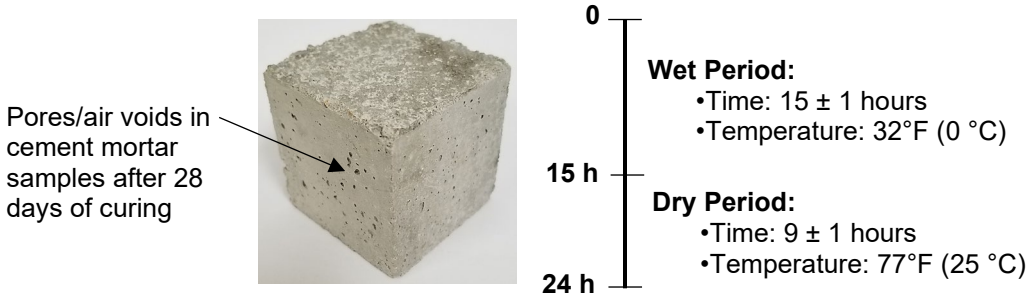

Figure 3-1: Experimental protocol for wet-dry exposure cycles and typical OPC mortar specimen after 28 days of curing.

3.2.3 Physical Characterization: Mass Change, Scaling, and Compressive Strength

Mass change, scaling, and compressive strength tests are conducted to determine the physical deterioration in the cement mortar specimens that are exposed to W-D cycles of deicing solutions in the absence and presence of polyol-based corrosion inhibitors. Cementitious materials may undergo mass gain or mass loss due to scaling damage or filling up micropores with dried deicer particles. The mass changes and surface scaling damage in the cement mortar specimens are recorded after every 10 W-D exposure cycles. For observing scaling damage and mass changes, test specimens are taken out of the deicing solution containers and placed at room temperature for 5 hours to achieve adequate drying. Based on visual observation, a scaling rating of 1-5 is assigned to the specimen based on the extent of surface scaling. The description of scaling rating is adopted from the literature (see Table 3-1) [37]. The compressive strength tests of deicer-exposed cement mortar specimens are conducted using ASTM C109 specifications [115]**.** The compressive strength is one of the most important durability indicators that is used to quantify the deicer and corrosion inhibitor-induced deterioration in cementitious materials. The experimental scheme with

information about the deicing solutions, exposure conditions, and the number of cycles after which each test is conducted are summarized in Table 3-1. The results obtained from scaling, mass change, and compressive strength tests for reference deicing solution, polyol corrosion inhibitor-based deicing solution, and tap water are discussed in Section 3.3.1, 3.3.2, and 3.3.3, respectively.

Table 3-1: Experimental scheme.

Deicing chemical	Exposure condition	No. of samples	Testing performed after following W-D cycles			
			Mass change	Scaling	Compressive strength	XRD, SEM, EDS analysis
NaCl NaCl + Sorbitol NaCl + Maltitol NaCl + Mannitol	Wet-Dry (W-D) cycles	3 per test per cycle	0, 10, 20, 30, 40, 50, 70, 90	0, 10, 20, 30, 40, 50, 70, 90	0, 15, 30, 45, 60, 90	0, 60

3.2.4 Chemical Characterization: XRD and SEM, and EDX Analysis

Three types of chemical/surface characterization tests are performed to determine the chemical composition of the products formed in the specimens as a result of cement hydration and exposure to deicing solutions in the absence and presence of small concentrations of polyol-based corrosion inhibitors. This includes X-ray diffraction (XRD), scanning electron microscopy (SEM), and energy-dispersive X-ray spectroscopy (EDX) analysis. XRD, SEM, and EDX analyses are conducted at the beginning of the study and after 60 W-D exposure cycles. For XRD analysis, a powder cement sample is extracted from the surface layer of the specimen. Bruker AXS' D8 Discover multipurpose X-Ray Diffractometer is employed for XRD tests. The XRD patterns of the cement mortar specimens are then obtained over a 2-theta range of 5-70° and generator settings of 40 kV and 30 mA. SEM and EDX analysis are conducted at a location of 1 cm from the surface of the specimens. The purpose of the SEM and EDX studies is to locate the presence of voids and microcracks in the specimens. Moreover, the EDX studies are aimed to identify the penetration of deicing salt ions near the surface of the specimens. The XRD analysis is conducted to determine the composition of any distinct compounds that are formed in cement mortar after exposure to the deicing solutions. The SEM micrographs and EDX spectra of cement mortar specimens are obtained using a JEOL JSM-6490LV scanning electron microscope. The results obtained from SEM, EDX, and XRD analysis are discussed in Section 3.3.4.

3.3 Results and Discussions

In this section, the physical and chemical deteriorations observed in the cement mortar specimens as a result of exposure to the traditional NaCl deicing solution in the absence and presence of the polyol corrosion inhibitors (sorbitol, maltitol, and mannitol) are discussed in terms of scaling damage, scaling ratings, mass loss or mass gain, compressive strength, and chemical changes. Moreover, the results obtained from this study are also compared with the results available in the literature for the most common deicers and corrosion inhibitors.

3.3.1 Scaling

Scaling can be defined as the superficial damage (flaking or peeling) of the top surface of the cementitious materials after exposure to deicing chemicals or freeze-thaw conditions [116]. Scaling is a commonly used indicator of deicer-induced deterioration in cement-based materials [36, 106, 116]. The surface scaling phenomena observed in the reference deicing solution (Sol-A: 23% wt. NaCl) and polyol-based deicing solutions (23% wt. NaCl + 1% wt. sorbitol: Sol-B, 23% wt. NaCl + 1% wt. maltitol: Sol-C, and 23% wt. NaCl + 1% wt. mannitol: Sol-D), for the 90 cycles exposure, are provided in Figure 3-2 and Figure 3-3, respectively. As observed in Figure 3-2, after 20 wet-dry exposure cycles, cement mortar specimens corresponding to all four types of deicing solutions exhibited a similar extent of surface scaling damage. In all specimens, small flakes are visible at the edges of the specimens. With further increase in the W-D exposure cycles, more flakes and buildup of deicer precipitates became visible at the surface and pores (see Figure 3-3). Moreover, the visual observation of specimens suggests that cement mortar specimens that are subjected to Sol-A and Sol-D suffered slightly greater scaling damage (both at the edges and interior surfaces) when compared to the cement mortar specimens that are Sol-B and Sol-C. The scaling damage observed in the specimens is typically observed in commonly used chloride-based deicing solutions (NaCl, $CalC_2$, and $MgCl_2$) in both W-D and Freeze-Thaw (F-T) exposure tests [37]. The scaling damage observed herein can be attributed to the excessive ingress of deicing solution into the cement mortar and subsequent accumulation, precipitation, and crystallization of deicing salts upon drying. These mechanisms are known to exert pressure and cause mechanical stresses within the cement mortar pores and thus cause scaling damage [114–116]. Furthermore, the chloride ions from the deicing solution can cause decalcification and form oxychloride crystals that can cause damage in the cement paste, particularly when a high concentration of NaCl (e.g., 23 wt.%) is used as a deicer [113, 114, 117, 118].

Based on visual observations of each specimen after different W-D exposure cycles, a visual scaling rating is assigned to the cement mortar specimens. The visual scaling rating of specimens ranges from 0 (no scaling) to 5 (severe scaling), and the description of each scaling rating, as adopted from Wang et al. [37], is summarized in Table 3-2. The visual observation-based scaling ratings of cement mortar specimens after exposure to the W-D exposure cycles of the salt brine deicing solution in the absence and presence of polyol corrosion inhibitors are provided in Figure 3-4. For comparison, Figure 3-4 also includes the scaling rating of cement mortar specimens that are exposed to W-D exposure cycles of tap water. Based on the visual observation of surface images of the cement mortar specimens after 20 wet-dry exposure cycles, all specimens are assigned a scaling rating of 1, which corresponds to slight scaling damage (see Figure 3-2 and Figure 3-4). At 40 W-D exposure cycles, the specimens exhibited a scaling rating of 2 (slight to moderate scaling), and beyond 45 W-D exposure cycles, the specimens are assigned a scaling rating of 2.5 or 3 (slight to moderate or moderate scaling). These results show that polyol-based deicing solutions cause slight to moderate and moderate scaling damage in cement-based materials and are no different from the scaling damage observed in the case of the specimens exposed to salt brine deicer without polyols. In essence, the addition of 1.0 wt.% polyol corrosion inhibitors does

not cause any additional scaling damage than that is observed in the specimens exposed to 23% wt. NaCl solution.

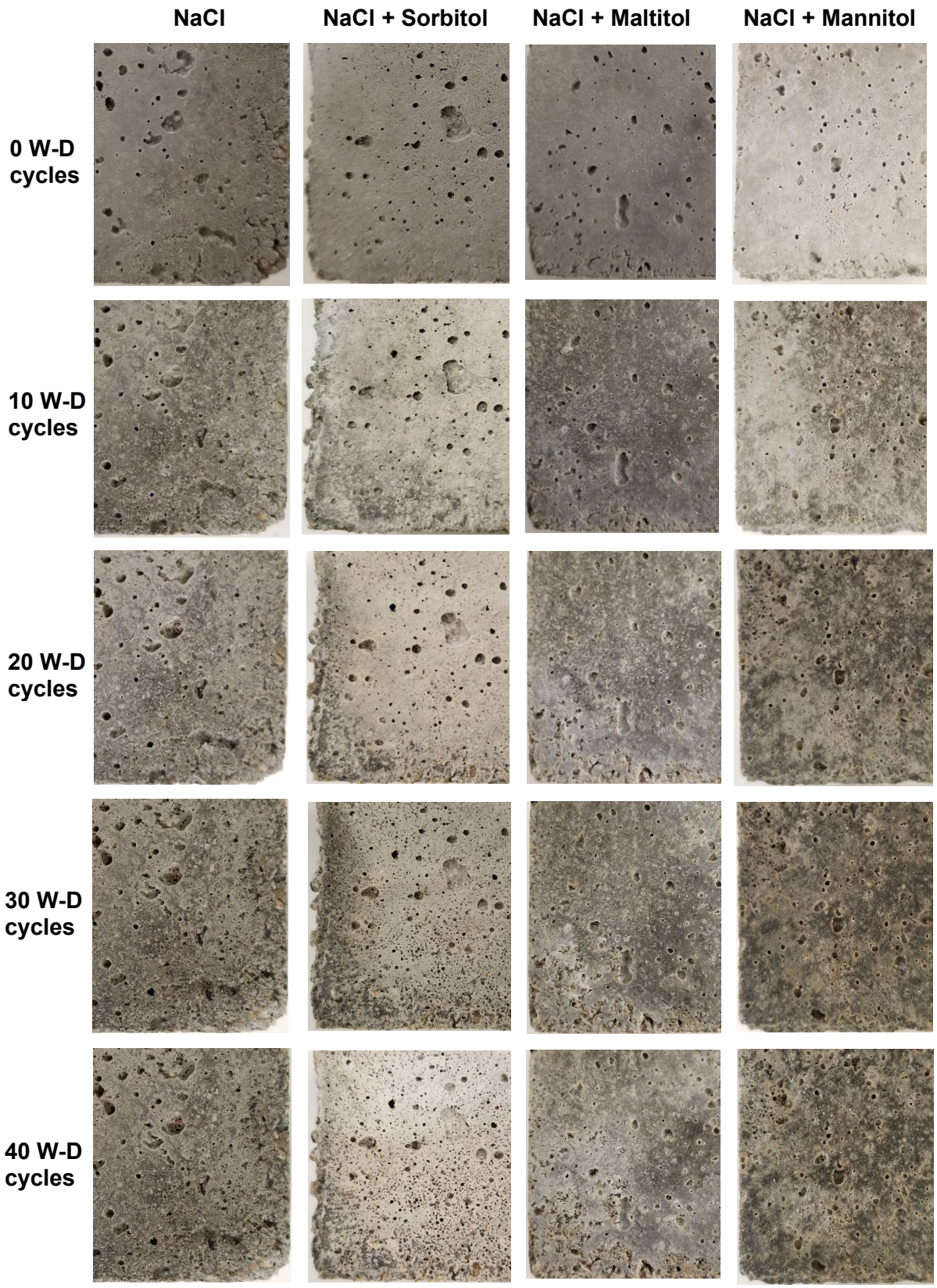

Figure 3-2: Visual appearance of cement mortar specimens after 0-40 W-D exposure cycles.

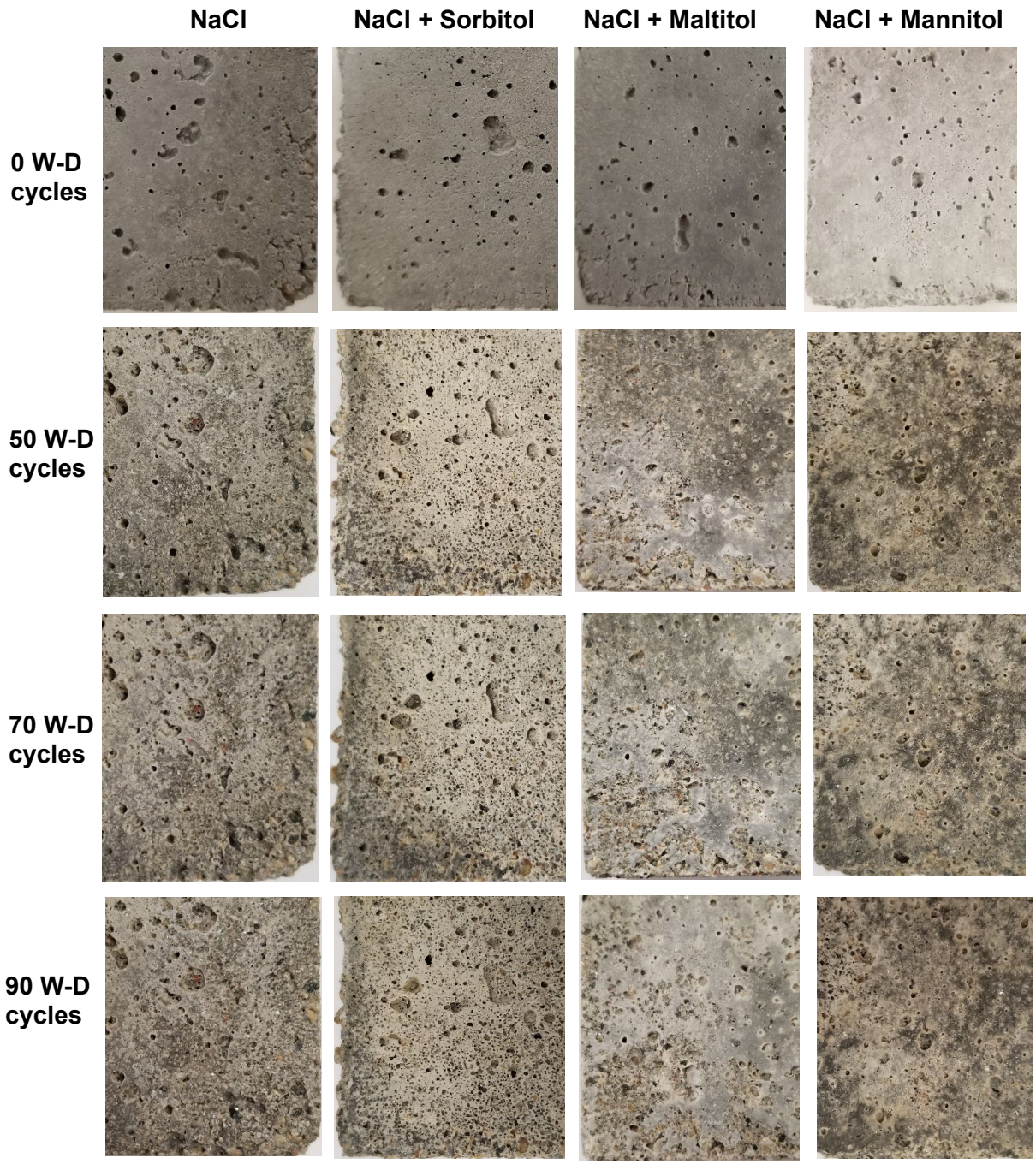

Figure 3-3: Visual appearance of cement mortar specimens after 0, 50-90 W-D exposure cycles.

Table 3-2. Description of the visual rating of scaling damage in cement mortar specimens.

Rating	Description
0	No scaling
1	Slight scaling (small flakes visible on sample surface)
2	Slight to moderate scaling (large flakes visible on the sample surface and sample edge damage noticeable)
3	Moderate scaling (sample edge damage and some fine aggregate visible)
4	Moderate to severe scaling
5	Severe scaling (chunks coming out of surfaces and edges, scaling depth > 0.3 cm, and fine aggregate visible over the entire surface)

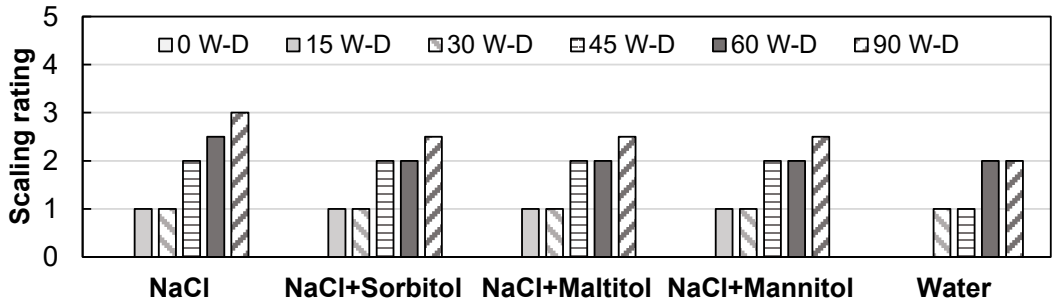

Figure 3-4: Visual observation-based scaling rating assigned to the OPC mortar specimens after exposure to W-D cycles of NaCl salt brine deicer with and without polyol corrosion inhibitors.

3.3.2 Mass Change

Mass change of specimens after exposure to a deicing solution is commonly used to characterize the deicer-induced damage in cement-based materials [37, 72]. The mass change indicates physical and chemical mechanisms that occur in cement mortar specimens after exposure to deicing solutions. An increase in the mass of cement mortar can be attributed to the continuous cement hydration, precipitation of deicing salts, and formation of micropores or increased surface area due to cracking available absorbing liquid or solid particles. Surface scaling can cause micro-cracks and increased surface area, which can lead to high retention of the deicers upon drying, and thus mass gain is observed. On the other hand, mass loss is usually indicative of breaking off of aggregates and cement hydration products from the surface, which is usually driven by the scaling-induced disintegration of particles on the surface. The mass change in specimens is determined after every 10 W-D exposure cycles, and the average mass change observed in the cement mortar specimens is plotted in Figure 3-5. The negative mass change denotes an increase in the mass, whereas the positive mass change indicates a mass loss in the cement mortar specimens. As observed in Figure 3-5, most of the specimens did not exhibit any considerable change in the mass when exposed to 30 W-D cycles, which can be attributed to the lesser extent of the scaling damage that was noticed in Figure 3-2. Further exposure to W-D cycles caused up to a 0.4% increase in

the mass of cement mortar specimens. This minor increase in the mass of cement mortar specimens can be attributed to the buildup of salt particles in the pore as well as an increase in the surface area of specimens due to microcracks formation at the surface. The increased surface area can retain more deicing solution and thus leads to mass gain [37]. The investigations conducted by Wang et al. [37] observed a similar mass gain in the case of W-D exposure tests for cement paste and concrete specimens. It is important to note that during the first 28 days of curing, the cement hydration also contributes to an increase in the mass. However, beyond 28 days, the contribution of cement hydration to mass gain can be expected to decrease, and hence that is the reason only a minor mass gain of 0.4% is observed in the current study as compared to other studies [37], and this mass gain can be primarily attributed to the precipitation of deicing salt and corrosion inhibitors. The mass change results suggest that polyol-based deicing solutions do not cause considerable change in the mass when applied to cementitious materials.

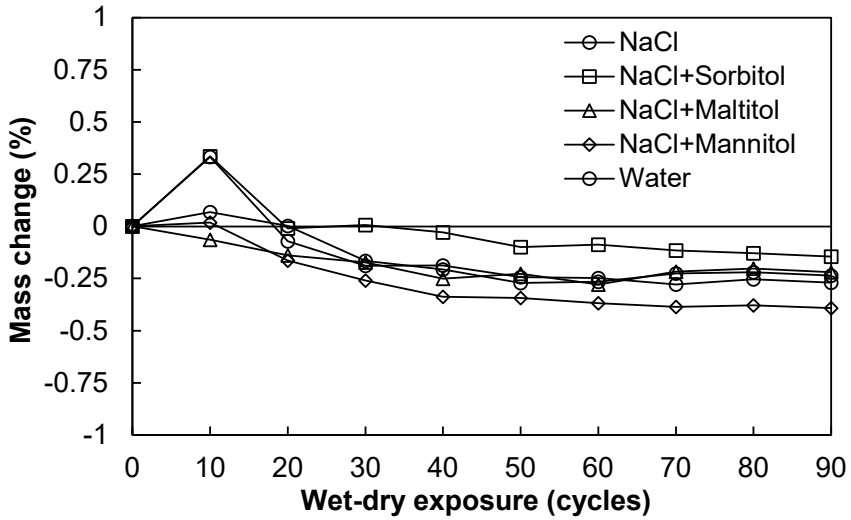

Figure 3-5: Mass change observed in the cement mortar specimens with respect to the number of W-D cycles of NaCl salt brine deicer with and without polyol corrosion inhibitors (note: negative mass change means mass gain).

3.3.3 Compressive Strength

The compressive strength of the cement mortar specimens can either decrease or increase, depending on the type of deicer and concentration of corrosion inhibitors. As discussed in Section 1, a higher concentration of corrosion inhibitors is linked with a reduction in the compressive strength of cementitious materials. It is also important to note that the deicing solution in itself can lead to a reduction in the compressive strength of cementitious materials due to the physical and chemical interactions between the deicing solution ions and cement hydration products. To elucidate the impact of polyol corrosion inhibitors, the compressive strengths of cement mortar specimens are determined after the 15^{th}, 30^{th}, 45^{th}, 60^{th}, and 90^{th} W-D exposure cycles using the procedure discussed in Section 2.3. The compressive strength results corresponding to the reference deicing solution, polyol-based deicing solution, and tap water after a specific number of W-D exposure cycles are provided in Figure 3-6. As observed in Figure 3-6, both reference cement

mortar specimens corresponding to NaCl deicer and cement mortar specimens that are subjected to polyol-based deicing solution exhibited almost similar compressive strength (65 MPa on average) after 15 W-D cycles. Beyond 15 W-D exposure cycles, the compressive strength of cement mortar specimens is observed to decrease until 60 W-D exposure cycles. The specimens that are subjected to NaCl brine deicer suffered approximately an 18% decrease in the compressive strength. On the other hand, most of the polyol-based deicing solutions experienced approximately a 10% decrease in compressive strength. Interestingly, at 90 W-D exposure cycles, most polyol-based deicing solutions are observed to regain their original strength (compressive strength observed at the onset of W-D exposure tests). The smaller decrease in the compressive strength of cement mortar in the case of polyol-based deicing solutions can be attributed to the smaller chloride penetration into the specimens due to the pore-blocking ability of agro-based deicers that was also observed in a previous study [37]. These results show that polyol-based deicing solutions cause either the same or relatively smaller decrease in compressive strength of cement-based materials when compared to the traditional salt brine deicers.

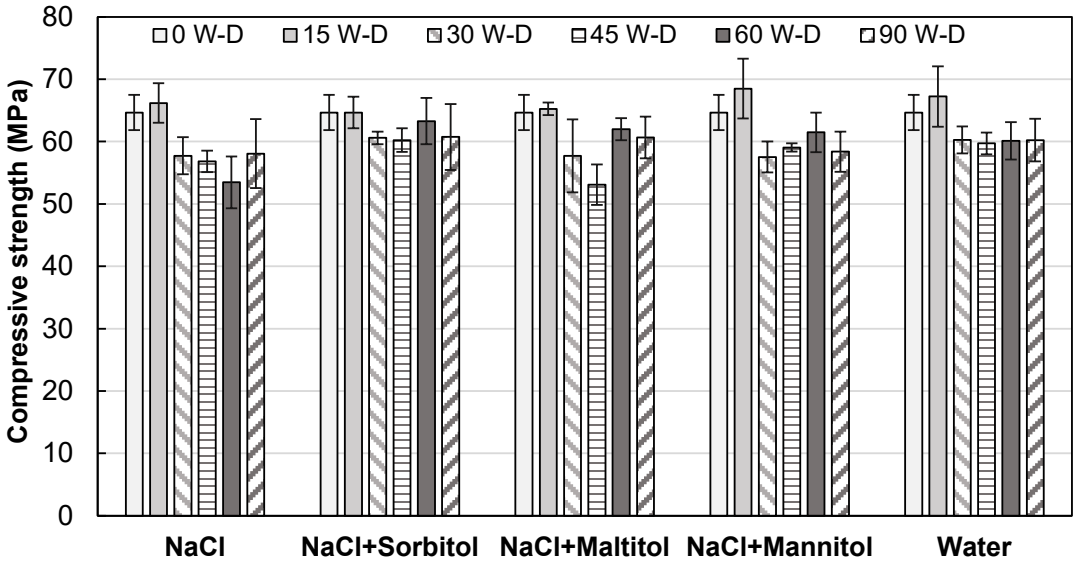

Figure 3-6: Compressive strength of cement mortar after exposure to W-D exposure cycles of NaCl salt brine deicer with and without polyol corrosion inhibitors.

3.3.4 Chemical Characterization: XRD, SEM, and EDX Analysis

Chemical composition analysis and morphological evaluation techniques are employed to evaluate the formation of any new products and cement hydration products when cement mortar specimens are subjected to W-D exposure cycles of salt brine deicing solution in the absence and presence of polyol corrosion inhibitors. Specifically, three types of chemical and surface characterization tests are conducted that include XRD analysis, determination of SEM micrographs, and EDX spectra. The sample preparation and testing procedure of each of these tests are discussed in Section 2.4. XRD analysis is conducted to assess the formation of any distinct chemical phases in the specimens after exposure to deicers W-D exposure cycles. XRD analysis is conducted at the beginning of the study (labeled as "No deicer exposure") and after 60 W-D

exposure cycles for both cement mortar specimens corresponding to both reference and polyol-based deicing solutions. The XRD spectra of cement mortar specimens are provided in Figure 3-7. As observed in Figure 3-7, the XRD spectra of test specimens show the presence of quartz, calcite, and hydration products such as calcium hydroxide and C-S-H that are typically observed in the OPC mortar that is exposed to NaCl-based deicing solution [37, 84, 119–121]. In all the spectra, the intensity of quartz dominated the other compounds which can be linked with the relatively low penetration of NaCl deicer [37]. The presence of NaCl in cement mortar specimens can be attributed to the precipitation of the deicing solution in the voids. In the case of a polyol-based deicing solution, hydrated forms of sorbitol, mannitol, or maltitol are observed in the corresponding solutions in addition to the products that are observed in the reference NaCl only deicing solution. However, no new product formation or leaching of calcium is observed in the spectra, which suggests that the lack of chemical interaction between the polyol hydrates and cement hydration products, and hence they do not have a negative impact on cement paste. Consequently, on slight to moderate scaling damage and relatively lesser deterioration in the compressive strength in the cement mortar specimens that are subjected to polyol-based deicers.

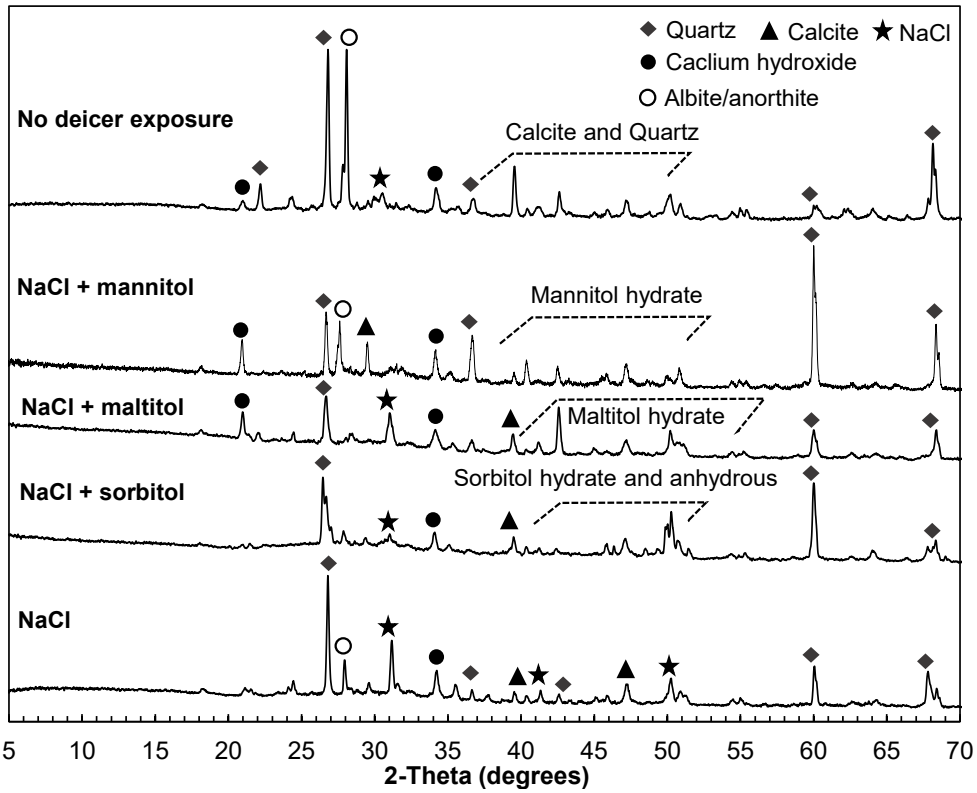

Figure 3-7: XRD spectra of cement mortar specimens after exposure to 60 W-D cycles of NaCl deicing solution in the absence and presence of polyol corrosion inhibitors.

To further assess the formation of any microcracks, micropores, or any new products, SEM micrographs are obtained for the cement mortar specimens after 60 W-D exposure cycles of the salt deicing solution and polyol corrosion inhibitor based deicing solutions using the procedure specified in Section 2.4. Moreover, the corresponding EDX spectra are also obtained to assess the

elemental composition of the morphology observed in the SEM micrographs. The SEM micrographs and EDX spectra of test specimens obtained after 60 W-D cycles are provided in Figure 3-8 and Figure 3-10, respectively. Moreover, the SEM micrograph and XRD spectra of cement mortar specimens after exposure to 60 W-D cycles of tap water are also obtained and are provided in Figure 3-9 for comparison purposes. As observed in Figure 3-8, the SEM micrographs of the cement mortar specimens corresponding to the reference deicing solution exhibit the formation of cracks in the cement matrix as well as some pores. Some precipitation of the deicing salts can also be noticed in the micrographs. The SEM micrographs of the cement mortar specimens that are subjected to 60 W-D exposure cycles of the NaCl deicer containing polyol corrosion inhibitors exhibited similar formation of cracks and pores. However, the extent of cracks and pores is observed to be relatively lower when compared to the cement mortar specimens that are exposed to the reference salt brine deicing solution. The EDX spectra of specific points in these micrographs are further obtained and presented in Figure 3-10. It can be noticed that in most cases, the EDX spectra show high peaks corresponding to calcium and oxygen, which represent the cement hydration products. Similarly, the spots in the vicinity of the cracks showed peaks of Na and Cl elements which points towards the presence of the deicing salts precipitates, an observation consistent with the XRD spectra (see Figure 3-7). On the other hand, the EDX spectra obtained in the case of specimens that are exposed to tap water exhibited the formation of typical hydration products (see Figure 3-9), whereas microcracks are also observed in the SEM micrograph corresponding to the tap water specimen. However, no deposits or products are observed along the crack. The microcracks observed in the SEM micrographs could result from 1) the formation of expansive oxychloride products due to the penetration of chloride ions and precipitation/crystallization of deicing salt or polyols. Such microcracks can also be triggered by the preparation of specimens for SEM analysis due to the brittleness of the cement matrix. Moreover, cracks of similar nature were also observed in a recent study by Cheng et al. [122], wherein OPC cement mortar specimens were subjected to wetting and drying exposure cycles of multiple corrosive ions, including NaCl. Overall, relatively the specimens that are subjected to NaCl deicer exhibited similar morphology and similar elemental composition regardless of the presence of polyol corrosion inhibitors.

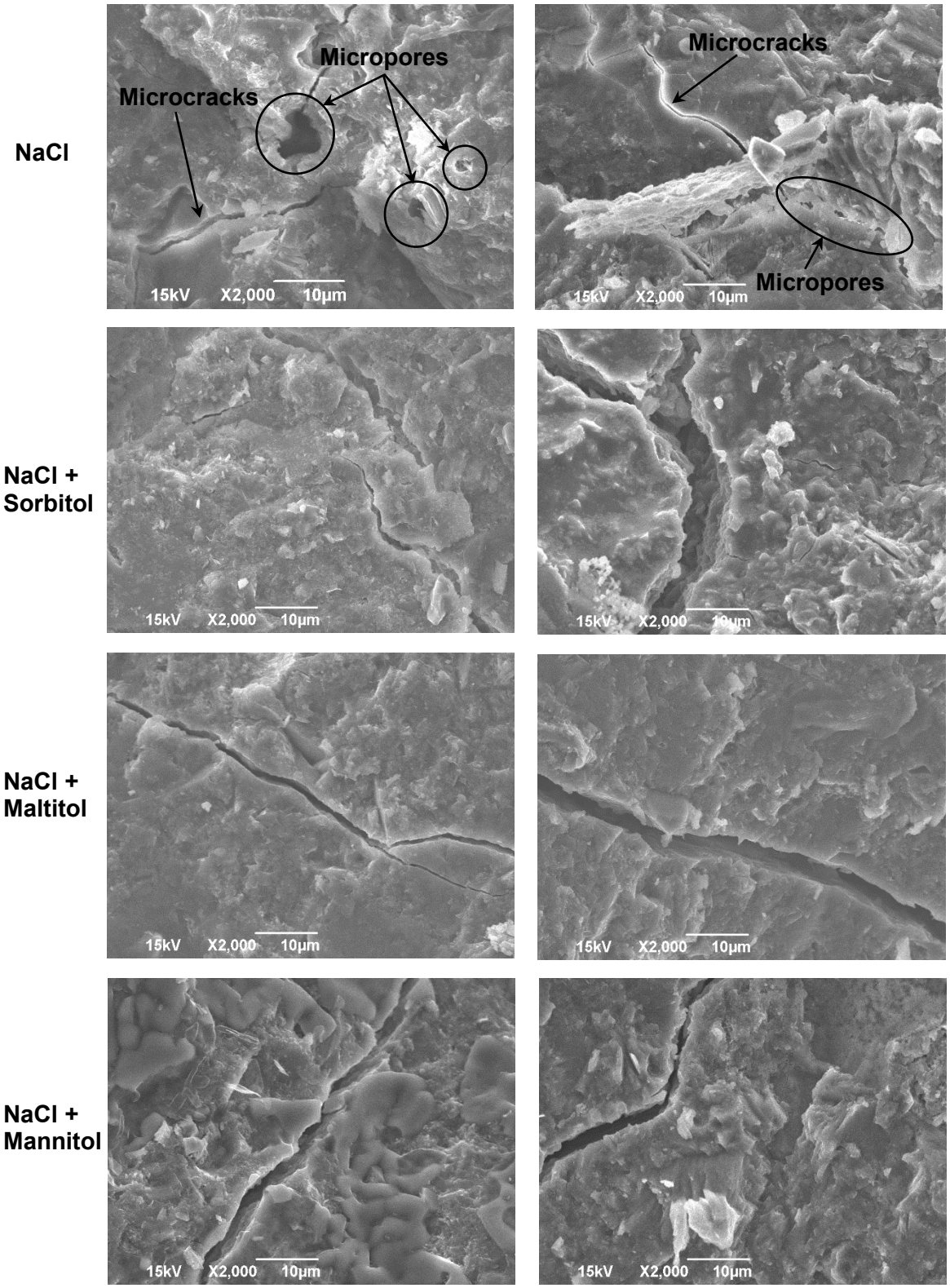

Figure 3-8: SEM micrographs of cement mortar specimens after exposure to 60 W-D cycles of NaCl deicing solution in the absence and presence of polyol corrosion inhibitors.

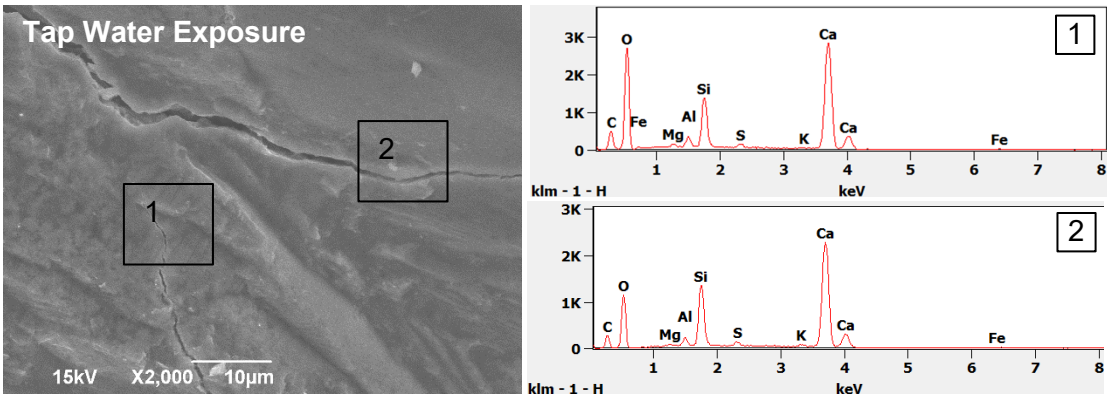

Figure 3-9: SEM micrograph and EDX spectra of cement mortar specimens after exposure to 60 W-D cycles of tap water.

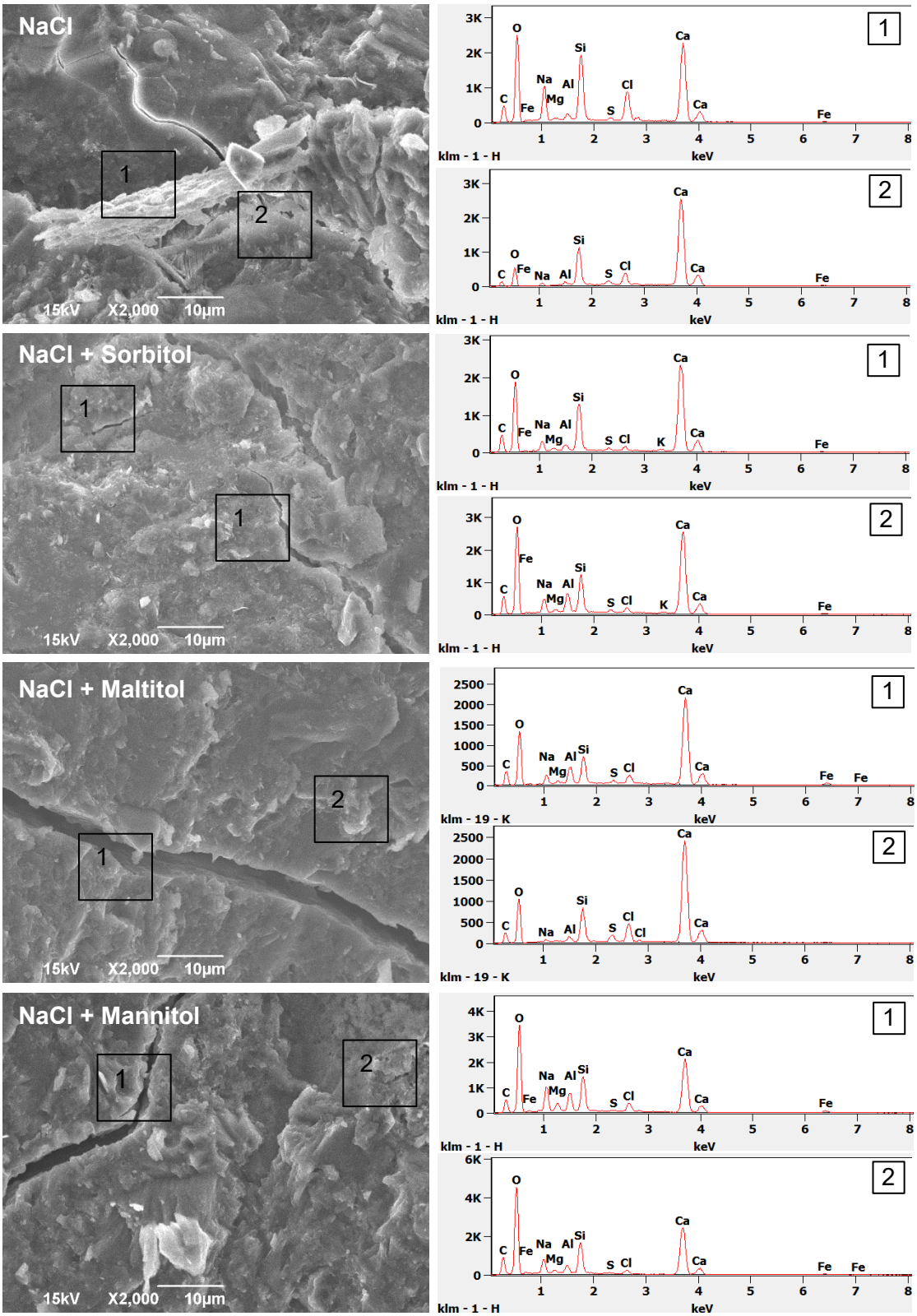

Figure 3-10: EDX spectra of cement mortar specimens after exposure to 60 W-D cycles of NaCl deicing solution in the absence and presence of polyol corrosion inhibitors.

3.4 Performance Comparison with the Literature and Discussion

The percentage decrease in the compressive strength of cement mortar specimens obtained in this study (60 W-D cycles) is compared with the percent decrease in the compressive strength of cement mortar or concrete specimens that are reported in the literature for different types of corrosion inhibitors and agro-based deicers. The results of this study and those obtained from the literature are provided in Figure 11. A comparison of compressive strengths revealed that for most corrosion inhibitors, the compressive strength of OPC materials decreases by 10-16% whereas, for some corrosion inhibitors, the compressive strength can decrease as high as 39%. It is also observed that surface-applied deicing solutions containing corrosion inhibitors and migrating corrosion inhibitors result in lesser deterioration in concrete compressive strength as compared to admixed corrosion inhibitors. The polyol corrosion inhibitors investigated herein resulted in less than 10% reduction in compressive strength of cement mortar and thus perform relatively better when compared to many commonly used admixed corrosion inhibitors in concrete.

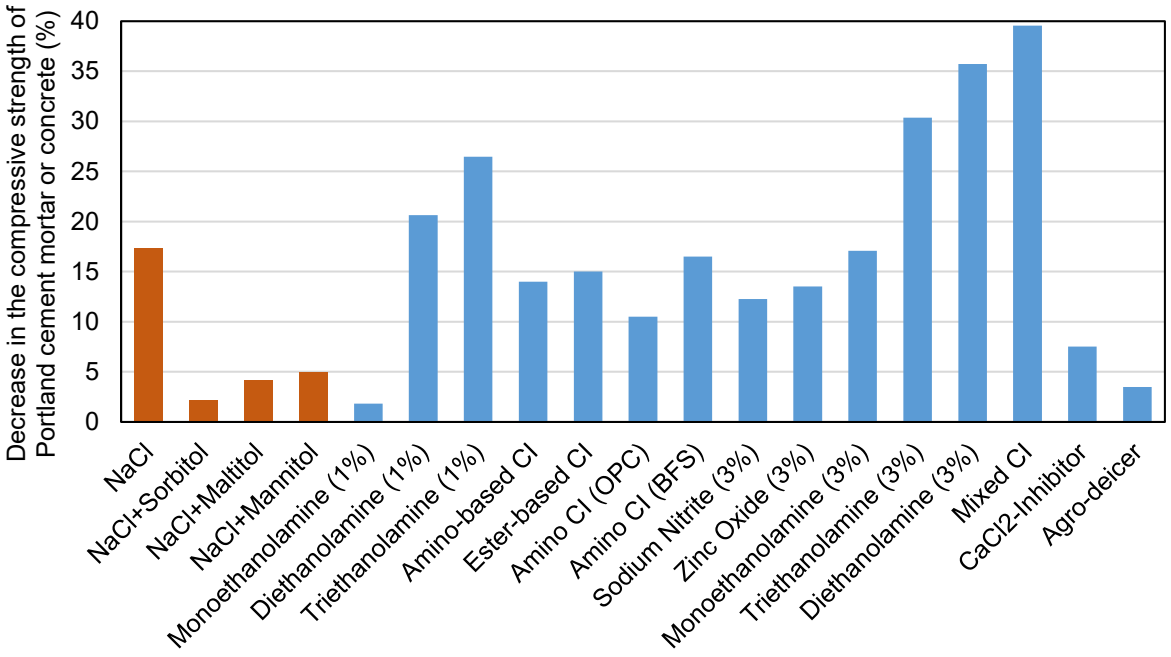

Figure 3-11: A comparison of compressive strength deterioration of cement mortar and concrete caused by different corrosion inhibitors and deicers.

The mass changes and scaling damage results are not widely reported for many corrosion inhibitors. However, for common deicers, mass change and scaling damage results are available. Previous studies conducted on NaCl and $CaCl_2$ deicers, as well as CaCl2 deicers with corrosion inhibitors, also resulted in slight to moderate scaling damage (i.e., scaling rating of 2 to 3) in the case of W-D exposure cycles in cement paste and concrete [37]. Similarly, the mass change was less than 1% for the specimens beyond 28 days of W-D cycles. To summarize, the polyol corrosion inhibitors do not cause further deterioration in the properties of cement-based materials and have

a relatively less negative impact on the compressive strength (see Figure 3-11) and other durability properties of cement mortar and cement concrete when compared to other corrosion inhibitors.

4 Soy-protein and Corn-derived Polyol based Coatings for Corrosion Mitigation in Reinforced Concrete

4.1 Introduction to Rebar Coatings

To mitigate corrosion and its deleterious effects in RC structures, different prevention strategies are employed. The corrosion prevention measures in RC structures are guided by two basic principles: (1) prevent the reaction between the chloride ions and steel rebar by forming a barrier between the chloride ions and steel surface, and (2) prolong the time needed for the chloride ions to penetrate the concrete and thus delay the initiation of corrosion reaction in the embedded rebars. The most common corrosion prevention measures in the RC industry include the use of coatings [122–126] (e.g. epoxy coatings, galvanizing, copper cladding, etc.), surface treatment [127–129] (e.g. sandblasting, water immersion, etc.), corrosion-inhibitor based deicers [76, 80, 130–133] (e.g. agro-based deicers), admixed and migratory corrosion inhibitors for concrete [16–22, 134] (e.g. nitrites, amines, alkanolamines, and propriety blends, etc.), cathodic protection [44, 134, 135], corrosion-resistant rebars [137–139], and using concrete with supplementary cementitious materials [9, 137] (e.g. silica fume, fly ash, and blast furnace slag, etc.). Among these corrosion prevention techniques, the coatings for rebars and the use of corrosion inhibitors are among the popular techniques in RC structures due to their effectiveness and ease of usage.

The rebar coating industry currently uses four types of coating technologies that are recognized by ASTM International and the Concrete Reinforcing Steel Institute (CRSI). These include epoxy-coated rebars (ASTM A775, A884, A934) rebars, galvanized rebars (ASTM A767), dual-coated (ASTM A1055), and vinyl-coated (ASTM A933) [123] rebars. Among these coatings, epoxy-coating is the most widely used coating in North America. Approximately 10% of all reinforcing bars in North America are estimated to be coated. As per the 2011 National Bridge Inventory, more than 74,097 bridge decks in the U.S. have epoxy-coated rebars. Epoxy-coated rebars commonly employ fusion-bonded epoxy (FBE) coating. The epoxy coatings provide a barrier system that insulates the steel rebars from the chloride ions and water molecules and thus ensures a significant delay in the initiation of corrosion in rebars. The FBE coatings are linked with the improved corrosion resistance of steel rebars and lead to an overall delayed initiation of corrosion in rebars [62, 122, 126] as observed in many field observations of bridges. Despite their largely satisfactory performance, there have been instances of premature corrosion in the FBE coated rebars in bridges as early as 7 years after construction [62, 122, 126]. The premature corrosion in epoxy-coated rebars is commonly attributed to the defects in the coating that occur during fabrication, handling, and transportation of rebars, and vibration during concreting. The presence of defects and their ability to trigger localized corrosion and subsequent pitting is one of the main disadvantages of the epoxy coatings apart from their additional development requirement for rebars in concrete. Rebar epoxy coatings (such as FBE) are made of constituents that are declared carcinogenic by environmental protection agencies and such types of coatings are being banned in many countries. To prevent the early defects in the epoxy coating rebars, different researchers have investigated the performance of the epoxy coatings that are modified with

different nano and micro materials such as graphene [140], carbon nanotubes [141], silica [12], and nano clay [46]. While these modifications improved corrosion resistance and integrity of the epoxy coatings, the high cost of the modified epoxy coatings remains a barrier for their large-scale commercial usage. Moreover, the toxicity and environmental concerns of the modified epoxy coatings remain a concern. In this regard, coatings synthesized from plant-based materials present an effective and sustainable solution to overcome the problems associated with epoxy coatings. While many plant-derived materials have been investigated for their corrosion inhibition performance in corrosive media [46], only a few studies have explored the potential of plant-derived materials in the preparation of bio-based coatings for steels [141–143]. Although plant extracts-based coatings exhibited promising anticorrosion performance, their large-scale availability remains a major barrier in their application in infrastructure. For successful implementation of a bio-based coating in infrastructural applications, the basic raw material needs to be abundantly available, and they must exhibit desirable anticorrosion performance. In this regard, soybean, an abundantly available agricultural commodity in the U.S., presents an attractive alternative for preparing bio-based coatings. Soy-based products (specifically, the products derived from soybean oil) have shown promising corrosion inhibition in the recently conducted investigations. Moreover, soy protein has excellent adhesion properties and have been used as a wood adhesive by partially or fully replacing the formaldehyde-based wood adhesives [144, 145]. This chapter focused on investigating the corrosion protection of soy protein-based coatings. Specifically, soy protein coatings are synthesized from the soy protein isolate, the protein-rich component of the soybean. The objective of this chapter is the synthesize and characterize the physical and chemical properties, and corrosion prevention performance of the soy protein coatings that can be used for in-situ application in old RC structures to fix the damaged epoxy coated rebars and thus protect the rebars from corrosion. The detailed experimental procedure and the characterization techniques employed for understanding the chemical and physical characteristics and corrosion prevention performance of the proposed soy protein coatings are discussed in the subsequent sections.

4.2 Experimental Procedure

This section describes the synthesis process of soy protein coatings and the experimental techniques that are employed for characterizing the physical and chemical characteristics of the soy protein coatings. This section further describes the corrosion performance evaluation of the soy protein coatings.

4.2.1 Soy Protein Isolate

Soy protein isolate is obtained from a commercial supplier and has 90% protein content as per the supplier-provided product sheet. SPI is a mixture of different proteins that are categorized into four protein classes based on their sedimentation coefficients: a) 2S (polypeptides), b) 7S (β-conglycinin), c) 11S (glycinin), and d) 15S (dimer of glycinin) [144, 145]. Among these categories, 7S (β-conglycinin) and 11S (glycinin) constitute 35% and 52% of the SPI protein content, respectively [145, 146]. Thus, together these protein categories account for more than 80 wt% of

SPI protein. 7S and 11S components are further composed of about 20 different amino acids combinations each of which has functional groups such as -OH, -COOH, etc., attached to the polypeptide chains of the protein molecule. Unfolding protein chains and exposing these functional groups via chemical modification dictate the mechanical and chemical properties of the SPI-based coatings.

4.2.2 Synthesis of Soy-Based Coatings

Soy protein coatings are prepared by using soy protein isolate (SPI, the protein-rich component of soybean with 90% protein content) as a base material and food-grade sorbitol as a plasticizing agent. Both the ingredients are obtained from a commercial supplier. Additionally, 1N NaOH solution is prepared for denaturing the SPI mixture. The SPI concentrations in the soy protein coating formulations ranged from 5% to 15% (%wt. of deionized water). Moreover, each soy protein coating formulation further included 10%, 20%, or 30% of sorbitol (%wt. of SPI). Generally, protein-based films and coatings are brittle and the addition of plasticizers becomes necessary to impart reasonable ductility to the film/coating. To this end, additives with hydrophilic groups (e.g., glycol, sorbitol, etc.) are commonly used as plasticizers in edible coatings [147, 148]. Polyol plasticizers (e.g. Sorbitol) have the ability to reduce the intermolecular bonding (internal hydrogen bonding) between the protein chains due to their highly hydrophilic character [149, 150]. In essence, they interject themselves between the protein chains and thus disrupt and reduce the forces that hold the chains together and increase the intermolecular spacing [149]. In this study, sorbitol is used as a plasticizer as it is agro-derived and effective plasticizer. Sorbitol is primarily derved from corn and it has successfully been used as a plasticizer, corrosion inhibitor, and salt brine freezing point depressant in the recent past [76, 79, 132]. The sorbitol plasticizer is limited to 30% (%wt. of SPI) as a higher plasticizer content may increase the permeability and decrease the mechanical strength of the resulting SPI coatings.

Soy protein coatings are prepared by mixing SPI in deionized water and stirring for 10 minutes to achieve uniform dispersion of soy protein in water. Sorbitol plasticizer is then added to the aqueous soy protein mixture in varying concentrations (10%, 20%, 30% wt. of soy protein isolate) and stirred for further 20 minutes. The pH level of the resulting soy protein mixture is then adjusted to 12 by adding 1N NaOH solution to achieve denaturing of soy protein. Denaturing helps unfold the protein chains and expose the functional groups that can lead to improved adhesion and higher water resistance (improved barrier properties) [145, 151]. The soy protein mixture with adjusted pH level is then placed on an orbital shaker set at 210 rpm and 45 °C for 4 hours. The high-temperature treatment can aid the denaturing process. The coatings are cured at a temperature of 40 °C for 48 hours. The resulting soy protein coating material is stored at 5 °C before application on rebars. The soy protein coating synthesis process is depicted in Figure 4-1. In total, 12 soy protein coating formulations are prepared by employing 5%, 10%, and 15% SPI (wt% of deionized water) and for each weight percentage of SPI four weight percentages of plasticizer are used (0%, 10%, 20%, 30% Sorbitol (wt% of SPI)). The synthesized coatings are labeled as S-#-*-$ where S refers to Soy Protein, # refers to wt.% of SPI isolate in deionized water, * refers to the pH level (alkalinity) of the soy protein suspension, and $ denotes the sorbitol weight in the mixture as a

weight percent of SPI. For instance, specimen S-5-12-20 has 5% SPI, a pH level of 12, and 20% wt. (% SPI) of sorbitol.

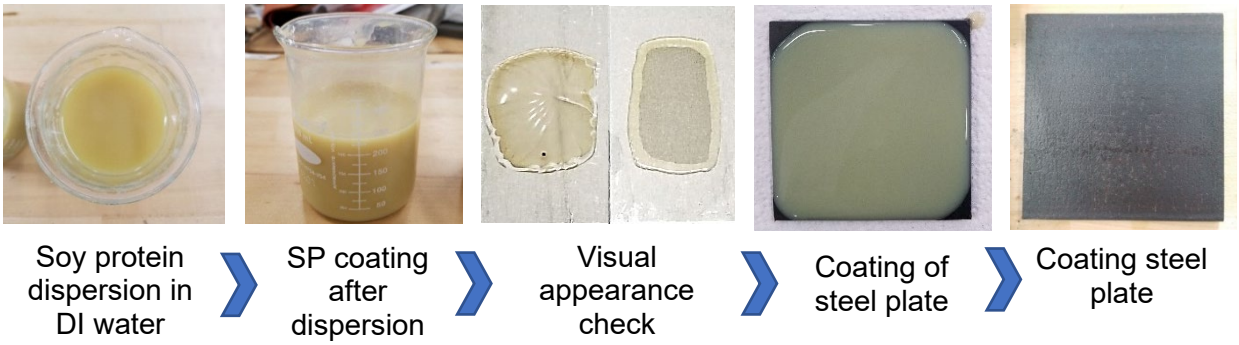

Figure 4-1: Typical workflow for each soy protein coating formulation trial.

4.2.3 Physical and Chemical Characterization Tests

Physical and chemical characteristics of each class of soy protein coatings are determined by conducting visual brittleness tests, viscosity tests, abrasion resistance tests, and Fourier Transform Infrared (FTIR) spectroscopy. The visual brittleness tests are conducted to evaluate the apparent brittleness or ductility of the cured soy protein coatings. For this purpose, soy protein coatings are applied on steel plates and are kept at 30°C for 48 hours for drying. The surface of the dried coating is then visually monitored for determining the apparent brittleness of the cured soy protein coatings. For determining the abrasion resistance of the cured coatings, abrasion resistance tests are conducted using Falling Sand Abrasion Tester using the procedure specified in ASTM D968 [152]. The Falling Sand Abrasion Tester is shown in Figure 4-2. For determining the abrasion resistance of the soy protein coatings, soy protein-coated steel panels are subjected to silica abradants from an 8-inch diameter sand reservoir via a guide tube. The soy protein-coated steel panels are placed at 45°. Silica particles are continuously pinged on the coated steel panel until 4-mm diameter of the substrate becomes visible as the coating worn off the steel substrate. The viscosity tests are performed to determine the consistency and workability of the soy protein coatings containing varying amounts of SPI and Sorbitol plasticizer. The viscosities of soy protein coatings are determined using HAAKE Viscotester® 550. HAAKE viscotester® 500 consists of a standard cylindrical spindle and the data acquisition (DAQ) system that measures and records the shear stress and shear rate of a given fluid (see Figure 4-3). The detailed procedure for viscosity determination can be found elsewhere [78]. Finally, the chemical bonds and functional groups that are present in the cured soy protein coatings are determined using FTIR tests. The FTIR spectra of each coating formulation are determined using Thermo Scientific Nicolet 8700 Fourier Transform Infrared Spectrometer. A spectral range of 4000-600 cm^{-1} is adopted in the FTIR tests.

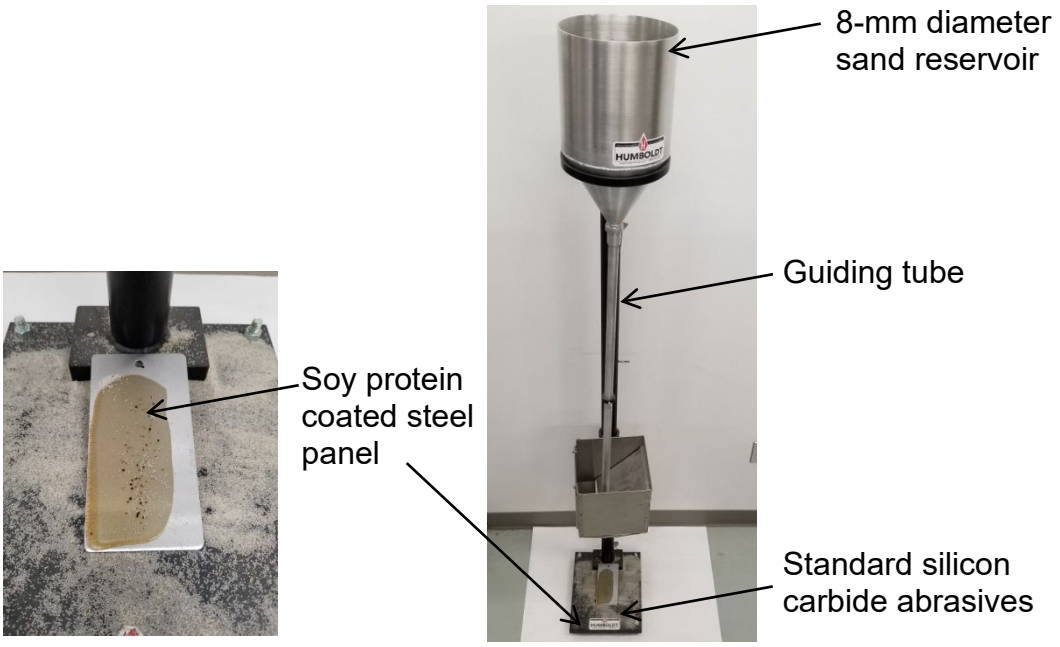

Figure 4-2: Falling Sand Abrasion Tester for determining the abrasion resistance of the soy protein-coated steel panels.

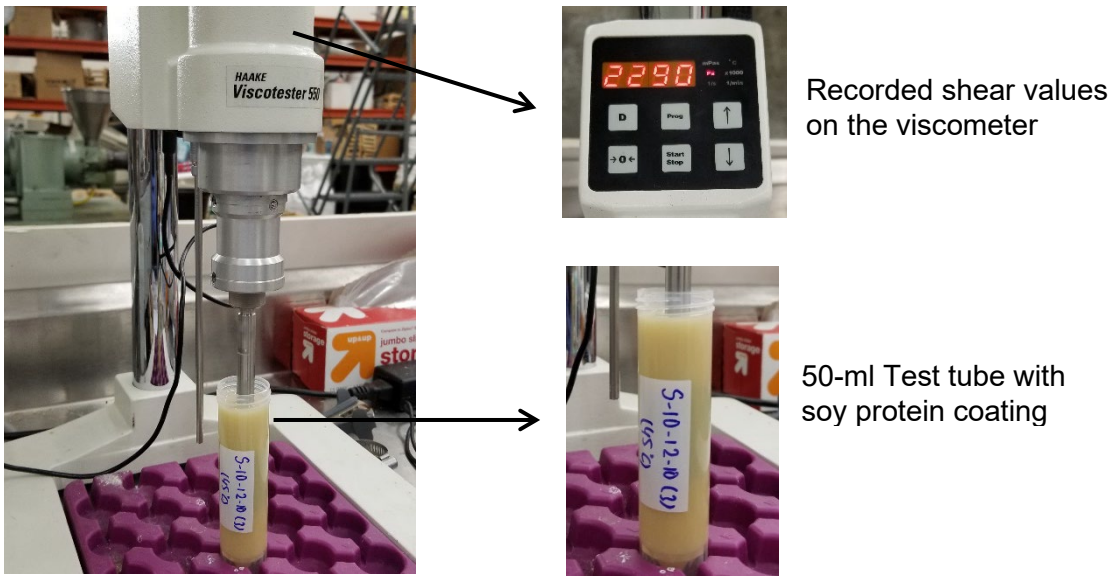

Figure 4-3: Viscosity test setup.

4.2.4 Corrosion Performance Characterization

The corrosion potential and corrosion rates of embedded rebars that are coated with polyol-based coatings are determined using rapid macrocell tests. For this purpose, a rapid macrocell test setup is built using the procedures specified in the Strategic Highway Research Program (SHRP) manual. The rapid macrocell test setup consists of two containers with concrete pore solutions and the presence of sodium chloride (NaCl) in one solution, one rebar sample in one of the containers

which act as an anode, two rebar samples immersed in the second container that acts as a cathode, and an electrical pathway between the anode and the cathode. The test setup is illustrated in Figure 4-4. Concrete pore solution for anodic and cathodic containers is prepared by mixing 974.8 g of distilled water, 18.81 g of potassium hydroxide (KOH), and 17.87 g of sodium hydroxide (NaOH) for preparing 1 L solution. Moreover, 15% of sodium chloride is added to the anodic container. Before immersing rebar specimens in the containers, specimens are thoroughly cleaned and degreased using acetone solution and air-dried. The rebar samples are then dip-coated with two coats of polyol-based soy protein coatings for 48 hours (see Figure 4-5). A period of 24 hours is adopted per coat for curing at 45°C. The coated rebar specimens are then embedded in 1:4 ordinary Portland cement mortar that is prepared using a 0.4 w/c ratio and about 6% air entrainment in the mix (see Figure 4-6). After curing for 14 days, the mortar-cladded rebar samples are dried for 24 hours and immersed in the containers (3-inch immersion depth for rebars). The voltage drop and subsequent corrosion rates across the embedded rebar specimens are then monitored for 120 days.

In addition to rapid macrocell corrosion tests, potentiodynamic polarization tests are also conducted herein to determine the corrosion current densities and corrosion rates. For this purpose, double-coated rebar specimens and coated panels are prepared using each of the coating formulations. Potentiodynamic polarization tests are then formed on the specimens using a standard 3-electrode electrochemical cell which included the coated specimens as working electrode, saturated calomel as reference electrode, stainless steel wire mesh as a counter electrode. During potentiodynamic polarization tests, the potential of the working electrode (coated specimen) is varied from cathodic to the anodic direction (anodic scan) within a range of ±500 mV with reference to the steady-state potential at a scanning rate of 2 mV/s. Tafel analysis is then performed on the polarization curves to obtained corrosion current densities and corrosion rates.

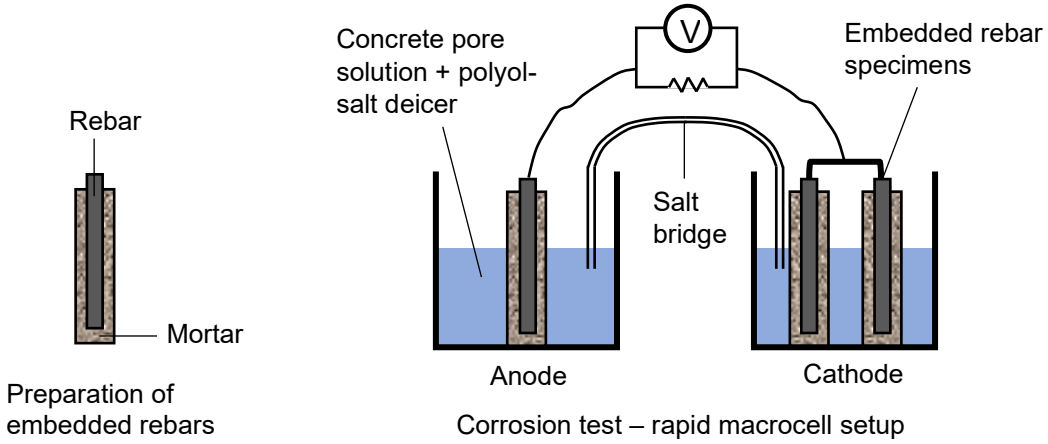

Figure 4-4: Schematic of macrocell corrosion test setup.

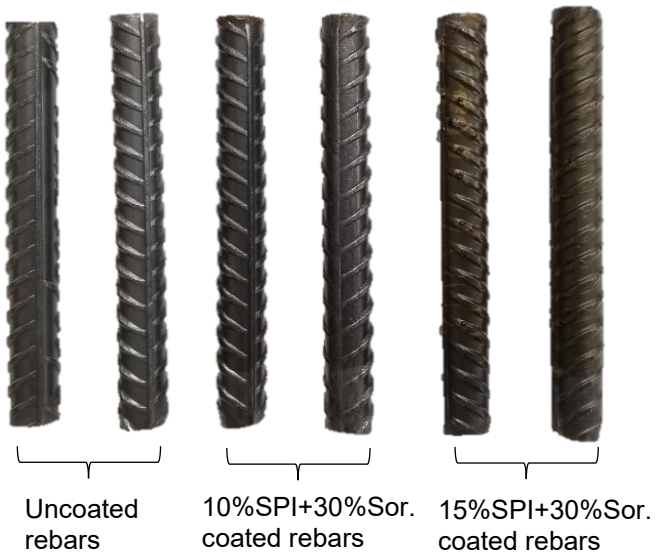

Figure 4-5: Uncoated (control) rebars and 10% and 15% soy protein-coated rebar specimens.

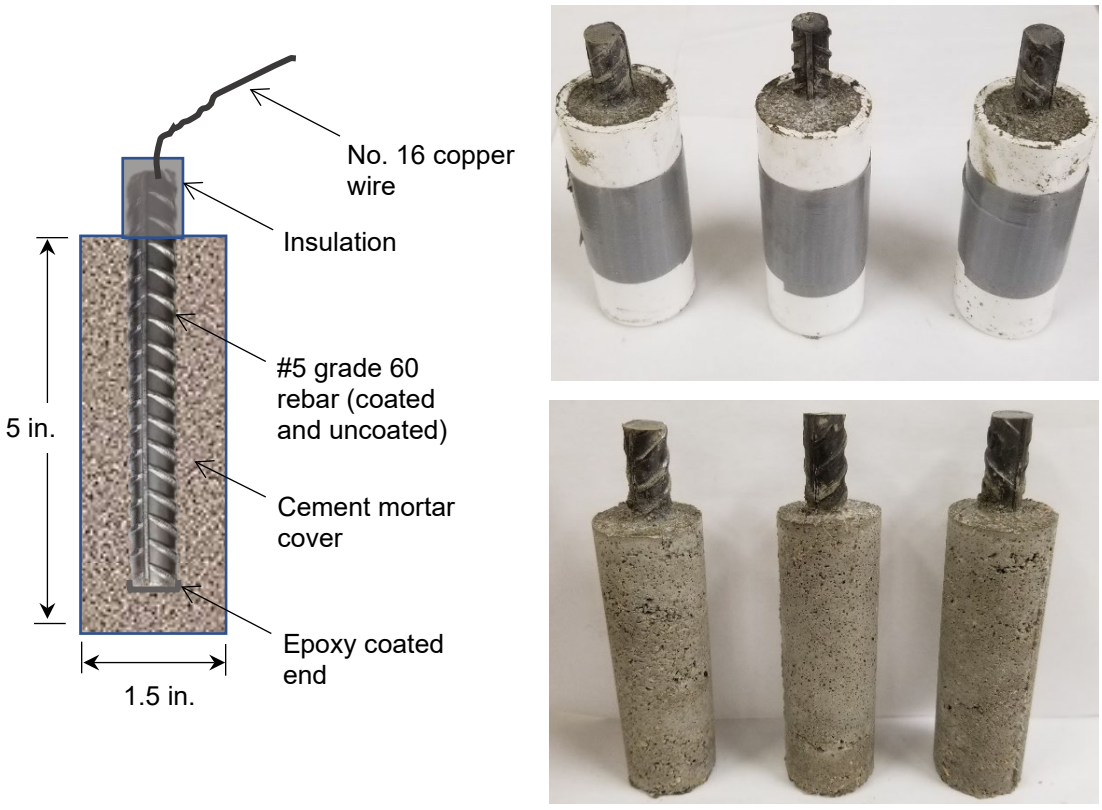

Figure 4-6: Rapid macrocell corrosion test specimens' preparation (uncoated and coated rebars embedded in cement mortar).

4.3 Results and Discussion

This section discusses the physical and chemical characteristics of the soy protein coatings that are synthesized in this study. Moreover, the corrosion protection performance of the coatings, which is obtained from potentiodynamic polarization tests and rapid macrocell tests, is further discussed in this section.

4.3.1 Visual Brittleness of Cured Soy Protein Coatings

The brittleness of the hardened soy protein coating is qualitatively assessed based on visual observation of the specimens. For this purpose, the soy protein coatings corresponding to each coating formulation (wt.% of SPI and wt.% of Sorbitol) are spread on mild steel plates and then cured for 48 hours, as discussed in Section 3.2. The cured coatings are then observed visually and the photograph of each coating is provided in Figure 4-7. As observed in Figure 4-7, the coatings with 0% Sorbitol plasticizer are visibly brittle regardless of the wt.% of SPI in the coating. However, the addition of Sorbitol plasticizer is observed to significantly decrease the brittleness in the coatings. The highest improvement in the integrity (non-brittleness) is noted in the coatings corresponding to 30% Sorbitol content.

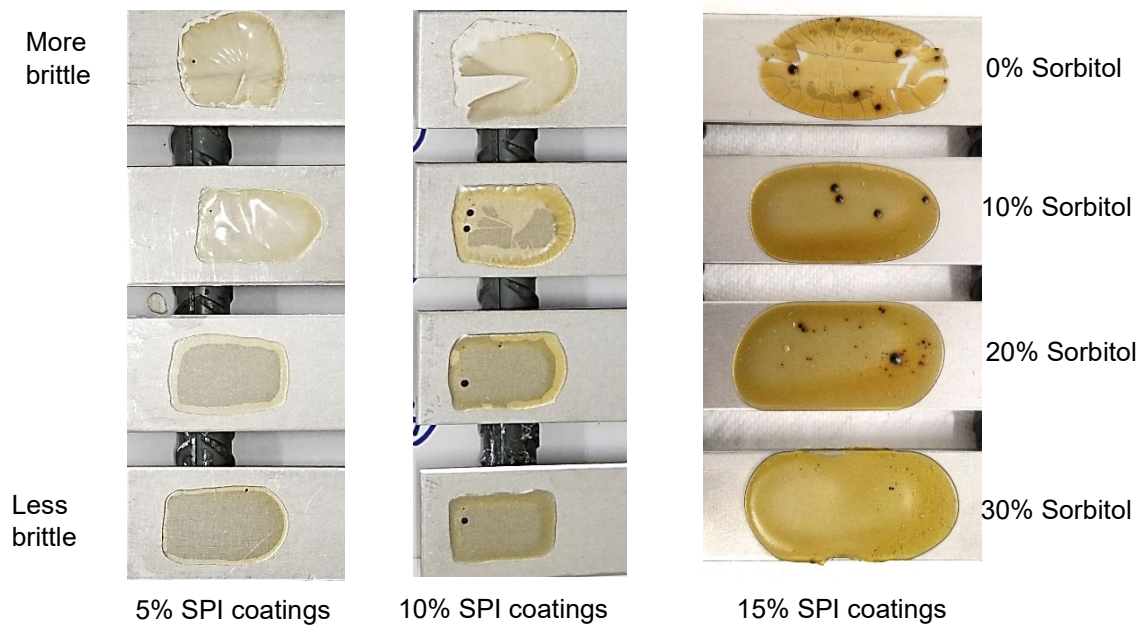

Figure 4-7: Visual brittleness of soy protein coatings with different concentrations of sorbitol.

4.3.2 Viscosities of Soy Protein Coatings

The viscosity tests are performed to determine the consistency and workability of the soy protein coatings containing varying amounts of SPI and Sorbitol plasticizer. The results obtained from the viscosity tests are provided in Figure 4-8. As observed in Figure 4-8, the viscosities for 5% SPI coatings ranged from 1.15 m.Pa.s (corresponding to 30% sorbitol) to 1.43 m.Pa.s (corresponding to 0% Sorbitol in coating). The increase in the concentration of SPI in the coatings is observed to increase the viscosities of the coating formulations due to the increase in the solid

content of the mixture. In the case of 10% SPI coatings, the viscosities are observed to be in the range of 6.00-6.80 m.Pa.s. Similarly, the viscosities are observed to further increase in the case of 15% SPI coatings wherein viscosities are observed to be 24.8-26.4 m.Pa.s. It is further observed that the increase in the concentration of Sorbitol plasticizer in the coatings resulted in a minor reduction in their viscosities. This can be attributed to the plasticizing ability of Sorbitol. Sorbitol can act as lubricant and thus facilitate the movements of the macromolecules over each other thereby increasing the workability and reducing the viscosity of the SPI coating [149, 153]**.** These results show that 10% and15% SPI coatings formulations have adequate viscosities for application on the rebar surface for achieving desirable corrosion protection.

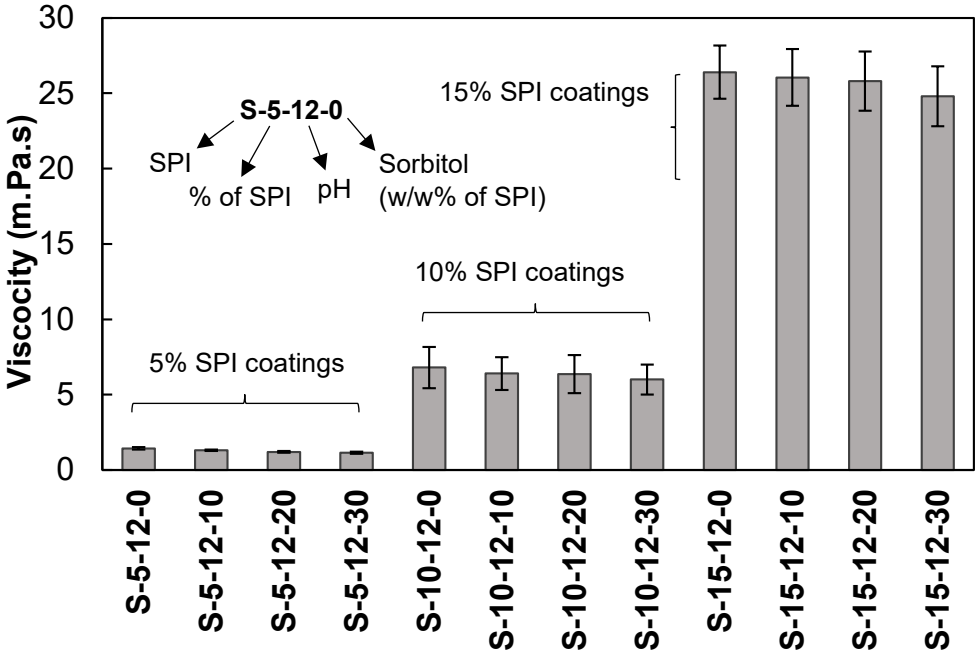

Figure 4-8: Viscosities of soy protein coatings with different weight concentrations of SPI and sorbitol.

4.3.3 Abrasion Resistance of Soy Protein Coatings

The abrasion resistance of the soy protein coatings is determined using the Falling Sand Abrasion Test method that was previously discussed in Section 3.3. The abrasion resistance of the coatings reported in terms of volume of sand per mil of coating (L/mil, is provided in Figure 4-9. As observed in Figure 4-9, the soy protein coatings with 5% SPI content have the least abrasion resistance, and the coating detached from the steel substrate during the initial impingement of sand abrasives. On the other hand, coatings with 10% and 15% SPI content exhibited substantial abrasion resistance which can be attributed to the increase in the SPI content and the corresponding increase in the solid content. The abrasion resistance of the soy protein coatings studied herein ranged between 6-142 L/mil. In the absence of sorbitol plasticizer, the coatings had poor abrasion resistance regardless of the SPI content. This can be attributed to the frigility and brittlness of the SPI coatings in the absence of the plasticizers. However, the addition of sorbitol plasticizer substantially increased the abrasion resistance of the coatings (up to 8 fold increase in the case of

10% SPI coatings and up to 13 fold increase in the case of 15% SPI coatings). This increase can be attributed to the flexibility that is imparted by the high concentration of sorbitol plasticizer in the SPI coatings [153]. The highest abrasion resistance is noted in the case of 10% and 15% SPI coatings with 30% sorbitol content. This shows that soy protein coatings with an appropriate amount of sorbitol coatings have adequate abrasion resistance for in-situ application.

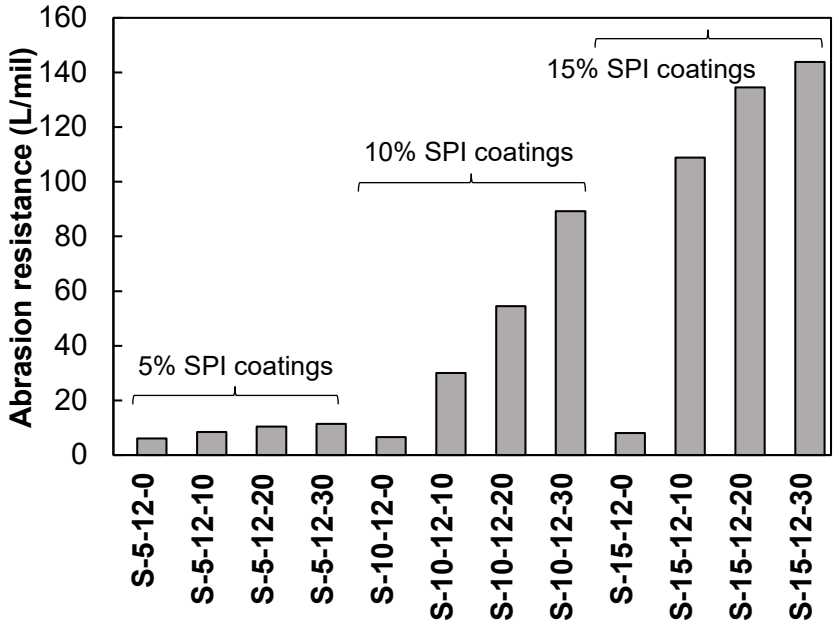

Figure 4-9: Viscosities of soy protein coatings with different concentrations of sorbitol.

4.3.4 FTIR Results

The functional groups present in the cured soy protein coating materials are determined using FTIR spectroscopy. The FTIR spectra for the cured polyol soy protein coatings are provided in Figure 4-10. As shown in Figure 4-10, peaks corresponding to various stretching vibrations (such as O-H, N-H, C-H, C-O, C=O) are observed that indicate the presence of different functional groups (hydroxyl, amid, methyl, methylene, secondary amide, and carboxyl group). Almost identical functional groups are observed in all coatings. The FTIR spectra at the medium range show peaks corresponding to Amide I (1720-1600 cm^{-1}) and Amide III (1400-1200 cm^{-1}) band patterns which show the unfolding of secondary structures in the soy protein. Moreover, it is observed that the –OH functional group almost vanished in the case of 15% SPI coatings. The presence of the observed functional groups in the FTIR spectra of the coatings exhibits the successful alkali modification of the soy protein mixture [154]. Moreover, the disappearance of the hydrophilic groups (such as hydroxyl and carboxyl) in the spectra corresponding to the 15% SPI coatings shows that the addition of high sorbitol content improved the water-resistance of the cured soy protein coatings besides imparting ductility [149].

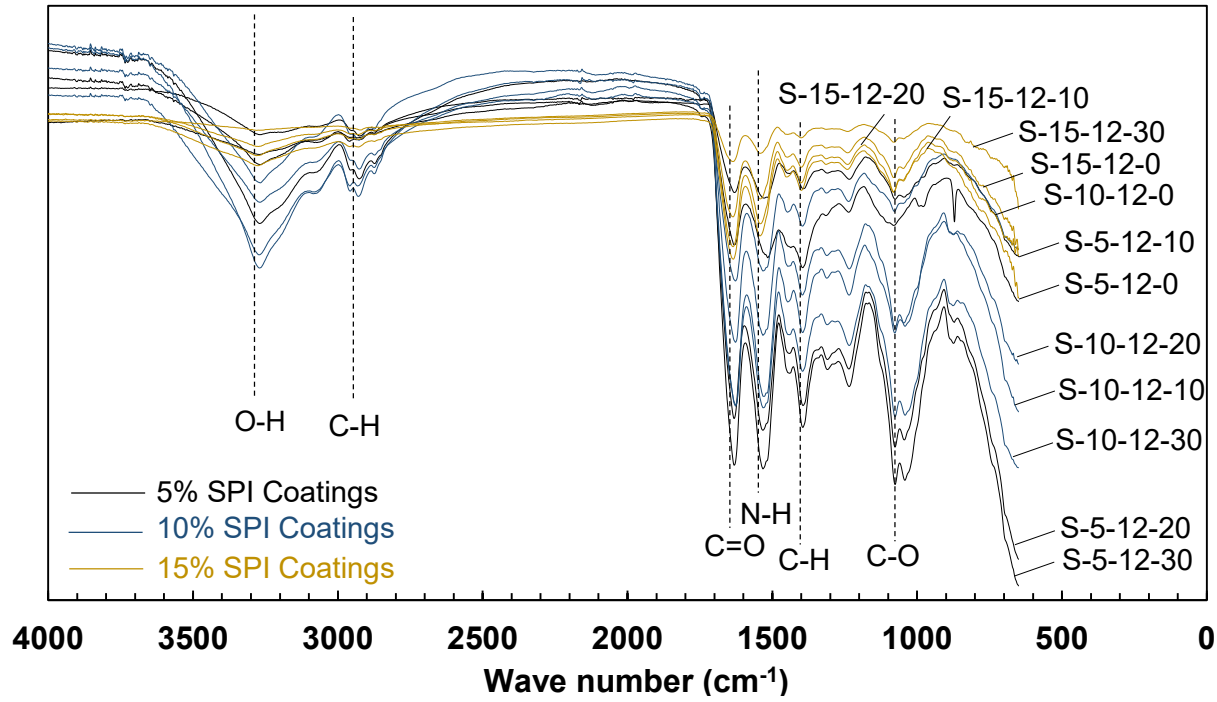

Figure 4-10: FTIR spectra of soy protein coatings with different concentrations of sorbitol.

4.3.5 Corrosion Performance Characterization

The results obtained from physical and chemical characterization tests showed that coating formulations with 5% and 10% SPI content and 30% sorbitol exhibited adequate ductility and abrasion resistance besides reasonable viscosities and FTIR spectra. Therefore, corrosion performance is evaluated only for two types of coating formulations (S-10-12-30 and S-15-12-30) and bare rebars as the control specimen. The polarization curves obtained from the potentiodynamic polarization tests are provided in Figure 4-11. The Tafel analysis performance on these polarization curves showed that the application of 10% and 15% SPI coatings with 30% Sorbitol plasticizer content can reduce the corrosion current densities and corrosion current rates by 95% when compared to the corrosion current density and corrosion rate of bare steel specimens. To determine the long-term corrosion behavior of the soy protein coatings in the concrete environment, rapid macrocell corrosion tests are conducted for coated rebars. To this end, rapid macrocell corrosion tests are conducted using the procedure discussed in Section 3.4. The macrocell tests are run for 120 days and the corrosion rates incurred in the anodic rebar specimen are evaluated by monitoring the voltage drop between the anodic rebar and cathodic rebar across a 10-ohm resistor (see Figure 4-4). The corrosion rates are determined from the voltage drop values using Faraday's equation which is provided below.

$$Corrosion\ rate\ \left(\frac{\mu m}{yr}\right) = K\ \frac{V \cdot m}{n \cdot F \cdot D\ \cdot R \cdot A}$$

where, K = conversion factor (31.5×10^4), V = voltage drop across the resistor (mV), m = atomic weight of iron (55.8 g/g.atom), n = number of ion equivalents exchanged (for iron, n = 2), F =

Faraday's constant (96485 coulombs/equivalent), D = density of iron (7.87 g/cm^3), R = resistance of the resistor (10 ohms), A = surface area of the immersed anodic rebar (approximately 39.9 cm^2). The corrosion rates obtained from rapid macrocell corrosion tests are provided in Figure 4-12. As shown in Figure 4-12, cement mortar embedded coated rebar specimens have considerably less corrosion rates as compared to cement mortar embedded bare rebar specimens. In the case of uncoated rebar, the average corrosion rate remained in the vicinity of 0.25 μm/yr. The application of 10% SPI+ 30% Sorbitol coating on the rebar decreased the average corrosion rates to the range of 0.16 μm/yr. The lowest corrosion rate is observed in the case of 15%SPI+30%Sorbitol coated rebar specimens wherein the corrosion rates mainly hover around 0.12 μm/yr, which is 50% less than the uncoated rebar. These results together with the results obtained from the potentiodynamic polarization tests validate the effectiveness of the soy protein coatings in mitigating corrosion in rebars.

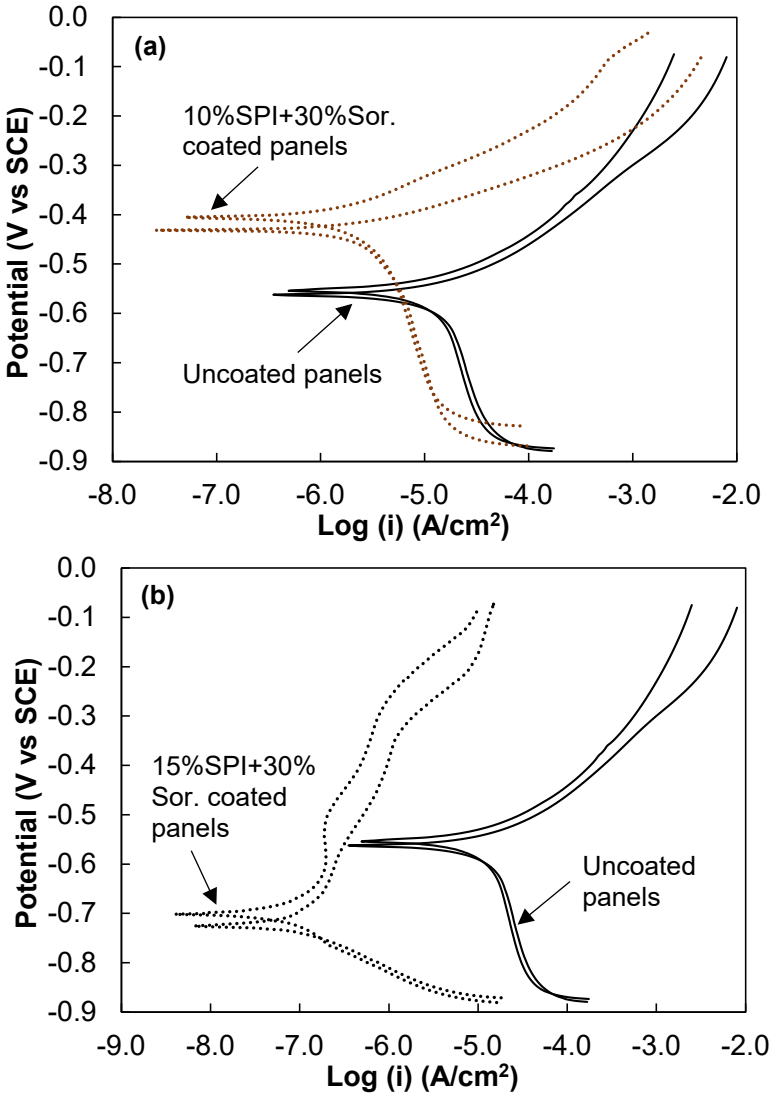

Figure 4-11: Potentiodynamic polarization curves of (a) 10% SPI coated steel panels and (b) 15% SPI coated steel panels, with 30% (w/w% of SPI) sorbitol as a plasticizer.

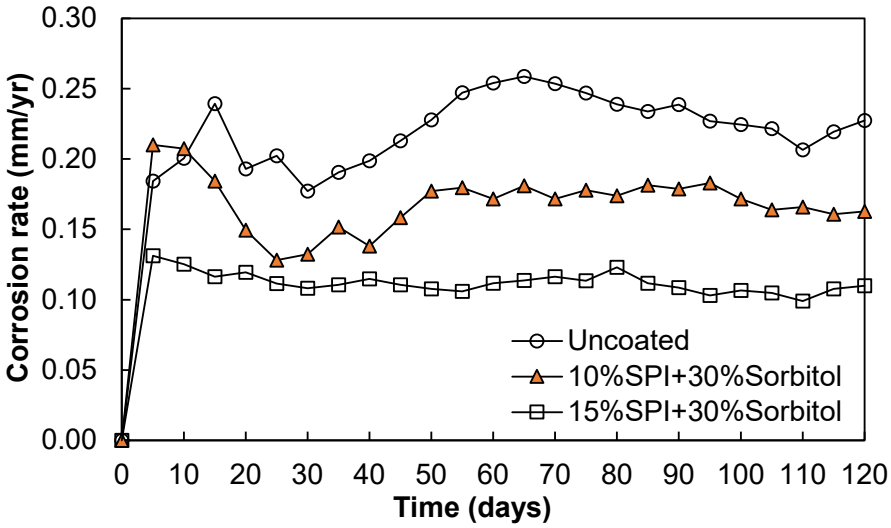

Figure 4-12: Corrosion rates obtained from rapid macrocell corrosion tests for uncoated rebars and soy protein-coated rebars that are embedded in Portland cement mortar.

5 Enhancement of Corrosion Resistance and Bond Strength in Rebars Employing Abrasives-Infused Soy-Protein Isolate Coatings

5.1 Introduction to Improved Biobased Coatings

Epoxy coatings are susceptible to damage during transportation requiring special handling. Corrosion of damaged epoxy coatings will lead to severe localized deterioration of metal, leading to catastrophic outcomes. With this, secondary coats were developed to repair the epoxy coatings in the field. The soy-protein coating that was discussed in the previous chapter was found to be an excellent secondary coat and showed some promise as a stand-alone coating material in a previous study. However, secondary coatings will further decrease the bond with concrete reducing the composite behavior of the reinforced concrete. The goal of this chapter is to improve the corrosion resistance of soy-protein coatings without compromising their bond performance with concrete.

5.2 Biobased Coating Materials and Coating Synthesis

5.2.1 Selection of Soy-Protein Isolates, Sorbitol, and Abrasives

To prepare a biobased coating for corrosion mitigation, we require a base material with specific functional groups that exhibit adhesion and hydrophobicity. In this study, we have chosen food-grade SPI as the base material due to its chemical structure and functional groups that determine biobased coatings' mechanical and chemical properties [155]. SPI is composed of four distinct protein classes: polypeptides (2S), β-conglycinin (7S), glycinin (11S), and a derivative of glycinin (15S), which can be differentiated based on their sedimentation rate coefficient "S" [156] (Svedberg unit which is the measure of time a particle takes to travel in a gradient and is equal to 10^{-13} seconds). Among these protein classes, β-conglycinin (7S) and glycinin (11S) comprise approximately 80% of the total SPI weight. These proteins also contain amide groups (-NH and -NH_2) that contribute to the adhesive power of SPI-based coatings [157]. By modifying the chemical structure of SPI in an alkaline medium with a pH of 12 using a 1 N NaOH solution, we can expose the amide groups and activate the adhesion and hydrophobic characteristics.

Previous studies have shown that soy-protein-based coatings tend to be brittle, and it is necessary to incorporate a suitable plasticizing agent to improve workability and prevent cracking [39, 40]. Polyols, commonly used as low-calorie sweeteners in the food industry, are widely employed as plasticizing agents [148]. In this research, sorbitol is used as a plasticizing agent. It inserts itself between the protein chains of SPI, reducing intermolecular forces and increasing spacing [149]. In a previous paper [158], the authors developed a SPI coating that effectively inhibits chloride-induced corrosion. However, this coating compromises the bond between the rebar and concrete. To address this issue and further enhance corrosion resistance, abrasives are added in this study. The selection of abrasives is based on their chemical passiveness, anti-corrosion performance, dispersion ability, and potential to improve the microstructure of the cement matrix. In light of these considerations, we have chosen nano silica fume (SiO_2) with 96.6% silica and an average particle size of 150 nm, zinc oxide (ZnO) with an average particle size of 1.5 μm, and aluminum oxide (Al_2O_3) with an average particle size of 5 μm [42–44]. To improve the dispersion of these abrasives in soy-protein mixture and prevent rapid agglomeration, a combination of all three abrasives is employed. Previous studies have demonstrated the successful dispersion of SiO_2, Al_2O_3, and ZnO in a water-based solution, which can be attributed to the

creation of intermolecular attractions such as hydrogen bonding and temporary dipoles [13, 44, 45].

5.2.2 Preparation of Modified Soy-Protein Coatings

To prepare modified soy-protein (MSP) coatings, organic SPI dispersed in deionized water is utilized as the base material [158]. Additionally, food-grade sorbitol is employed as a plasticizing agent [149], and a combination of oxides (SiO_2, Al_2O_3, and ZnO) is used as abrasives to enhance the bond performance of coated rebars with the cement matrix and improve corrosion mitigation. Five different coating formulations are developed, each varying the types and amounts of abrasives while keeping the dosage of the base material and plasticizer constant (see Table 5-1). The formulations include Control (without abrasives), MSP-10-5-0 (10% SiO_2 and 5% Al_2O_3 by weight of sorbitol plasticizer), MSP-10-0-5 (10% SiO_2 and 5% ZnO by weight of sorbitol plasticizer), MSP-10-5-5 (10% SiO_2, 5% Al_2O_3, and 5% ZnO by weight of sorbitol plasticizer), and MSP-10-10-10 (equal percentages of 10% SiO_2, Al_2O_3, and ZnO by weight of sorbitol plasticizer). The dosage of abrasives is selected to ensure appropriate consistency, uniform dispersion, and a non-brittle surface after curing.

Table 5-1: MSP coating formulations with varying amounts of abrasive oxide weights.

	Formulation	**SPI (%[#])**	**Sorbitol (%[$])**	**SiO_2 (%[*])**	**Al_2O_3 (%[*])**	**ZnO (%[*])**
1	Control	10	30	0	0	0
2	MSP-10-5-0	10	30	10	5	0
3	MSP-10-0-5	10	30	10	0	5
4	MSP-10-5-5	10	30	10	5	5
5	MSP-10-10-10	10	30	10	10	10

[#]The weight of SPI is taken as % wt. of deionized water, [$]the weight of sorbitol is taken as the % wt. of SPI and *the weight of SiO_2, ZnO, and Al_2O_3, are taken as % wt. of sorbitol plasticizer.

The preparation of MSP coatings involves five steps (see Figure *5-1*). In the first step, a mixture of uniformly dispersed abrasives is prepared. This is achieved by adding 10% SiO_2 into warm deionized water at 35ºC and thoroughly mixing for 5 minutes while maintaining a pH of 12 using a 1N NaOH solution. Subsequently, Al_2O_3 and ZnO are added, if necessary, along with their respective dosages and stirred for an additional 5 minutes. Previous studies have shown that increasing temperature, pH, and using a combination of abrasives promote the dispersion of oxide species and reduce agglomeration [13, 40, 46]. To avoid a cracked coating after curing, the maximum dosage of any abrasive (SiO_2, Al_2O_3, and ZnO) is limited to 10% by the weight of the sorbitol. In the second step, 10% SPI by weight of deionized water is added to the prepared abrasive mixture and dispersed for 10 minutes using a magnetic stirrer. This addition of SPI thickens the liquid paint mixture, necessitating the use of a plasticizing agent to achieve the desired flowability.

The third step focuses on achieving adequate paint workability/flowability. A sorbitol dosage of 30% by weight of SPI is employed while maintaining a temperature of 45ºC. By adding sorbitol during the SPI mixing stage and increasing the temperature to 45ºC, along with a high pH

of 12, denatured the proteins within the SPI [149], and the amide (-NH_2) groups are exposed, leading to improved adhesion and hydrophobicity [40, 41]. In the fourth step, the freshly prepared MSP liquid paints are placed on an orbital shaker at 210 rpm for 3 hours at a temperature of 45ºC to obtain a stable and uniform paint mixture. Subsequently, the final product is seasoned for 24 hours at the same temperature in an airtight container before being applied to steel plates and rebars for further investigation. The prepared specimens are then characterized and tested.

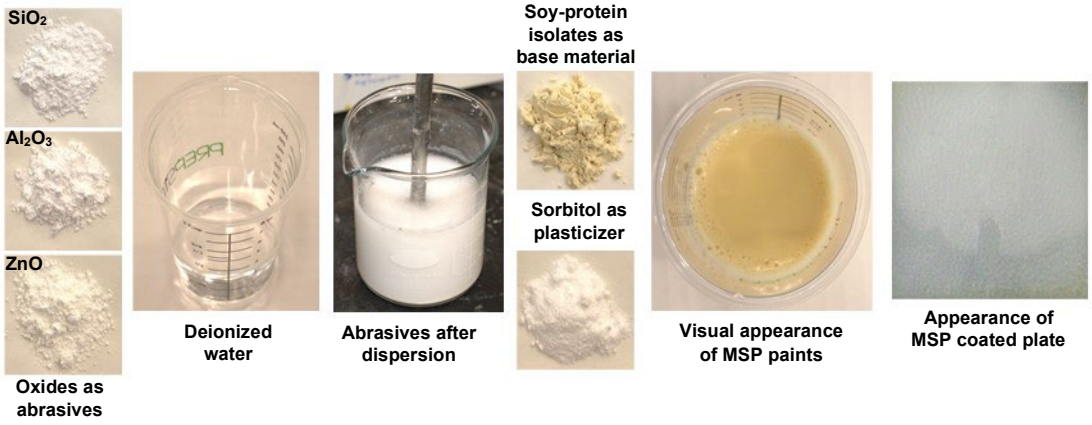

Figure 5-1: Synthesis of modified soy-protein paints employing three different oxides (SiO_2, Al_2O_3, and ZnO) as abrasives.

5.3 Experimental Program

To ensure the durability of rebars in transportation and harsh concreting environments, it is crucial to apply paint mixtures that offer robust protection. These paints should possess suitable viscosity, which affects the coating procedure (such as dip or spray) and the quality of the final cured coating. Additionally, the coatings need to provide reliable and consistent corrosion protection by achieving uniform thickness. To address these practical considerations, the MSP paints are characterized to evaluate their viscosity, abrasion resistance, and coating thickness.

5.3.1 Physical Characterization

5.3.1.1 Viscosity of MSP Paint

A viscosity test was conducted to assess the impact of abrasives on the workability and consistency of MSP paints. Previous studies have reported the viscosity range of SPI paints to be 4.00 cP to 6.80 cP at a temperature of 25°C [158]. Other paints used for rebars [165], wood [164], and concrete [42] exhibit viscosities ranging from 10 cP to 850 cP. While higher viscosities may be favorable for spray coating, they can pose challenges such as limited penetration into the coating surface, weak bonding, and entrapment of air bubbles within the coated surface.

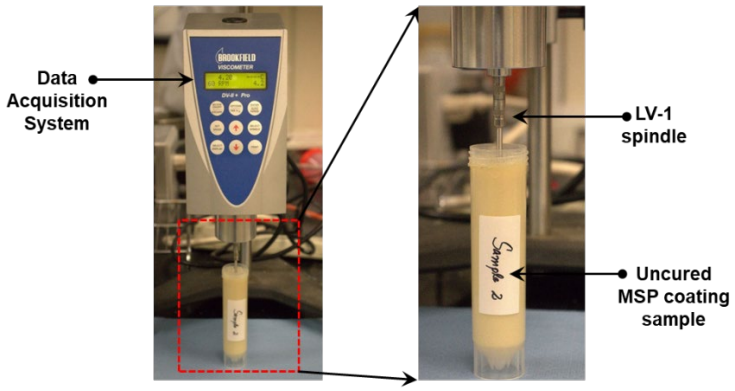

Figure 5-2: Test set-up for viscosity measurement using Brookfield viscometer®.

In this research, the viscosity of all five MSP coating formulations was measured using a Brookfield viscometer® (see Figure 5-2). The viscometer includes a data acquisition system and two cylindrical spindles: a low viscosity (LV) spindle for materials like ink and oil and a regular viscosity (RV) torque spindle for medium viscosity materials like cream and paints. The LV spindles are further categorized into four divisions (LV1 through LV4) based on the magnitude of torque they produce against the shearing fluid. The speed of these LV spindles can be adjusted from 0.3 to 60 rpm. Since the MSP paints in this study are water-based and exhibit lower viscosity [158], an LV1 spindle operating at 60 rpm was chosen. The viscosity values were determined using the following equation [166]

$$Viscosity\ (cP) = \frac{Shear\ stress}{Shear\ strain} \qquad \text{Eq. 1}$$

For the viscosity test, 50 ml of MSP paints were placed in a 13.5 mm diameter tube. The LV1 spindle was carefully inserted into the tube, avoiding rapid insertion that may introduce air bubbles on the spindle's surface, leading to inaccurate viscosity readings. The LV1 spindle was allowed to rotate until the viscosity values were recorded. The test was conducted at a temperature of 20°C, as specified by the equipment manufacturer. Five repetitions of the test were performed for each coating formulation, and the mean value was reported as the final viscosity value.

5.3.1.2 Thickness of MSP Coating

Achieving a consistent thickness is crucial to ensure quality control and accurately assess the bond strength between the concrete and coating. Maintaining uniform and reliable coating on the substrate is also essential to prevent differential weathering and corrosion. In this study, the thickness of the MSP coating was measured using a digital micrometer that adheres to ASTM D1005 standards [167] (see Figure 5-3). The process began by cleaning steel plates and rinsing them with acetone to eliminate any surface dust or dirt. A single coat of MSP paint was then applied and cured for 24 hours at a temperature of 45°C. After the initial 24-hour curing period, another layer of MSP paint was applied and allowed to cure for an additional 24 hours at the same temperature. A hand-held micrometer screw gauge with an accuracy of ± 1.27 µm and a resolution of 0.001 millimeters was employed to determine the thickness of the MSP coating on the plates.

The coating thickness was evaluated at five different spots on each plate, and the mean value was calculated and reported as the coating thickness.

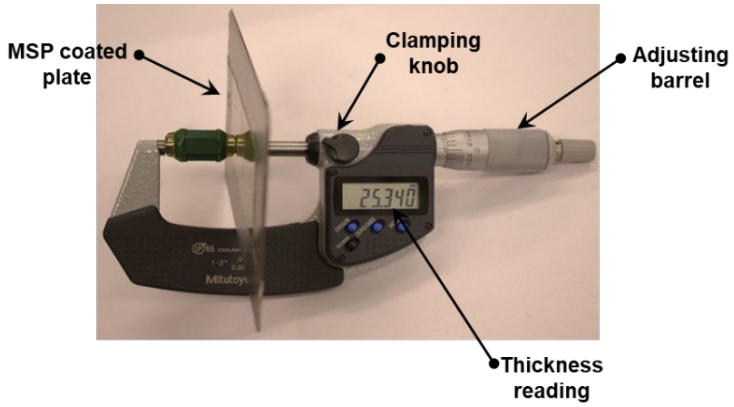

Figure 5-3: Test set-up for the evaluation of modified soy-protein coating thickness using a portable digital micrometer.

5.3.1.3 Abrasion Resistance of MSP Coating

The abrasion resistance of MSP coatings is a crucial factor to investigate, considering the harsh conditions involved during transportation and abrasion during the concreting process. To measure the abrasion resistance, a falling abrasive technique conforming to ASTM D968 standards [168] was employed. In this technique, silicon carbide was used as the abrasive material. The abrasive was allowed to fall from a height of 36" through a guiding tube onto a panel coated with MSP, which was positioned at a 45º angle and located one inch below the end of the guiding tube (see Figure 5-4). The preparation procedure and curing time for the MSP-coated plates remained consistent with those described for thickness measurement. The abrasion resistance was quantified as the amount of abrasive per unit abraded thickness of the MSP coatings. A specified volume of 1600 liters of abrasives was poured into the funnel of the falling abrasion test setup until a region with a diameter of 4 mm was worn down to the substrate. The opening slit of the funnel was adjusted to ensure a rate of abrasive flow of 2 liters of sand every 21-23.5 seconds. The abrasion resistance was determined using the following equation.

$$A_{vol} = V/T \qquad \text{Eq. 2}$$

where, A_{vol} is the volume of abrasives required to erode a unit thickness of the coating, V denotes the volume of abrasives in liters, and T represents the thickness of the eroded coating in millimeters.

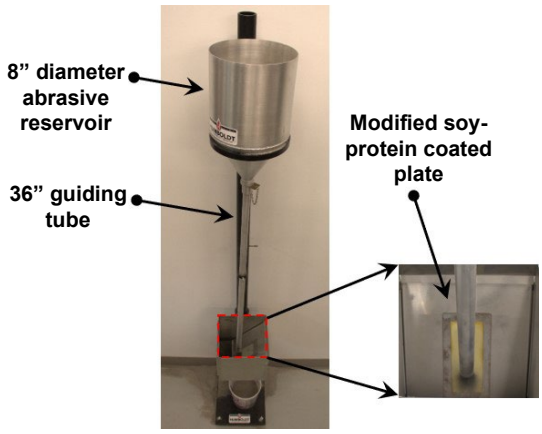

Figure 5-4: Falling cone abrasion resistance setup used to evaluate abrasion resistance of MSP coatings in comparison to Control coatings.

5.3.2 Chemical Characterization

5.3.2.1 FTIR Analysis

In a recent study, a biobased coating was prepared using SPI as the base material. Chemical characterization revealed that SPI contains amide groups (-NH and -NH_2), which serve as crosslinkers and contribute to the adhesion ability of the coating [158]. In this study, Fourier Transform Infrared Spectroscopy (FTIR) was conducted to determine the presence of necessary functional groups in the prepared MSP coatings, enabling adhesion with the rebars. The FTIR spectra of SPI, sorbitol, SiO_2, Al_2O_3, ZnO, and all coating formulations (Control, MSP-10-5-0, MSP-10-0-5, MSP-10-5-5, and MSP-10-10-10) were obtained and compared to assess the interaction within the composite ingredients.

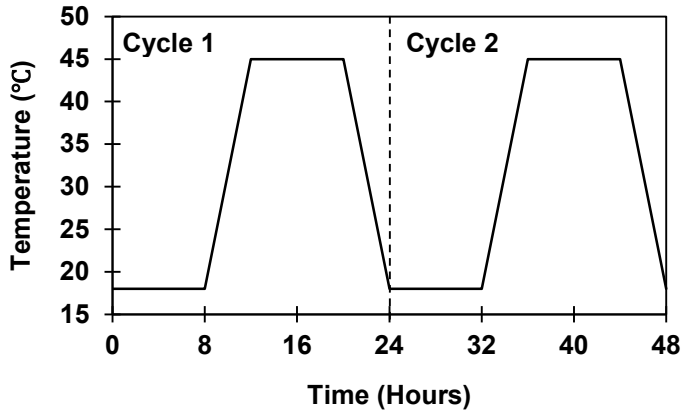

Figure 5-5: Thermal cycles showing the upper temperature bound (45°C), lower temperature bound (18°C), and transitioning ramps for two thermal cycles.

To prepare the specimens for FTIR analysis, 30 mg of potassium bromide (KBr) was thoroughly mixed with 0.03 mg of the investigating specimen (SPI, sorbitol, SiO_2, Al_2O_3, ZnO, and all coating formulations). The mixture was then compressed under a maximum load of two tons using a hydraulic jack for two minutes, forming a thin circular pellet. The prepared pellet was

placed in front of the Infra-Red (IR) beam in the FTIR apparatus for characterization. KBr, an optically transparent material, allowed the IR spectrum to pass through, and the investigating specimen absorbed specific wavelengths within the spectral range of 4000 – 400 cm^{-1}, resulting in absorbance peaks on the FTIR spectra. These peaks correspond to vibrations (stretching or bending) of the functional groups [159].

5.3.2.2 Chemical Compatibility after Thermal Cycling

Furthermore, to investigate the chemical compatibility among the individual ingredients of the coating, MSP coatings were subjected to 50 cycles of heating and cooling. The coatings underwent a predetermined temperature cycle, involving heating at 45°C for 8 hours, followed by a linear decrease in temperature to 18°C over a 4-hour window. Subsequently, the coatings were held at 18°C for 8 hours before the temperature was linearly raised back to 45°C to complete a single temperature cycle. The heating and cooling durations and temperatures are depicted in Figure 5-5. FTIR spectra were obtained before and after the thermal cycles, allowing for a comparison to identify any changes in the locations of functional groups, the emergence of new compounds, and the disappearance of previously existing functional groups. This analysis provides insights into the chemical behavior of the individual coating ingredients under thermal conditions.

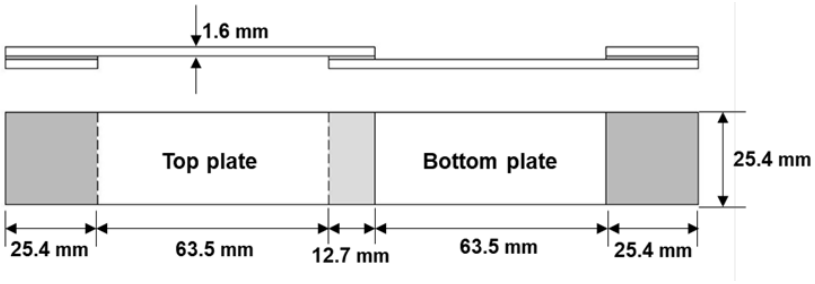

Figure 5-6: Geometry and dimensions of specimens used for lap-shear tests.

5.3.3 Mechanical Properties of Coatings

5.3.3.1 Lap Shear Test

The adhesive behavior of the biobased coating is crucial for assessing the coating's integrity with the rebar. To characterize the adhesion behavior of MSP coating formulations compared to the Control coating, a lap shear test (LST) was conducted following ASTM D1002 standards [169]. The schematic representation of the LST specimen is shown in Figure 5-6. The purpose of the LST is to evaluate the coating material's ability to withstand in-plane shear forces. Two mild steel plates with dimensions of 101 mm × 25.4 mm × 1.6 mm, adhering to ASTM D1002 guidelines [52], were utilized for the LST specimens. The specimen's length, width, and overlapping area were determined based on the plate thickness. Before the test, the steel plates were thoroughly cleaned and degreased using ethanol wipes, followed by air drying. A 25.4 mm × 12.7 mm area from the end of each plate was coated with MSP paints, creating an overlap to sandwich the liquid paint material. This region was securely held in place by a clip to prevent movement.

Furthermore, the non-overlapping ends of the specimens were coated with MSP paints and abutted with plates that are secured similarly to ensure alignment with the direction of the applied

force and avoid any eccentricity (see Figure 5-7). Subsequently, all specimens were cured at 45°C for 48 hours before testing. The LST was repeated five times for each coating formulation, and the mean value was recorded as the ultimate shear force for that specific coating. In total, 25 specimens were prepared to conduct the LST for all formulations. This experimental setup allowed for the evaluation of the adhesive strength between the coating and the mild steel plates, providing insights into the performance of the MSP coatings under in-plane shear forces.

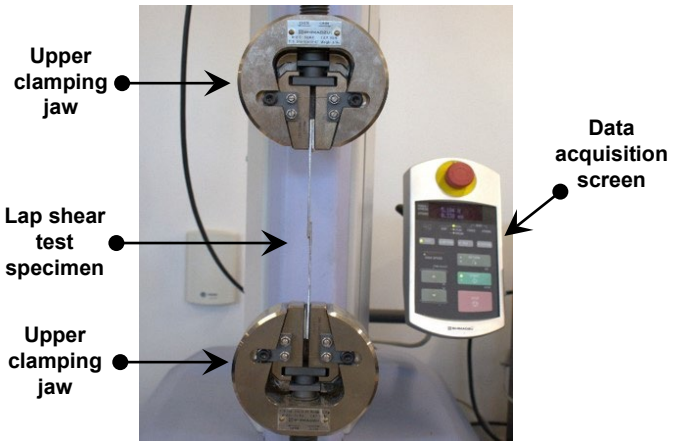

Figure 5-7: Test set-up for lap-shear tests.

5.3.3.2 Pull-out Test

Previous studies have highlighted a decrease in bond strength when epoxy paints are applied to rebars in reinforced concrete (RC) structures due to the formation of a weak interfacial transition zone (ITZ) between the coated rebar and cement matrix [170]. This issue can be addressed by increasing the embedment length [14, 15, 54]. Thus, in this research, we aimed to enhance the bond strength between the cement matrix and MSP-coated rebars by incorporating SiO_2, which improves bond strength through pozzolanic activity [172], and Al_2O_3 and ZnO, known to enhance cement composite microstructures through a packing effect [55, 56]. Packing refers to interparticle spaces and the efficiency of space utilization within the cementitious matrix. The bond strength of MSP-coated rebars embedded in concrete was evaluated using a pullout test following ASTM C900 standards [175]. To prepare the test specimen, a 450 mm long and 12.7 mm diameter grade 60 mild steel rebar was cleaned of surface rust using a steel wire brush, washed with acetone, and air-dried. Two layers of MSP coating were applied, with each layer cured for 24 hours at 45ºC. The dual-coated rebars were then positioned centrally in cylindrical molds before pouring the concrete.

A concrete mix with a cement, sand, and aggregate ratio at 1:1.5:2.5 was prepared, maintaining a water-to-cement (w/c) ratio of 0.30. To achieve the desired workability, a Glenium-based superplasticizer was added, accounting for a maximum of 0.90% of the cement weight in water. The mixing procedure followed ASTM C685 guidelines [176]. After 24 hours, the cylindrical concrete specimens containing the embedded dual-coated rebars were removed from the molds and placed in a water-curing tank until further testing. After being removed from the curing tank, the specimens were air-dried for a few hours before testing. A schematic representation of the pullout test specimen and test setup is depicted in Figure 5-8 (a-b). A total of

30 cylindrical specimens, each with a height and diameter of 100 mm, were cast and tested at 7 and 28 days.

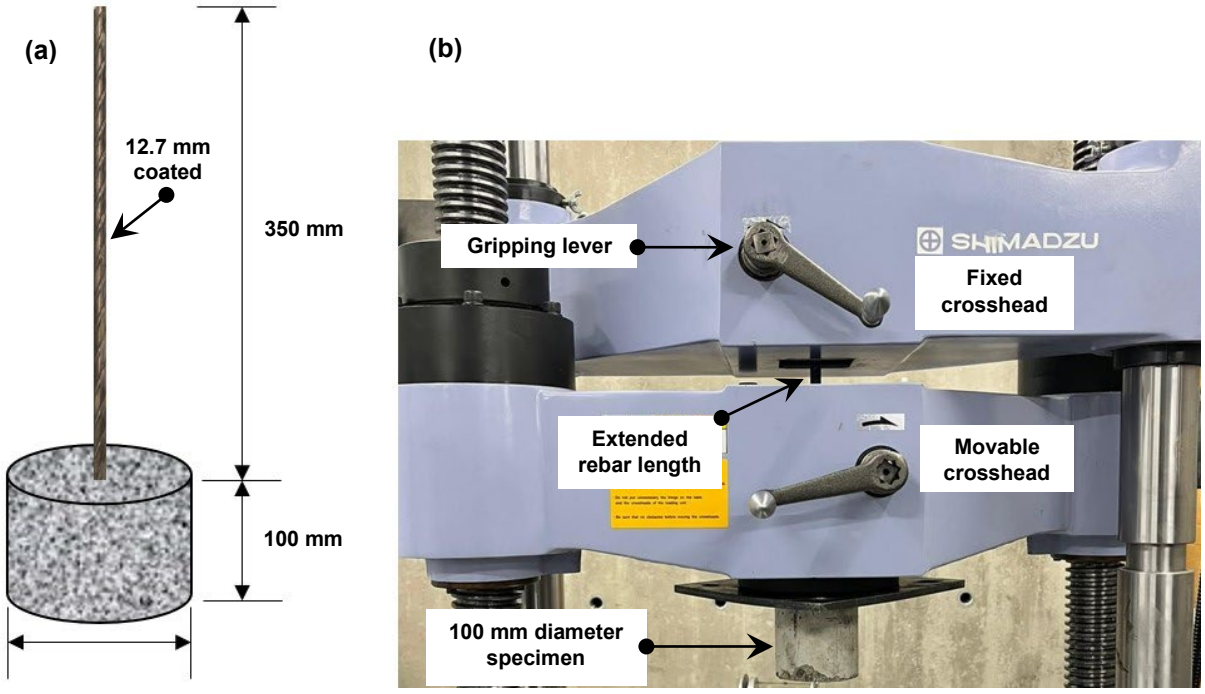

Figure 5-8: (a) Schematics of pullout test specimen, and (b) Shimadzu universal testing machine showing the pullout test setup.

5.3.4 Electrochemical Analysis

5.3.4.1 Salt Spray Test

Salt spray testing is a commonly used method in the coating industry to simulate the corrosive effects of chloride-rich environments on coatings during their service life [40]. The duration of the test varies depending on the coating type, typically ranging from 8 to 3000 hours [59–61]. This study conducted a salt spray test for 240 hours (excluding inspection time) to evaluate the relative corrosion protection performance of MSP coatings compared to Control coatings, following ASTM B117 standards [178].

To prepare the specimens, ASTM A36 steel plates [180] were thoroughly cleaned using a steel wire brush, rinsed with acetone, and air-dried. A single layer of MSP paint was applied to the cleaned plates, then cured for 24 hours at 45ºC.. Subsequently, a second coat of MSP paint was applied and cured for an additional 24 hours at the same temperature. After a total curing time of 48 hours, the coated specimens were placed in a salt spray chamber specifically designed for the test. The salt spray chamber consists of a fog chamber, salt solution reservoir, compressed air nozzles, specimen racks, and a heating assembly. For the test, the MSP-coated specimens were positioned on the specimen racks in a consistent pattern and evenly spaced to prevent the dripping of salt solution from one specimen onto another. The salt solution used in the test contained 5% sodium chloride by weight of water, with a pH range of 6.5 to 7.2, and was maintained at a temperature of 35°C.

5.3.4.2 Potentiodynamic Polarization Test

Previous studies have utilized various electrochemical techniques to quantify the corrosion protection mechanism of coatings, including a) linear polarization tests [181], b) potentiodynamic polarization tests [182], and c) electrochemical impedance spectroscopy [183]. Among these techniques, the potentiodynamic polarization test has been widely used due to its ability to provide detailed information about corrosion mechanisms, corrosion rates, passivation ranges, and pitting potential behavior [184]. Additionally, this test is cost-effective, provides instant data, and yields reproducible results [182]. Therefore, this study conducted, the potentiodynamic polarization test was conducted following ASTM G59 standards [185] to investigate the corrosion current densities and the corresponding corrosion rates.

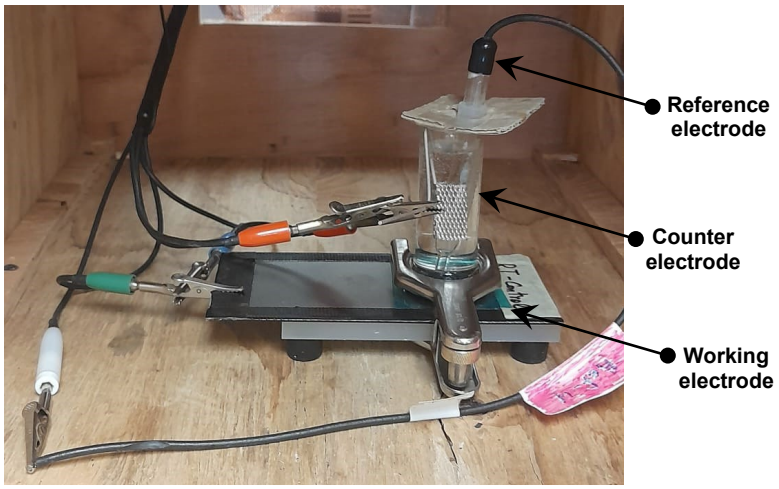

Figure 5-9: Potentiodynamic polarization test set-up for measuring corrosion current densities for MSP coatings.

To prepare the MSP-coated specimens for the potentiodynamic tests, ASTM A572 steel plates [186] were cleaned using a steel wire brush, washed with acetone, and air-dried. A single layer of MSP paint was applied to the cleaned plates and cured for 24 hours. Subsequently, a second coat of MSP paint was applied and cured for an additional 24 hours. In total, 15 specimens were prepared for testing. For the electrolyte, a solution of 3.5% NaCl by weight of water was prepared. The potentiodynamic polarization test setup consisted of a coated specimen as the working electrode, a saturated calomel electrode as the reference electrode, and a stainless steel wire mesh as the counter electrode (see Figure 5-9). The working electrode was covered with plastic tape, exposing a circular area of 7.07 cm^2 for analysis. All potentials were measured against the saturated reference electrode. In the potentiodynamic polarization tests, the potential of the working electrode can be subjected to anodic polarization or cathodic polarization. In this study the potentiodynamic polarization tests were conducted by ramping the working electrode potential from -1.2 V to 0.2 V, with a scanning rate of 10 mV/s. The higher potential range was chosen to capture the passivation range and pitting behavior of the MSP-coated plates.

5.3.4.3 Macrocell Corrosion Studies

In order to assess the long-term corrosion rate of MSP coatings, an accelerated macrocell corrosion test was conducted. The test protocol followed the guidelines of the Strategic Highway Research Program (SHRP) [187] and involved two half-cells, namely the anodic and cathodic half-cells (see Figure 5-10). To create a simulated concrete pore solution, distilled water was combined with sodium hydroxide (NaOH) and potassium hydroxide (KOH) per the SHRP guidelines. In each half-cell, 974.8g of distilled water, 17.87g of NaOH, and 18.81g of KOH were added. To induce corrosion at the anodic electrode, 45.6g of sodium chloride was added to 1 liter of the simulated concrete solution in the anodic half-cell. For accelerating the corrosion and simulating top rebar corrosion in bridge decks (with aggressive dissolution in a smaller anodic region), two embedded rebars were utilized as the cathode. The rebars were cleaned using a steel wire brush and rinsed with acetone. Subsequently, they were coated with two layers of MSP paints and cured for 24 hours at 45°C between each coat. The dual-coated rebars were then embedded in cement mortar, de-molded after 24 hours, and cured underwater for 14 days. Afterward, the specimens were air-dried for 24 hours before being immersed in the simulated concrete pore solution to set up the macrocell corrosion test. Throughout 120 days, the voltage drop and corresponding corrosion rate across the two half-cells were continuously monitored to evaluate the performance of the MSP coatings.

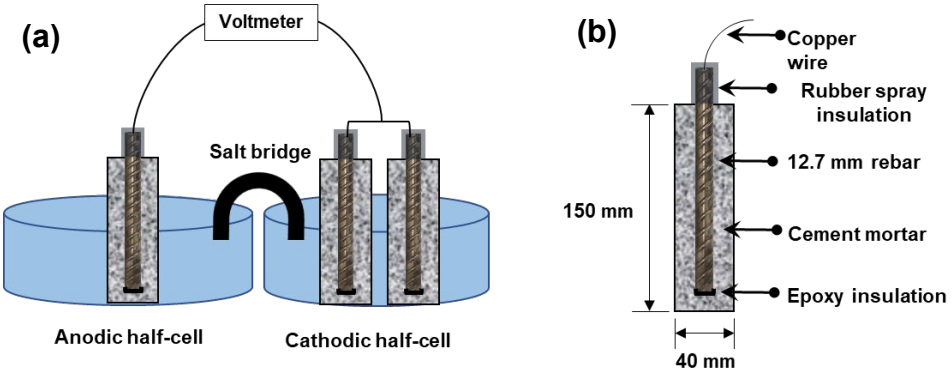

Figure 5-10: Schematics of (a) test assembly of accelerated macrocell corrosion test, and (b) dual-coated rebar embedded in cement mortar.

5.4 Results and Discussion

5.4.1 Physical Characterization Results

5.4.1.1 Viscosity of MSP Paints

The viscosity of the Control paint, which does not contain any abrasives, was measured to be 4.1 cP. As mentioned earlier, viscosity is an important parameter that influences the choice of coating procedure. To determine the viscosity of the MSP paints and assess their suitability for coating purposes, viscosity tests were performed following the procedure described in Section 5.3.1.1. In our study, the viscosity of the MSP paints ranged from 4.1 to 7.2 cP for all the formulations. Among the tested MSP paints, MSP-10-5-0 and MSP-10-0-5 exhibited viscosity values similar to the Control paint without abrasives. This indicates that adding abrasives up to 15% by weight of the sorbitol (plasticizer) has no significant impact on viscosity. On the other

hand, MSP-10-5-5 and MSP-10-10-10 showed 33% and 43% higher viscosity values, respectively, compared to the Control paint. The higher viscosity in these formulations enhances the rheology of the MSP paint and provides anti-sagging behavior. This anti-sagging behavior helps in achieving a stable coating formation on the rebars. This can be attributed to the higher concentration of abrasives in the MSP paints, which increases the required shear force to mobilize one layer of paint with respect to the other layer. This observation is supported by previous studies [7, 67] that have indicated that paints with added abrasives tend to have higher viscosities. The viscosity values of the Control and MSP coatings are provided in Figure 5-11, showing a linear dose-dependent relationship with the concentration of abrasives beyond 15% with no dependence for abrasives concentration less than 15% wt. of plasticizer.

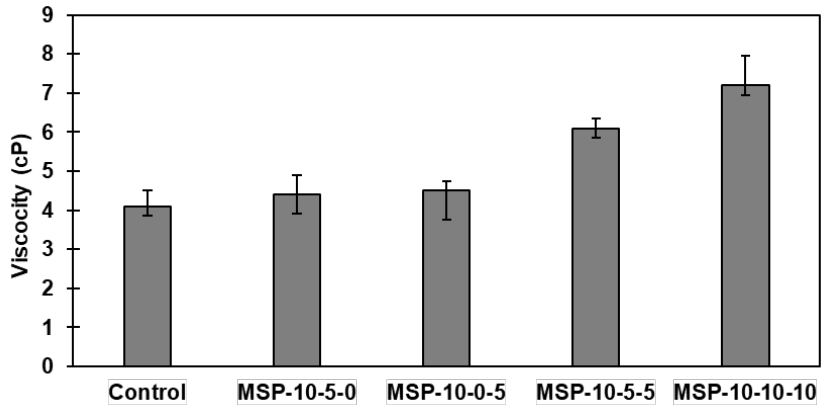

Figure 5-11: Viscosity of modified soy-protein paints with varying fractions of abrasives evaluated using Brookfield viscometer®.

5.4.1.2 Thickness of MSP Coatings

Previous studies have emphasized the challenge of achieving a consistent coating thickness in bio-based coatings due to variations in the biomaterials quality [37, 38, 68]. In this study, the thickness of MSP coatings was measured using the procedure described in Section 5.3.1.2. Five readings were taken to evaluate the thickness of each coating and the variations from the mean values were within an acceptable range of 7%, indicating reasonable quality control for bio-based coatings.

It is evident that the coating thickness is strongly influenced by the viscosity of the uncured liquid paint, as shown in Figure 5-12, which aligns with existing literature [191]. This is particularly relevant in this study, as the dip coating method relies on the cohesion between paint layers to achieve a uniform coat [192]. A paint with higher viscosity tends to result in a thicker coating layer. The MSP coating thickness of double coats in this study ranged from 0.194 mm to 0.416 mm. It is worth noting that a paint mixture with a higher quantity of abrasive exhibits higher viscosity, leading to a thicker cured coating. The Control coating formulation, which did not contain any abrasives, is the thinnest coating with a thickness of 0.194 mm. MSP-10-5-0 and MSP-10-0-5 showed comparable coating thickness values of 0.2124 mm and 0.2022 mm, respectively, owing to their comparable viscosities. In contrast, MSP-10-5-5 and MSP-10-10-10 exhibited coating thicknesses of 0.288 mm and 0.416 mm, respectively. The higher concentration of

abrasives in MSP-10-5-5 and MSP-10-10-10 reduces the effective water-to-abrasives (w/a) ratio increasing the viscosity, resulting in a thicker coating. Commercially available coatings typically have thicknesses ranging from 0.020 mm to 0.250 mm [70, 71]. Moreover, the observed coating thickness is consistent with available literature [194], further validating the findings of this study.

5.4.1.3 Abrasion Resistance of MSP Coatings

The abrasion resistance of MSP coatings was assessed using a falling sand abrasion tester, as described in Section 5.3.1.3. In accordance with ASTM D968 [168], abrasion resistance is defined as the volume of silicon carbide abrasive, measured in liters, required to abrade a 1/1000th inch of coating material when poured from a height of 36 inches. The abrasion resistance of the MSP coating is reported in terms of the volume of sand used per mil of coating (Liter/mil). Images of MSP-coated panels taken before and after the abrasion tests can be seen in Figure 5-13.

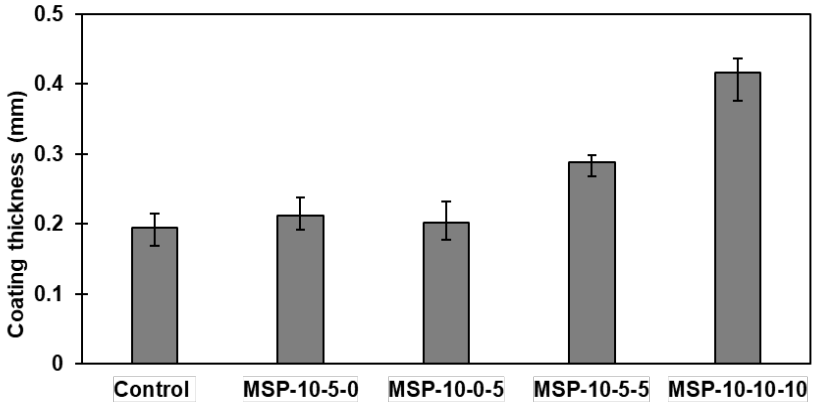

Figure 5-12: Thickness of dual-coated MSP coatings with various weight fractions of abrasives.

After the abrasion test, discoloration was observed in all coating formulations. This discoloration can be attributed to the adsorption of dust particles from the silicon carbide abrasives into the SPI matrix, as well as oxidation resulting from the friction between the abrasives and coatings, which leads to a slightly elevated temperature. Among all the coatings, the Control coating (with a thickness of 0.194 mm) completely eroded after the pouring of 367 liters of abrasives, yielding an abrasion resistance of 48 liters/mil. This result aligns with a previous study [158]. In contrast, none of the MSP-coated plates exhibited any noticeable decrease in coating thickness, even after pouring 1600 liters of abrasives. This can be attributed to the enhanced abrasive strength of the reinforcing abrasive particles [8, 44, 45]. Since no measurable reduction in thickness was observed, the experiment was halted, as this coating will primarily be used as a secondary coat for the in-situ repair of damaged epoxy-coated rebars.

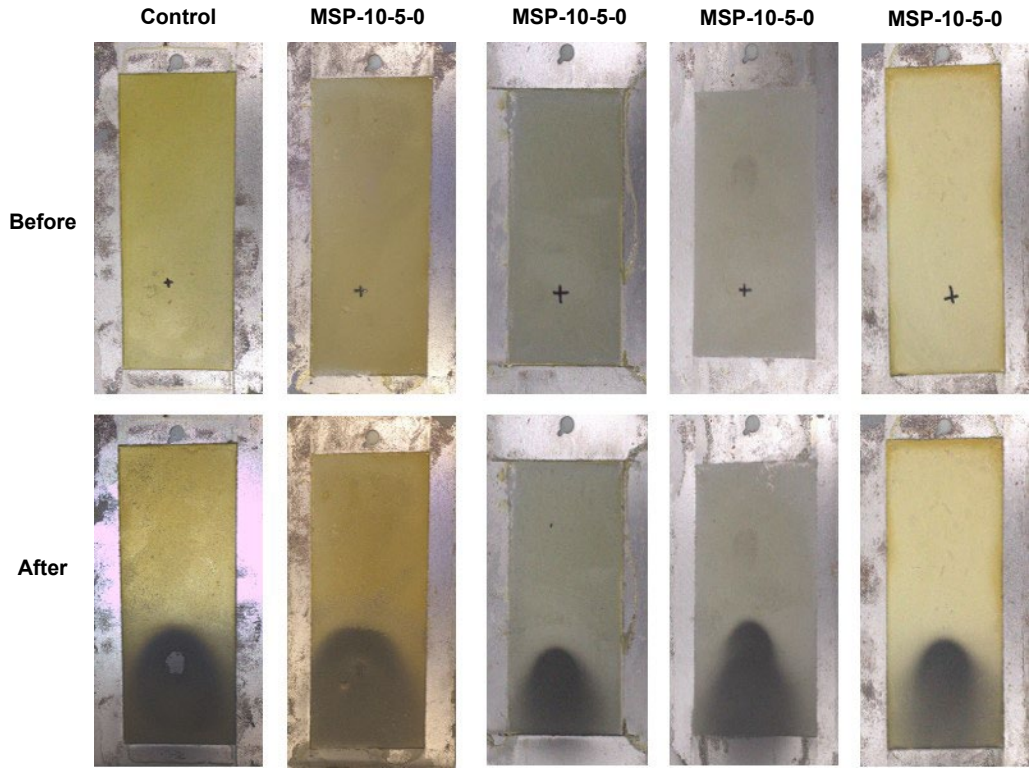

Figure 5-13: Visual appearance of MSP coatings before and after abrasion resistance test conducted employing ASTM D968 [168]. The discolored locations are the regions of contact between the abrading solids and coating material.

5.4.2 Chemical Characterization

5.4.2.1 FTIR Analysis of MSP Coatings

The adhesion strength of coatings with rebars and the cohesion within the coating layers primarily depends on the functional groups present in the coating. As mentioned earlier, the physical and chemical processes employed in the synthesis of MSP coatings were aimed at optimizing the performance of these functional groups. To confirm the presence of the desired functional groups, FTIR analyses were conducted following the procedure outlined in Section 5.3.2.1, and the results are shown in Figure 5-14. Additionally, the important functional groups relevant to the coatings are summarized in Table 5-2. Figure 5-14 illustrates that MSP coatings exhibit functional groups that undergo stretching and bending vibrations [195]. Stretching and bending vibrations are types of molecular vibrations that occur within functional groups present in a coating material. These vibrations involve the oscillation of atoms within the functional group, leading to changes in bond lengths and angles. Stretching vibrations occur when the bonds within a functional group are stretched or compressed, resulting in changes in bond lengths. Bending vibrations, on the other hand, involve the bending or flexing of bonds within a functional group. In this vibration, the bond angles change as atoms move towards or away from each other, causing the bonds to bend. Both stretching and bending vibrations contribute to the overall properties and performance of a coating.

The absorbance spectra of all MSP coating formulations displayed similar characteristic peaks, including those at 3305 cm^{-1}, 2930 cm^{-1}, 1736 cm^{-1}, 1658 cm^{-1}, 1449 cm^{-1}, 1369 cm^{-1}, 1087 cm^{-1}, 1030 cm^{-1}, and 662 cm^{-1}. The band at 3305 cm^{-1} corresponds to the strong stretching vibration of hydroxyl groups (-OH) [155], while 2930 cm^{-1} represents the stretching vibration of methylene ($-CH_2$) [196]. The stretching vibration of the amide group (-NH) was observed at 1736 cm^{-1} [75,76], and its bending vibration at 1658 cm^{-1} [198]. The bending vibration of methyl groups ($-CH_3$) was detected at 1449 cm^{-1} [199], and a weak hydroxyl (-OH) bending at 1369 cm^{-1} [76,77]. Furthermore, characteristic peaks related to the abrasives were observed at 1087 cm^{-1}, 1030 cm^{-1}, and 662 cm^{-1}, indicating the stretching of SiO_2 [200], bending vibration of Al_2O_3 [201], and bending of ZnO [198], respectively.

Among these functional groups, the -OH group contributes to improved hydrophobicity [155], while the amide groups (-NH & $-NH_2$), resulting from the unfolding of secondary protein structures, are associated with enhanced adhesion strength through the increased crosslinking ability of MSP coatings [75, 76]. It is important to note that this FTIR analysis was conducted on fresh coatings, however the coatings undergo thermal cycles during their service life, which may promote unintended chemical interactions among the coating's constituents. This aspect will be explored further in the next section.

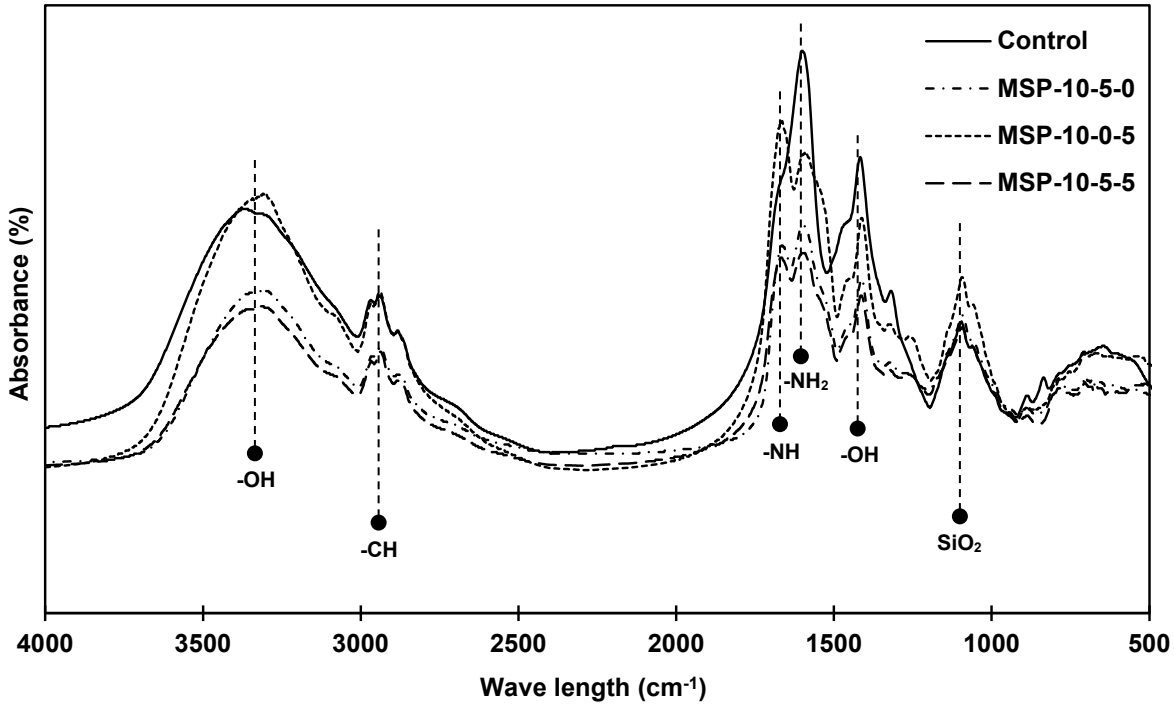

Figure 5-14: FTIR spectra showing the characteristic peaks of different functional groups in MSP coatings and the necessary functional groups for adhesion and hydrophobicity of MSP coatings.

Table 5-2: Characteristic functional groups in the coating and their corresponding band frequencies.

Bands (cm^{-1})	Assignment of Bands	Refs.

3305	Strong stretching of hydroxyl (-OH) group	[155]
2930	Strong stretching vibration of methylene (-CH)	[196]
1736	Amide stretching (-NH)	[75,76]
1658	Amide bending ($-NH_2$)	[198]
1449	Methyl bending ($-CH_3$)	[199]
1369	Hydroxyl (-OH) bending	[76,77]
1087	Silica (SiO_2) stretching	[200]
1030	Alumina (Al_2O_3) strong bending	[201]
662	Bending vibration of Zinc oxide (ZnO)	[198]

5.4.2.2 Chemical Compatibility of MSP Coatings

The prepared MSP coatings will be employed in a variety of coating scenarios for corrosion mitigation of rebars in the longer run, where they could be exposed to heating and cooling cycles. Therefore, chemical compatibility was investigated in this research by comparing the FTIR curves of the MSP coatings before and after the thermal cycles test. Herein, 50 thermal cycles are employed using the procedure discussed in Section 5.3.2.2. The FTIR curves of MSP-10-5-0, MSP-10-0-5, and MSP-10-5-5 are taken before and after the thermal cycle test and are shown in Figure 5-15. While the FTIR curve for MSP-10-10-10 is not shown here as it is the exact duplicate of MSP-10-5-5 (because both the coatings contain the same constituents). It is noticed that the FTIR spectra before and after thermal cycles overlapped and no new peaks originated, confirming that there is no change in chemical composition; hence the ingredients of the prepared MSP coatings are chemically compatible [75, 80].

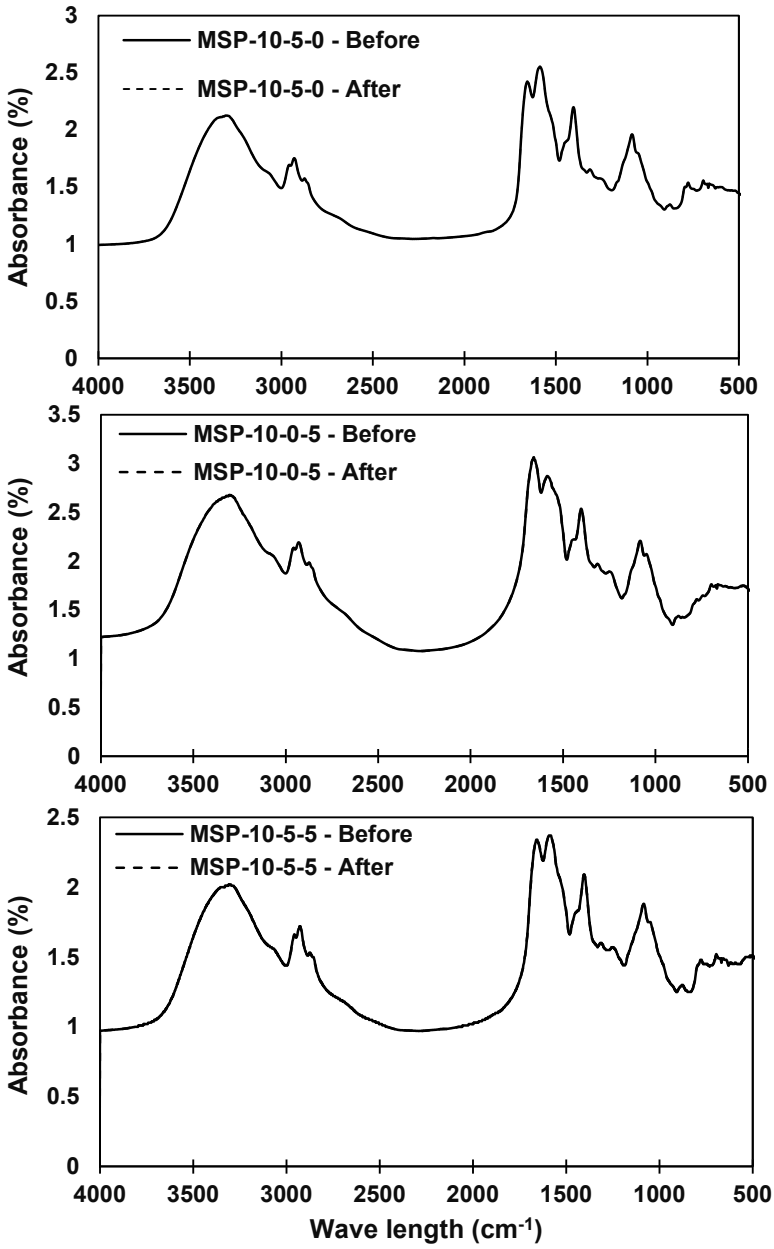

Figure 5-15: FTIR spectra of all the MSP coatings before and after the thermal cycler test. The before and after curves overlapped and can be noticed as a single curve.

5.4.3 Mechanical Characterization

5.4.3.1 Lap Shear Strength of MSP Coatings

Various tests have been used in the past to assess a coating's adhesion, such as the pull-off adhesion test, tape test, scrape test, and lap shear test [203]. This study compares the relative adhesion performance of MSP coatings to the Control coating using the LST, which offers a quantitative measure of adhesion and is a simple and cost-effective method. The test specimens are prepared following the procedure outlined in Section 5.3.3.1**.** Furthermore, a study has reported that changes in surface roughness can enhance coating adhesion by promoting mechanical

interlocking between the substrate and the coating material [194]. To ensure accuracy and avoid any discrepancies, the bonding region was carefully prepared without intentional impressions or exogenous roughness before sample preparation.

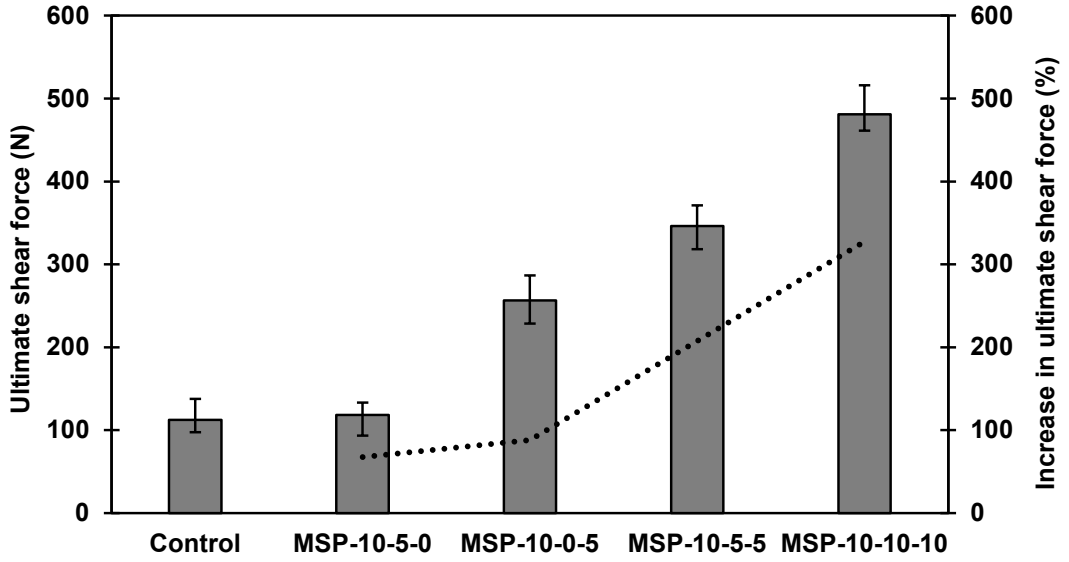

Figure 5-16: Comparison of the ultimate shear force (N) of the MSP coatings with the Control coating.

Figure 5-16 presents the results of the ultimate shear force and the percentage increase in the ultimate shear force of the MSP coatings compared to the Control coating with no abrasives. The ultimate shear force values for the Control, MSP-10-5-0, MSP-10-0-5, MSP-10-5-5, and MSP-10-10-10 coatings were 112.65 N, 118.30 N, 256.63 N, 346.23 N, and 481.11 N, respectively. It is evident that the ultimate shear force increases with higher abrasive dosages. The Control coating, which contains no abrasives, exhibits the lowest ultimate shear force, while MSP-10-10-10, with the highest abrasive dosage, shows a significant increase in ultimate shear force. Additionally, a linear increase in the ultimate shear force is observed for coatings with abrasives more than 15% by weight of the plasticizer. This can be attributed to the increase in the viscosity which increases the coating's thickness resulting in higher shear strength. The percentage increase compared to the Control coating is approximately 67% for MSP-10-5-0, 88% for MSP-10-0-5, 207.6% for MSP-10-5-5, and 327.43% for MSP-10-10-10. It is important to note that the test was repeated five times for each coating formulation, and the results showed variation not exceeding 10%, complying with ASTM D1002 [169].

5.4.3.2 Bond Strength with Concrete of MSP Coatings

Although epoxy coatings have shown promise for mitigating rebar corrosion in reinforced concrete structures [10, 36], these coatings often suffer from reduced adhesion, frictional forces, and mechanical interlocking with the concrete due to their chemically inactive surface and smooth nature [10, 11, 15, 36, 47]. This results in weakened bond strength between the coated rebars and the surrounding cement matrix, with some studies reporting up to a 50% reduction in bond strength [43]. In this study, MSP coatings were developed using different concentrations of abrasives (SiO_2,

Al_2O_3, and ZnO), and it is hypothesized that these abrasives will enhance the bond performance of MSP-coated rebars in concrete. The bond performance was evaluated through the pullout test, measuring the ultimate bond strength (MPa). The pullout test specimens were prepared following the procedure outlined in Section 3.3.2 and cured underwater for testing ages of 7 and 28 days. The ultimate bond strength was calculated using Eq. 3:

$$\tau = \frac{P}{\pi \times d \times l} \qquad \text{Eq. 3}$$

where, τ represents the ultimate bond strength (MPa), P is the ultimate tensile load (kN), d is the rebar diameter of 12.7 mm, and l is the embedded length of the coated rebar in the cement matrix of 100 mm.

Figure 5-17 and Figure 5-18 illustrate the ultimate bond strength (MPa) and the percentage increase in ultimate bond strength of MSP-coated rebars embedded in concrete cylinders at two different ages. The results demonstrate that the ultimate bond strength increases with the testing age for all MSP-coated rebar specimens, as well as the Control specimen. Furthermore, the ultimate bond strength of all MSP-coated rebars surpasses that of the rebar coated with Control coating, irrespective of the type of abrasive used in the MSP coating preparation.

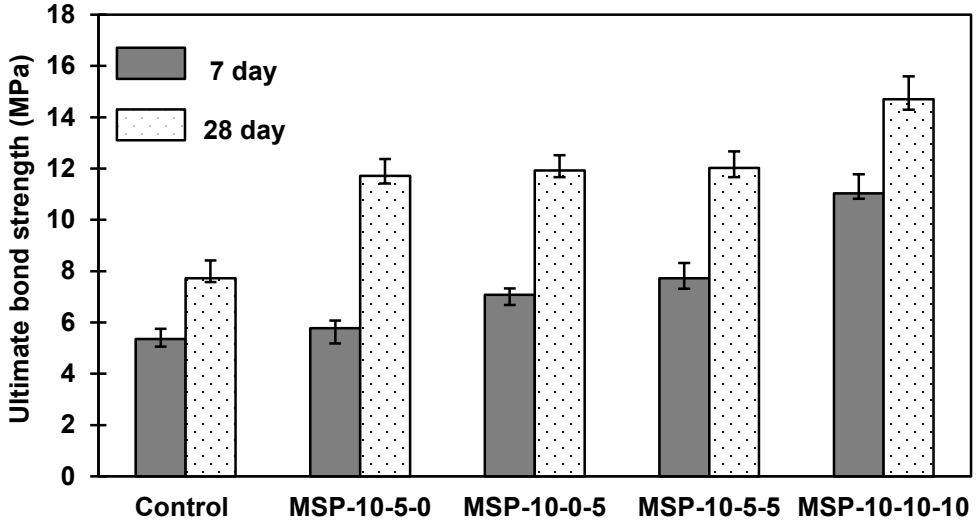

Figure 5-17: Ultimate bond strength of the MSP coated rebars specimens in comparison to the Control coated rebars after 7 and 28 days of curing.

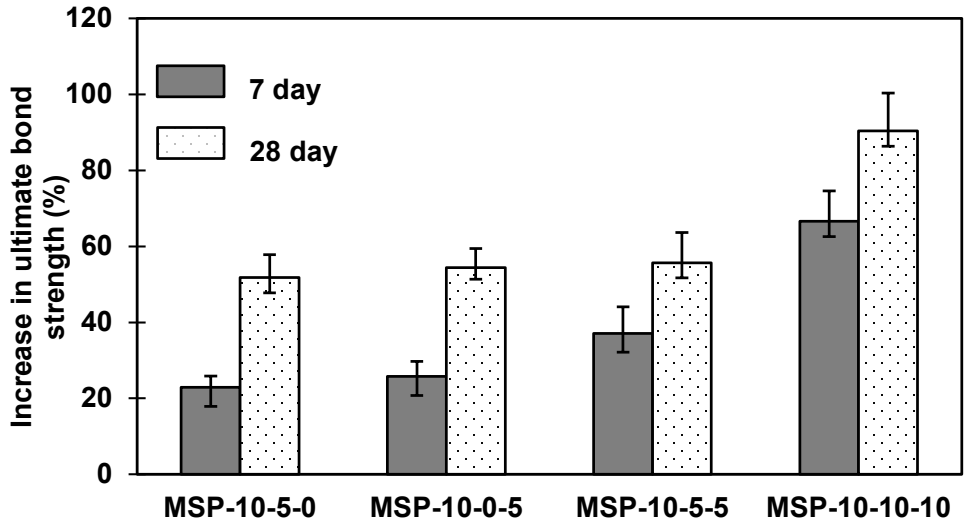

Figure 5-18: Percentage increase in ultimate bond strength of the MSP coated rebars specimens in comparison to Control coated rebar after 7 and 28 days of curing.

At 7 days of testing age, the ultimate bond strength was found to be 5.36 MPa for Control, 5.78 MPa for MSP-10-5-0, 7.08 MPa for MSP-10-0-5, 7.73 MPa for MSP-10-5-5, and 11.03 MPa for MSP-10-10-10. At 28 days of testing age, the ultimate bond strengths were 7.72 MPa for Control, 11.72 MPa for MSP-10-5-0, 11.90 MPa for MSP-10-0-5, 12.02 MPa for MSP-10-5-5, and 14.07 MPa for MSP-10-10-10. Additionally, the percentage increases in ultimate bond strength at 7 days of testing age for MSP-10-5-0, MSP-10-0-5, MSP-10-5-5, and MSP-10-10-10 coated rebars compared to the Control coated rebar were 22.91%, 25.75%, 37.12%, and 14.70%, respectively. At 28 days of testing age, the percentage increases in ultimate bond strength for MSP-10-5-0, MSP-10-0-5, MSP-10-5-5, and MSP-10-10-10 against Control coated rebar specimen were 51.81%, 54.4%, 55.69%, and 90.41%, respectively.

In summary, bond performance improved for all MSP-coated rebars compared to Control coated rebars. This improvement can be attributed to the enhanced interfacial transition zone (ITZ) developed between the MSP-coated rebars and the surrounding concrete. It is established that nano SiO_2 generates pozzolanic activity [172], while Al_2O_3 and ZnO enhance the concrete microstructure through a packing effect in the bonding area [55, 56], resulting in increased bond strength. However, a more in-depth microstructural investigation is recommended for future studies.

5.4.4 Corrosion Protection Tests

5.4.4.1 Salt Spray Tests

Previous studies have highlighted the deterioration of rebar coatings in in-situ conditions, particularly in environments with high moisture content and chlorides, such as bridge decks and concrete pavements [15, 35, 47]. Considering the susceptibility of the coatings synthesized in this study to similar conditions, it is crucial to assess their anti-corrosive performance in a chloride environment. To evaluate this, a salt spray test was conducted for 240 hours following the procedure outlined in Section 5.3.4.1. It is important to note that no specific guidelines or literature are available regarding the maximum duration of salt spray exposure for biobased coatings.

However, past studies have tested oxide coatings for up to 96 hours in the salt spray chamber [59, 61].

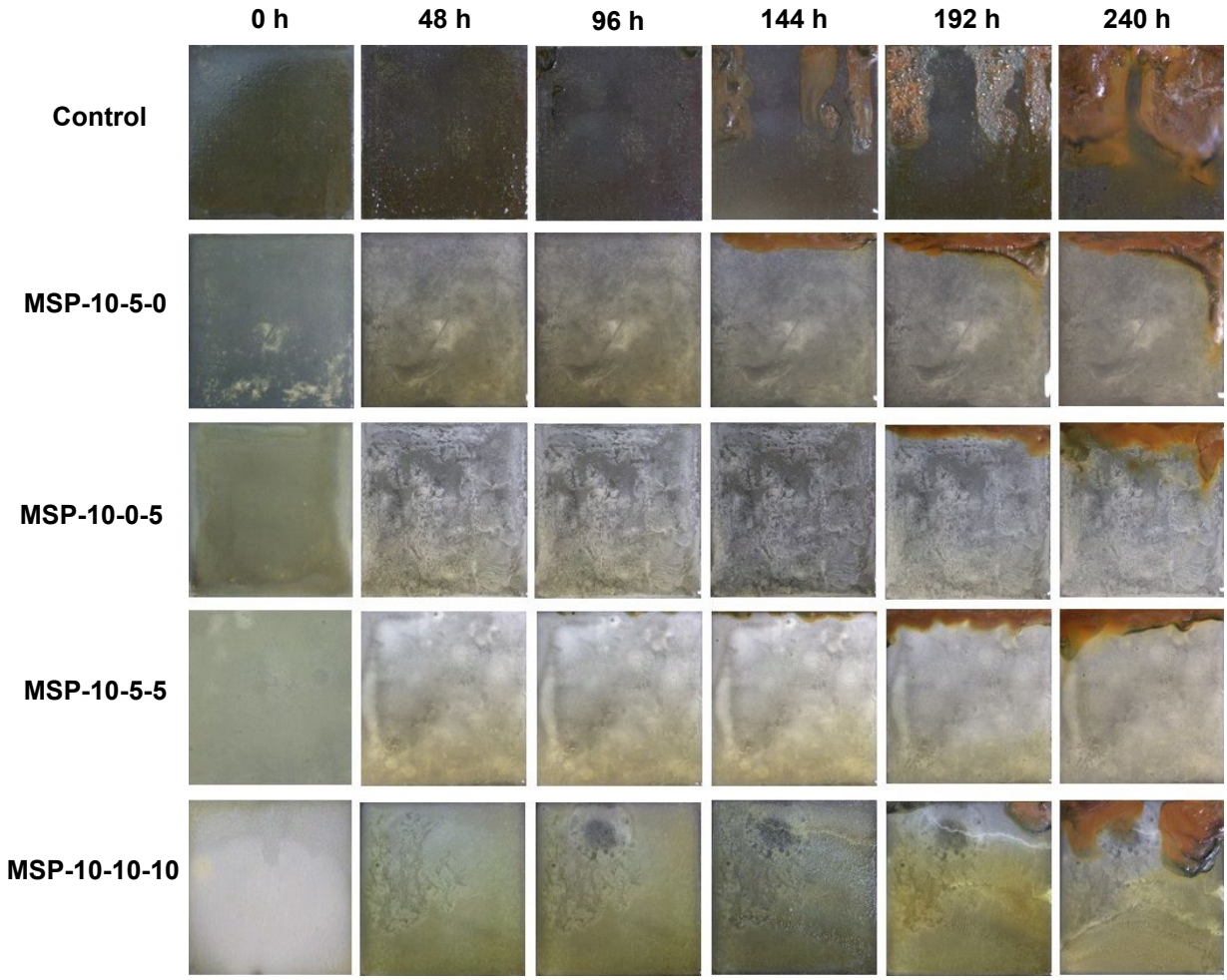

Figure 5-19: Periodical visual appearance of MSP-coated plates subjected to corrosive salt spray.

In this study, salt spray exposure was carried out until visible corrosion damage was observed in the MSP coating, which occurred after 240 hours. The salt spray was paused every 48 hours to visually examine the test specimens, and representative images are provided in Figure 5-19**.** The results of the test showed that the Control coating did not exhibit any signs of corrosion within the first 48 hours. However, after 96 hours, localized pits were observed near the upper edge of the plate, indicating a rupture in the protective film [20, 82]. By the end of the testing period, approximately 75% of the Control formulation coated plate's surface had uniformly corroded. In comparison, MSP-10-5-0 showed corrosion initiation after 144 hours, while the other MSP coatings (MSP-10-0-5, MSP-10-5-5, and MSP-10-10-10) displayed minimal corrosion, beginning after 192 hours from the start of testing.

Overall, MSP coatings exhibited superior anti-corrosion performance compared to the Control coating. The MSP coatings demonstrated prolonged resistance to corrosion in the chloride environment, primarily due to their increased thickness and higher abrasives content. Moreover,

previous studies have highlighted the beneficial effects of multiple oxides in the coating [83–85]. It is worth noting that all the coated specimens showed corrosion initiation from the top edge, as they were inclinedly placed on the rack with the top edge positioned higher than the lower edge. This inclined positioning led to brine flowing from the top to the lower edge, potentially rupturing the coating and exposing the surface to oxygen and water.

5.4.4.2 Polarization Tests on MSP Coatings

As mentioned earlier, the potentiodynamic polarization test was conducted to gain a comprehensive understanding of the corrosion resistance properties of MSP coatings. This technique measures the current generated between the working and reference electrodes due to the potential difference [182]. The potentiodynamic polarization tests were carried out following the procedure described in Section 5.3.4.2, and the Tafel plots are presented in Figure 5-20 (a-d). The electrochemical parameters assessed in this study include corrosion current densities, corrosion rates, and corrosion mitigation mechanisms through Tafel analysis. Each coating formulation underwent the test three times, and for the sake of brevity, only one representative curve is displayed as they all overlapped in Figure 5-20 (a-d). The corrosion rate was calculated using the following equation

$$Corrosion\ rate\ \left(\frac{mm}{year}\right) = 3.27 \times 10^{-3}\ \frac{i_{corr} \times EW}{d} \qquad \text{Eq. 4}$$

where, i_{corr} is the corrosion current density calculated from the Tafel exploration, EW is the equivalent weight, and for ASTM A572 [186] is equal to 28.25 g, while d is the density of the plate, and in this case, it is equal to 7.86 g/cm^3.

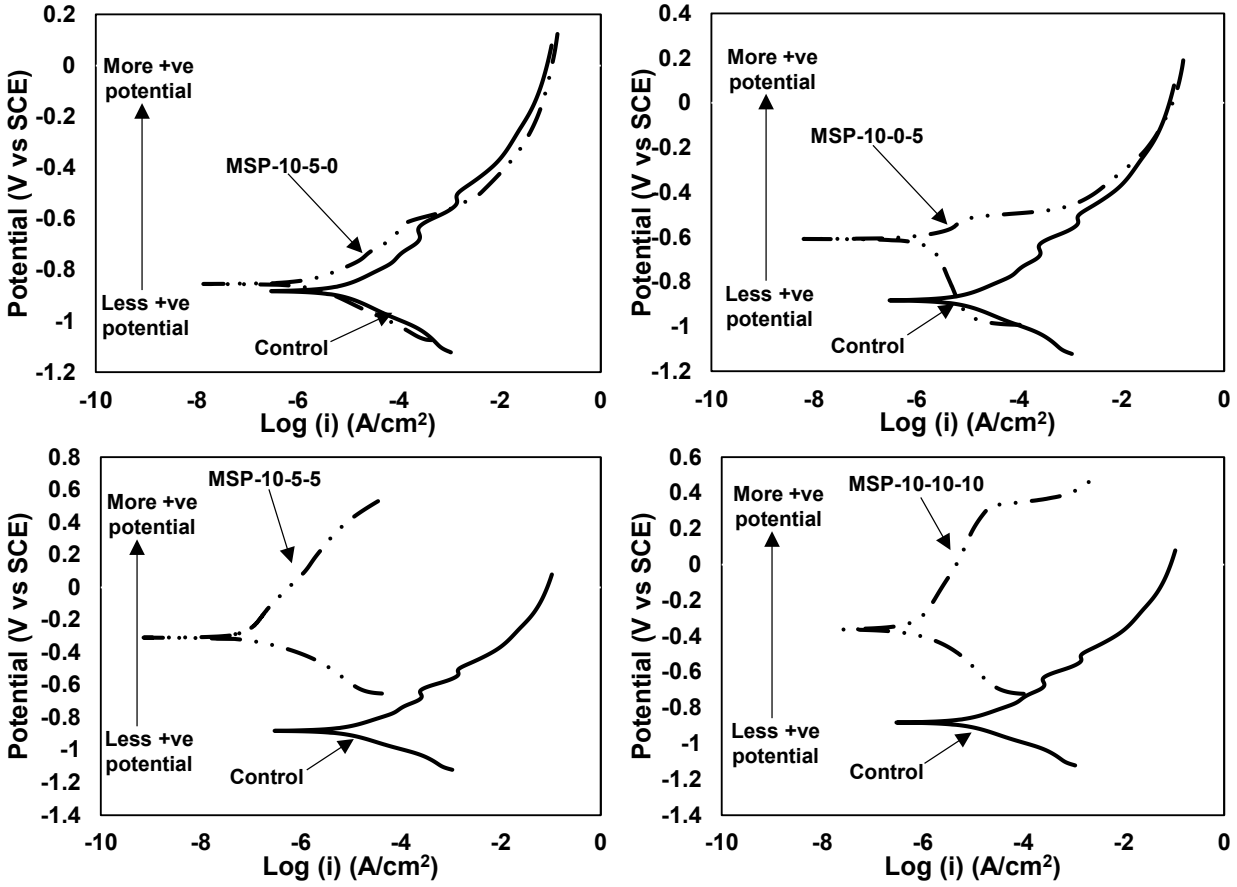

Figure 5-20: Potentiodynamic polarization curves of (a) MSP-10-5-0 (containing 10% SiO_2 & 5% Al_2O_3 abrasives) (b) MSP-10-0-5 (containing 10% SiO_2 & 5% ZnO abrasives) (c) MSP-10-5-5 (10% SiO_2, 5% Al_2O_3 & 5% ZnO abrasives) and (d) Sample (10% SiO_2, 10% Al_2O_3 & 10% ZnO abrasives) in comparison to the Control coating containing no abrasives.

The Tafel analysis revealed that the corrosion current densities and corrosion rates for all MSP coatings containing abrasives (SiO_2, Al_2O_3, and ZnO) were significantly reduced compared to the Control coating without abrasives. This decrease in corrosion current densities indicated a slower dissolution rate of MSP coatings compared to the Control coating [7, 63, 81]. The corrosion current densities for Control, MSP-10-5-0, MSP-10-0-5, MSP-10-5-5, and MSP-10-10-10 were found to be 16.75 $\mu A/cm^2$, 2.21 $\mu A/cm^2$, 2.27 $\mu A/cm^2$, 1.99 $\mu A/cm^2$, and 0.97 $\mu A/cm^2$, respectively. Converting these corrosion current densities using Eq. 4, the corrosion rates for Control, MSP-10-5-0, MSP-10-0-5, MSP-10-5-5, and MSP-10-10-10 were determined to be 0.197 mm/year, 0.026 mm/year, 0.027 mm/year, 0.023 mm/year, and 0.012 mm/year, respectively. The percentage decrease in corrosion current densities and corrosion rates for MSP-10-5-0, MSP-10-0-5, MSP-10-5-5, and MSP-10-10-10 was calculated to be 87%, 86%, 88%, and 94%, respectively. It can be observed that the decrease in corrosion current densities and corrosion rates enhanced with the increase in the abrasive concentrations. This decrease in electrochemical parameters can be attributed to the thick MSP coatings, acting as a physical barrier (discussed in Section 4.1.2), and to the formation of a passive oxide layer due to the presence of abrasives [81, 83].

Furthermore, the plots for MSP coatings in Figure 5-20 are located in a more positive potential region than the Control coating, which is located in a less positive potential region. This shift towards a more positive potential region indicates improved corrosion resistance of the MSP coating plates [203]. It can be concluded that a higher positive potential corresponds to lower tendency of metal corrosion. These observations strongly align with the results from the salt spray test, supporting the potential of MSP coatings as promising candidates for corrosion mitigation.

5.4.4.3 Macrocell Studies on MSP Coatings

The long-term anti-corrosion performance of MSP-coated rebars was evaluated using an accelerated macrocell corrosion test, following the procedure described in Section 5.3.4.3. The voltage drop across the anodic and cathodic rebars was monitored using a 10-ohm resistor, and the corrosion rate (μm/year) was determined using the Faraday equation (Eq. 5) provided below.

$$Corrosion\ rate\ (\mu m/year) = \mathrm{K}\frac{\mathrm{V} \times \mathrm{m}}{n \times \mathrm{F} \times \mathrm{D} \times \mathrm{R} \times \mathrm{A}} \qquad \text{Eq. 5}$$

where, the conversion factor (K) = 31.5 x 10^4, voltage drop (V) across the resistor in milli volts, the atomic mass of iron (m) = 55.8 g/g. atom, number of ion equivalents exchanged for iron (n) = 2, Faraday's constant (F) = 96500 C/equivalent, the density of iron (D) = 7.86 g/cm^3, the resistance of the resistor (R) = 10 ohms, the surface area of the immersed anodic rebar in simulated pore solution (A) = 39.9 cm^2.

Figure 5-21 displays the corrosion rate variation of all MSP coatings compared to the Control coating. The results show that all MSP-coated rebars experienced a significant reduction in corrosion rate compared to the Control coated specimen. This reduction can be attributed to the increase in the coating thickness and barrier protection caused by the presence of abrasives in the MSP coating. The average corrosion rates of the Control, MSP-10-5-0, MSP-10-0-5, MSP-10-5-5, and MSP-10-10-10 coatings were determined to be 0.50 μm/year, 0.41 μm/year, 0.35 μm/year, 0.25 μm/year, and 0.11 μm/year, respectively. Additionally, the percentage reduction in the corrosion rate of the MSP-coated rebars (MSP-10-5-0, MSP-10-0-5, MSP-10-5-5, and MSP-10-10-10) compared to the Control coated rebar was observed to be 18%, 30%, 50%, and 78%, respectively (see Figure 5-22). Furthermore, the study revealed that the corrosion rate decreased linearly as the amount of abrasives in the MSP coating increased. It is worth mentioning that MSP-10-10-10, which contained SiO_2, Al_2O_3, and ZnO abrasives, exhibited a consistent corrosion protection behavior depicted by its curve profile, which highlights the quality of the synthesized coatings. These results are consistent with the findings from the potentiodynamic polarization and accelerated salt spray studies presented earlier, further supporting the anti-corrosion potential of MSP coatings.

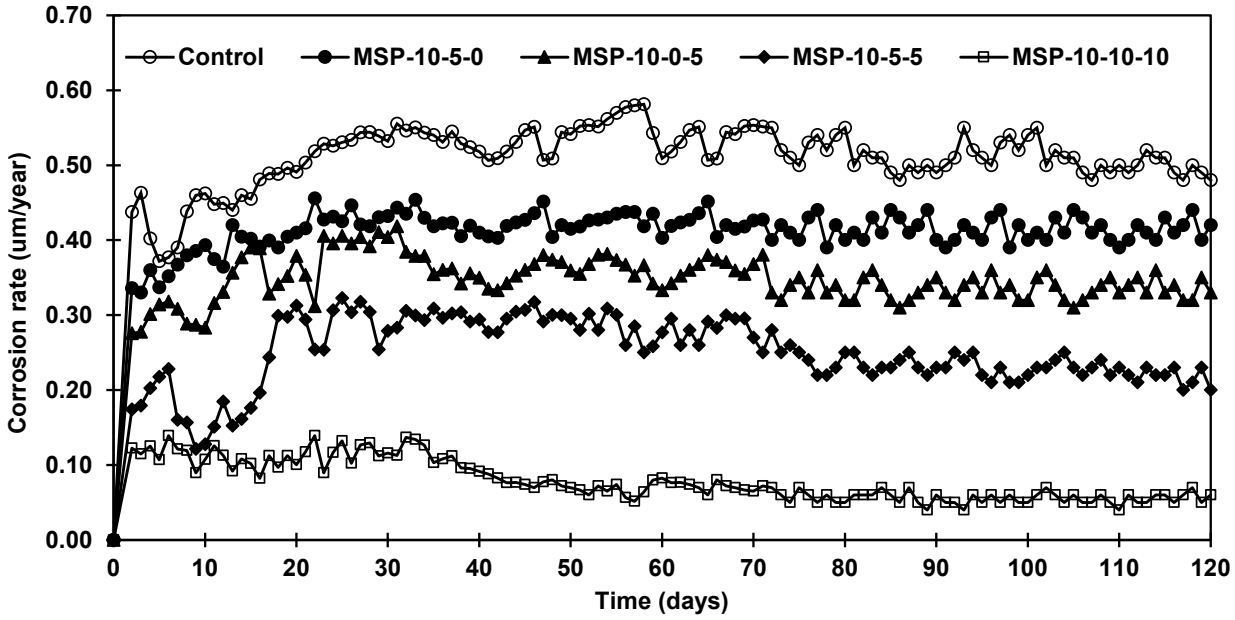

Figure 5-21: Corrosion rate of MSP coated rebars in simulated concrete pore solution over a period of 120 days.

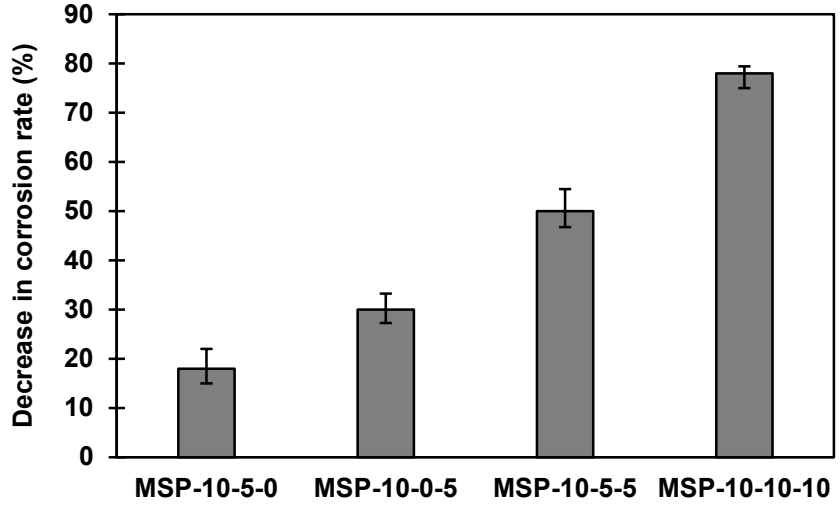

Figure 5-22: Percentage (%) decrease in the corrosion rate of MSP-coated rebars in simulated concrete pore solution.

6 Conclusions and Recommendations

This chapter summarizes the important conclusions of this project followed by a list of recommendations for future research.

6.1 Effect of Polyol Corrosion Inhibitors on Cementitious Materials

The impact of polyol corrosion inhibitors added to the deicing solutions on the compressive strength, scaling resistance, mass change, and chemical properties of ordinary Portland cement mortar is investigated in this study. The important conclusions obtained from this investigation are:

1. Exposure to the reference salt brine deicing solution results in a 12-17% reduction in the compressive strength of concrete after exposure to more than 60 W-D cycles. For the same number of exposure cycles, a relatively lower deterioration in the compressive strength of cement mortar is observed (2-8%) when 1.0 wt.% corn-derived polyols are added to the NaCl deicing solution. The relatively lower reduction in the compressive strength of cement mortar can be attributed to the relatively lower scaling damage and lack of significant chemical interaction between the corrosion inhibitors and cement hydration products due to the pore-clogging effect of polyols.
2. NaCl deicing solution causes slight to moderate scaling damage in cement mortar specimens which can be attributed to the penetration and precipitation of deicing molecules in the cement mortar. The addition of polyol corrosion inhibitors in the NaCl deicer did not result in any further scaling damage.
3. The addition of polyol corrosion inhibitors in the NaCl deicing solution (1.0 wt.% sorbitol, mannitol, or maltitol) does not cause a significant mass change in the cement mortar specimens, and hence it will not have a further negative impact on the properties of cement mortar when compared to NaCl deicing solution. This is reflected by the lower surface scaling and spalling of cement mortar.
4. The chemical composition analysis (XRD and EDX) revealed the presence of NaCl deicing salt precipitates as well as the presence of cement hydration products. However, no considerable decalcification is observed when the deicing solutions are applied on the hardened cement mortar surface, regardless of the presence of corrosion inhibitors. This demonstrates that the addition of polyol corrosion inhibitors does not alter the chemical composition of the hardened cement matrix and does not result in the formation of deleterious products, and thus does not cause further damage in cement mortar when compared to NaCl deicing solution.
5. The morphological analysis conducted using SEM revealed the formation of microcracks and some micropores in the specimens that are subjected to NaCl deicing solution both during the absence and presence of polyol corrosion inhibitors. The morphological pattern is similar in all specimens, which demonstrates that the addition of polyol corrosion inhibitors in the NaCl deicing solution did not cause any further microcracking or form any

superficial products. The microcracks observed in the SEM micrographs may be linked with the formation of expansive oxychloride crystals and deicer precipitates.

A comparative analysis of the type and dosage of polyol corrosion inhibitors investigated herein shows that the addition of polyol corrosion inhibitors does not cause further deterioration in the cement mortar when compared to the traditional salt brine deicer. Moreover, polyol corrosion inhibitors resulted in a relatively lower reduction in the cement mortar compressive strength when compared to the majority of the commonly used concrete corrosion inhibitors. The results obtained from this study further demonstrate that at an optimum amount (1.0% wt.) of corn-derived polyols, namely sorbitol, mannitol, and maltitol, can be added to the 23.0% wt. NaCl deicing solution without any concern for the deterioration in the properties of hardened concrete. Moreover, the addition of a similar or higher amount of these corn-derived polyols in the traditional NaCl deicing solution has been demonstrated to significantly reduce the corrosivity of the NaCl deicing solution without compromising the snow melting capacity of the NaCl deicing solution [76, 78].

6.2 Soy Protein Isolate Coatings as Secondary Coats for Rebars

Novel biobased coating is synthesized utilizing the soy protein isolate as the base material and sorbitol (a type of polyol) as the plasticizer. This coating is then evaluated for its mechanical and corrosion inhibition performance. The most important conclusion obtained from this study are as follows:

1. Soy protein coatings with 10-15% (%wt. of deionized water) SPI content and 10-30% (%wt. of SPI) corn-derived Sorbitol content render adequate properties for usage as anticorrosion coating material.
2. The FTIR results showed that heat treatment (45°C for 4 hours) and pH modification via NaOH successfully denatured soy protein dispersion and exposed the functional groups (such as amide) in the soy protein chains that imparted necessary properties for coating adhesion on the surface.
3. The increase in the SPI content in the soy protein coating increased the viscosity of the soy protein coatings which can be attributed to the increase in the solid content in the case of higher protein content. The average viscosities of soy protein coatings ranged between 2.5-27 m.Pa.s. The addition of sorbitol plasticizer leads to a slight decrease in the viscosities of the soy protein coatings which can be attributed to plasticizing and lubricating effect of polyols that enhance the mobility of macromoleclues in the SPI mixture.
4. Soy protein coatings without the inclusion of plasticizers remained highly brittle upon drying regardless of the SPI content. The addition of 10-30% sorbitol significantly reduced the visual brittleness in the cured and dried soy protein coatings which can be attributed to the improved flexibility and enhanced chain mobility in the sorbitol-based SPI coatings. The highest decrease in the brittleness is observed corresponding to the soy protein coatings with 10% and 15% SPI content, and 30% Sorbitol.

5. The increase in the concentration of sorbitol significantly enhanced the abrasion resistance of the soy protein coatings which can be attributed to the increase in the flexibility and reduced fragility in the SPI coatings containing a higher concentration of sorbitol plasticizer. The highest abrasion resistance is observed in the case of soy protein coating with 15% SPI and 30% Sorbitol (142 L/mil).
6. The potentiodynamic polarization tests showed that soy protein coatings with 10% or 15% SPI and 30% Sorbitol decreases the corrosion rates by more than 90%. The long-term corrosion rates obtained from the rapid macrocell corrosion rates showed cement mortar embedded rebars that are coated with soy protein coating (15% SPI+30%Sorbitol) incurred 50% less corrosion as compared to uncoated rebar specimens.

These results demonstrated that soy protein coatings have adequate physical and chemical characteristics for use as a supplementary protective coating material in mitigating corrosion in rebars. The proposed coating formulations can be applied in-situ to repair the damaged epoxy-coated rebars and can be used as supplementary coatings for old rebars.

6.3 Improving the Mechanical and Bond Performance of Biobased Coatings

All coatings including the biobased coatings compromise the bond with concrete. To improve the bond performance, inert oxide abrasives have been incorporated in to the coating. The following are the important conclusions of this study.

1) The viscosities of the MSP paints range between 4.1 cP and 7.2 cP, with no sign of cracking after curing. MSP-10-10-10 has the highest viscosity of 7.2 cP due to the presence of higher concentrations of all three abrasives.
2) The Control coating had an abrasion resistance of 48L/mil. On the other hand, all the MSP coatings, i.e., MSP-10-5-0, MSP-10-0-5, MSP-10-5-5, and MSP-10-10-10 exhibited negligible changes in coating thickness under abrasion and remained intact with the substrate even after exposure to 1600 liters of silicon carbide abrasive.
3) The FTIR characterization confirmed the presence of the necessary functional groups which dictate the adhesion and hydrophobicity of the coating. Moreover, comparing the FTIR curves before and after the thermal cycles test revealed no change in the placement of peaks, confirming that the ingredients of the MSP coatings are chemically compatible.
4) Results from the lap shear test (LST) showed that all the MSP coatings revealed adequate mechanical adhesion to steel plates compared to the Control coating. In comparison to the Control coating (112.65N), MSP-10-0-5 (256.63N) showed a 2-fold increase, MSP-10-5-5 (346.23N) had a 3-fold increase, and MSP-10-10-10 (481.11N) exhibited a 4-fold increase in the ultimate shear force.
5) Pullout tests at the age of 7 and 28 days showed an increase in ultimate bond strength for all the coating formulations when compared with the Control coating, which can be attributed to the increase in the coating's thickness from the infusion of abrasives. At 28 days of testing age, the ultimate bond strength increased by 51.81%, 54.4%, 55.69%, and 90.41% for MSP-10-5-0, MSP-10-0-5, MSP-10-5-5, and MSP-10-10-10, respectively.
6) The accelerated salt spray test for a duration of 240 hours showed that 75% of the Control coated plate's surface was uniformly corroded by the end of the testing period. Corrosion damage in MSP-10-5-0 was initiated after 144 hours, while the rest of the MSP coatings

i.e., MSP-10-0-5, MSP-10-5-5, and MSP-10-10-10 showed the least corrosion damage which initiated after 192 hours of salt spray.

7) The potentiodynamic polarization test that quantifies the instantaneous corrosion inhibition potential showed that MSP coatings containing abrasives reduced the current densities and the corrosion rates compared to the Control coating without abrasives by up to 94%. This improvement directly results from the stronger barrier effect offered by, the thicker MSP coatings. The percentage decrease in the corrosion rate for MSP-10-5-0, MSP-10-0-5, MSP-10-5-5, and MSP-10-10-10 is determined to be 87%, 86%, 88%, and 94%, respectively.
8) The macrocell corrosion studies quantify the long-term effectiveness of MSP coatings in protecting the rebars from corrosion. In comparison to the Control coating, MSP-10-5-0, MSP-10-0-5, MSP-10-5-5, and MSP-10-10-10 mitigate the corrosion of rebars by 18%, 30%, 50%, and 78%, respectively.

This research concludes that the investigated MSP coatings have the potential for mitigating corrosion without compromising bond performance, primarily due to the thick physical barrier resulting from the infusion of abrasives in the coatings. Furthermore, these findings suggest that MSP coatings can be effectively considered for standalone applications in reinforced concrete structures and also as a repair material for damaged epoxy-coated rebars.

6.4 Recommendations for Future Studies

The following are the recommendations for future research:

1) *Extend the shelf-life of biobased coatings*: Although the current study found the coatings to remain fresh for 3 months after synthesis, it is crucial to explore the performance of biobased paints aged beyond 6 – 12 months in future studies.
2) *Standardize the painting procedure*: While dip coating was used in this research project, it is important to explore other coating methods, particularly spray coating, as it offers a practical approach for field application of these paints.
3) *Explore concrete seals*: In addition to rebars, further exploration of these coatings as sealants for concrete pavements can be valuable to prevent chloride ion ingress during winter, while maintaining skid resistance.
4) *Conduct field testing and real-world application*: It is crucial to conduct field trials to evaluate the performance of biobased coatings on rebars in real-world environments, collaborating with industry partners to implement these systems in actual infrastructure projects and monitor their long-term effectiveness.
5) *Investigate compatibility with conventional protective systems*: To facilitate practical implementation, it is essential to investigate the compatibility of biobased coatings with existing corrosion protection systems such as epoxy coatings or galvanization. Research should focus on developing strategies to effectively combine or integrate biobased coatings with traditional methods, thereby enhancing corrosion resistance.

By following these recommendations, future research can make significant advancements in the development and practical application of biobased coatings for mitigating corrosion in rebars.

References

[1] American Society of Civil Engineers, "2017 Infrastructure Report Card: A comprehensive assessment of America's Infrastructure," *ASCE*, p. 111, 2017, [Online]. Available: https://www.infrastructurereportcard.org/

[2] M. Craighead, "A Comparison of Highway Construction Costs in the Midwest and Nationally," pp. 1–9, 2018, [Online]. Available: https://midwestepi.files.wordpress.com/2017/05/cost-per-lane-mile-nationally-and-in-the-midwest-updated-final.pdf

[3] A. Poursaee, *Corrosion of steel in concrete structures*. Elsevier Ltd, 2016. doi: 10.1016/B978-1-78242-381-2.00002-X.

[4] ACI Committee 222, "Protection of Metals in Concrete Against Corrosion," *Aci 222R-01*, pp. 1–41, 2001.

[5] ŠTAMPAJ, "Pourbaix diagram (stability diagram)," 1963, [Online]. Available: http://www.uobabylon.edu.iq/eprints/publication_12_18276_228.pdf

[6] Y. Zhou, B. Gencturk, K. Willam, and A. Attar, "Carbonation-Induced and Chloride-Induced Corrosion in Reinforced Concrete Structures," *J. Mater. Civ. Eng.*, vol. 27, no. 9, 2015, doi: 10.1061/(asce)mt.1943-5533.0001209.

[7] a276, "Standard Specification for Stainless Steel Bars and Shapes," *ASTM Int.*, vol. 10, pp. 1–7, 2012, doi: 10.1520/A0276.

[8] B. Fotovvati, N. Namdari, and A. Dehghanghadikolaei, "On coating techniques for surface protection: A review," *J. Manuf. Mater. Process.*, vol. 3, no. 1, 2019, doi: 10.3390/jmmp3010028.

[9] M. Criado, D. M. Bastidas, S. Fajardo, A. Fernández-Jiménez, and J. M. Bastidas, "Corrosion behaviour of a new low-nickel stainless steel embedded in activated fly ash mortars," *Cem. Concr. Compos.*, vol. 33, no. 6, pp. 644–652, 2011, doi: 10.1016/j.cemconcomp.2011.03.014.

[10] N. A. Farhan, M. N. Sheikh, and M. N. S. Hadi, "Experimental Investigation on the Effect of Corrosion on the Bond Between Reinforcing Steel Bars and Fibre Reinforced Geopolymer Concrete," *Structures*, vol. 14, no. March, pp. 251–261, 2018, doi: 10.1016/j.istruc.2018.03.013.

[11] Z. Zhou and P. Qiao, "Bond behavior of epoxy-coated rebar in ultra-high performance concrete," *Constr. Build. Mater.*, vol. 182, pp. 406–417, 2018, doi: 10.1016/j.conbuildmat.2018.06.113.

[12] A. Afshar, S. Jahandari, H. Rasekh, M. Shariati, A. Afshar, and A. Shokrgozar, "Corrosion resistance evaluation of rebars with various primers and coatings in concrete modified with different additives," *Constr. Build. Mater.*, vol. 262, p. 120034, 2020, doi: 10.1016/j.conbuildmat.2020.120034.

[13] M. Li, T. Su, Y. Chen, H. He, and X. Yang, "Salt spray aging effects on dynamic responses and failure characteristics of hybrid bonded-riveted CFRP/Al joints under high speed loading," *J. Manuf. Process.*, vol. 72, no. September, pp. 582–593, 2021, doi: 10.1016/j.jmapro.2021.10.048.

[14] Y. Li *et al.*, "A review on durability of basalt fiber reinforced concrete," *Compos. Sci. Technol.*, vol. 225, no. May, p. 109519, 2022, doi: 10.1016/j.compscitech.2022.109519.

[15] T. Ayub, N. Shafiq, and M. F. Nuruddin, "Mechanical properties of high-performance concrete reinforced with basalt fibers," *Procedia Eng.*, vol. 77, pp. 131–139, 2014, doi: 10.1016/j.proeng.2014.07.029.

[16] M. Ormellese, L. Lazzari, S. Goidanich, G. Fumagalli, and A. Brenna, "A study of organic substances as inhibitors for chloride-induced corrosion in concrete," *Corros. Sci.*, vol. 51, no. 12, pp. 2959–2968, 2009, doi: 10.1016/j.corsci.2009.08.018.

[17] M. I. Prieto, A. Cobo, Á. Rodríguez, and M. D. L. N. González, "The efficiency of surface-applied corrosion inhibitors as a method for the repassivation of corroded reinforcement bars embedded in ladle furnace slag mortars," *Constr. Build. Mater.*, vol. 54, pp. 70–77, 2014, doi: 10.1016/j.conbuildmat.2013.12.014.

[18] C. L. Page, V. T. Ngala, and M. M. Page, "Corrosion inhibitors in concrete repair systems," *Mag. Concr. Res.*, vol. 52, no. 1, pp. 25–37, 2000, doi: 10.1680/macr.2000.52.1.25.

[19] H.-S. Lee, V. Saraswathy, S.-J. Kwon, and S. Karthick, "Corrosion Inhibitors for Reinforced Concrete: A Review," *Corros. Inhib. Princ. Recent Appl.*, 2018, doi: 10.5772/intechopen.72572.

[20] V. Saraswathy and H. W. Song, "Improving the durability of concrete by using inhibitors," *Build. Environ.*, vol. 42, no. 1, pp. 464–472, 2007, doi: 10.1016/j.buildenv.2005.08.003.

[21] H. W. Song and V. Saraswathy, "Analysis of corrosion resistance behavior of inhibitors in concrete using electrochemical techniques," *Met. Mater. Int.*, vol. 12, no. 4, pp. 323–329, 2006, doi: 10.1007/BF03027549.

[22] A. Poursaee, *Corrosion protection methods of steel in concrete*. Elsevier Ltd, 2016. doi: 10.1016/B978-1-78242-381-2.00012-2.

[23] N. G. Thompson, M. Yunovich, D. R. Lankard, and L. M. Laboratories, "Procedures for Evaluating Corrosion-Inhibiting Admixtures for Structural Concrete(NCHRP-W29)," *NCHRP Web Doc.*, vol. 29, no. June, 2000.

[24] C. Venkatesh, S. K. Mohiddin, and N. Ruben, *Corrosion inhibitors behaviour on reinforced concrete—A Review*, vol. 25. Springer Singapore, 2019. doi: 10.1007/978-981-13-3317-0_11.

[25] A. Zomorodian, R. Bagonyi, and A. Al-Tabbaa, "The efficiency of eco-friendly corrosion inhibitors in protecting steel reinforcement," *J. Build. Eng.*, vol. 38, no. December 2020, p. 102171, 2021, doi: 10.1016/j.jobe.2021.102171.

[26] D. F. Griffin, "Corrosion inhibitors for reinforced concrete," *Am. Concr. Institute, ACI Spec. Publ.*, vol. SP-049, pp. 95–102, 1975, doi: 10.5772/intechopen.72772.

[27] M. Büchler, *Corrosion inhibitors for reinforced concrete*. Woodhead Publishing Limited, 2005. doi: 10.1533/9781845690434.190.

[28] A. Jupri, "No Title{$μ$}{\'$α$}{$νατζμεντ$}," *Rev Reprod*, vol. 28, no. October, p. 226765, 1998.

[29] K. Y. Ann, H. S. Jung, H. S. Kim, S. S. Kim, and H. Y. Moon, "Effect of calcium nitrite-

based corrosion inhibitor in preventing corrosion of embedded steel in concrete," *Cem. Concr. Res.*, vol. 36, no. 3, pp. 530–535, 2006, doi: 10.1016/j.cemconres.2005.09.003.

[30] G. De Schutter and L. Luo, "Effect of corrosion inhibiting admixtures on concrete properties," *Constr. Build. Mater.*, vol. 18, no. 7, pp. 483–489, 2004, doi: 10.1016/j.conbuildmat.2004.04.001.

[31] M. C. Brown, N. S. Berke, T. E. Cousins, and J. C. Duke, "Assessment of Commercial Corrosion Inhibiting Admixtures Admixtures for Reinforced Concrete," 1999.

[32] R. E. Weyers and M. M. Sprinkel, "CONTRACT REPORT PERFORMANCE EVALUATION IN CONCRETE EXPOSURE SPECIMENS Virginia Polytechnic Institute," *Virginia Transp. Res. Counc.*, no. January 2018, 1999.

[33] M. C. Brown, R. E. Weyers, and M. M. Sprinkel, "Effect of corrosion-inhibiting admixtures on material properties of concrete," *ACI Mater. J.*, vol. 98, no. 3, pp. 240–250, 2001, doi: 10.14359/10279.

[34] A.H Mohyedeein, "No 主観的健康感を中心とした在宅高齢者における 健康関連指標に関する共分散構造分析Title," *Mod. large Cult. Dimens. Glob.*, vol. 26, no. 1980, pp. 3–41, 1996, [Online]. Available: http://dx.doi.org/10.1016/j.cirp.2016.06.001%0Ahttp://dx.doi.org/10.1016/j.powtec.2016.12.055%0Ahttps://doi.org/10.1016/j.ijfatigue.2019.02.006%0Ahttps://doi.org/10.1016/j.matlet.2019.04.024%0Ahttps://doi.org/10.1016/j.matlet.2019.127252%0Ahttp://dx.doi.o

[35] T. A. Söylev and M. G. Richardson, "Corrosion inhibitors for steel in concrete: State-of-the-art report," *Constr. Build. Mater.*, vol. 22, no. 4, pp. 609–622, 2008, doi: 10.1016/j.conbuildmat.2006.10.013.

[36] H. U. Sajid, A. Jalal, R. Kiran, and A. Al-Rahim, "A survey on the effects of deicing materials on properties of Cement-based materials," *Constr. Build. Mater.*, vol. 319, no. December, 2022, doi: 10.1016/j.conbuildmat.2021.126062.

[37] K. Wang, D. E. Nelsen, and W. A. Nixon, "Damaging effects of deicing chemicals on concrete materials," *Cem. Concr. Compos.*, vol. 28, no. 2, pp. 173–188, 2006, doi: 10.1016/j.cemconcomp.2005.07.006.

[38] X. Shi, M. Akin, T. Pan, L. Fay, Y. Liu, and Z. Yang, "Deicer Impacts on Pavement Materials: Introduction and Recent Developments," *Open Civ. Eng. J.*, vol. 3, no. 1, pp. 16–27, 2009, doi: 10.2174/1874149500903010016.

[39] P. Carbon-, P. Low-, and P. Examinations, "Standard Specification for Epoxy-Coated Steel Reinforcing Bars 1," pp. 1–11, doi: 10.1520/A0775.

[40] I. Mohammadi, T. Shahrabi, M. Mahdavian, and M. Izadi, "Construction of an epoxy coating with excellent protection performance on the AA 2024-T3 using ion-exchange materials loaded with eco-friendly corrosion inhibitors," *Prog. Org. Coatings*, vol. 166, no. August 2021, p. 106786, 2022, doi: 10.1016/j.porgcoat.2022.106786.

[41] R. R. Lucas *et al.*, "Progress in Organic Coatings Bio-based one-component epoxy resin : Novel high-performance anticorrosive coating from agro-industrial byproduct," vol. 167, no. October 2021, 2022, doi: 10.1016/j.porgcoat.2022.106861.

[42] G. Zhang, Q. Xie, C. Ma, and G. Zhang, "Permeable epoxy coating with reactive solvent for

anticorrosion of concrete," *Prog. Org. Coatings*, vol. 117, no. December 2017, pp. 29–34, 2018, doi: 10.1016/j.porgcoat.2017.12.018.

[43] J. J. Chang, W. Yeih, and C. L. Tsai, "Enhancement of bond strength for epoxy-coated rebar using river sand," *Constr. Build. Mater.*, vol. 16, no. 8, pp. 465–472, 2002, doi: 10.1016/S0950-0618(02)00101-0.

[44] M. M. S. Cheung and C. Cao, "Application of cathodic protection for controlling macrocell corrosion in chloride contaminated RC structures," *Constr. Build. Mater.*, vol. 45, pp. 199–207, 2013, doi: 10.1016/j.conbuildmat.2013.04.010.

[45] Y. Sang *et al.*, "Synthetic polyaniline-boron nitride-aqueous epoxy resin composite coating for improving the corrosion resistance of hot-dip galvanized steel plates," *Appl. Surf. Sci.*, vol. 592, no. November 2021, p. 153229, 2022, doi: 10.1016/j.apsusc.2022.153229.

[46] N. Sharma, S. Sharma, S. K. Sharma, and R. Mehta, "Evaluation of corrosion inhibition and self healing capabilities of nanoclay and tung oil microencapsulated epoxy coatings on rebars in concrete," *Constr. Build. Mater.*, vol. 259, p. 120278, 2020, doi: 10.1016/j.conbuildmat.2020.120278.

[47] M. Rosenqvist, *Frost-induced deterioration of concrete in hydraulic structures Interactions between water absorption, leaching and frost action*. 2017. [Online]. Available: www.energiforsk.se

[48] T. C. Powers, "Freezing Effects in Concrete," *ACI Symp. Publ.*, vol. 47, doi: 10.14359/17603.

[49] J. J. Valenza and G. W. Scherer, "A review of salt scaling: II. Mechanisms," *Cem. Concr. Res.*, vol. 37, no. 7, pp. 1022–1034, 2007, doi: 10.1016/j.cemconres.2007.03.003.

[50] M. Holický and J. Kolísko, "Service life of concrete structures," *Solid State Phenom.*, vol. 309 SSP, pp. 267–271, 2020, doi: 10.4028/www.scientific.net/SSP.309.267.

[51] Kesler, "No Title البنك الاسلامي," vol. 21, no. 4, p. 162, 1985.

[52] S. Chatterji, "Mechanism of the CaCl2 attack on portland cement concrete," *Cem. Concr. Res.*, vol. 8, no. 4, pp. 461–467, 1978, doi: 10.1016/0008-8846(78)90026-1.

[53] L. Sutter, T. Van Dam, K. R. Peterson, and D. P. Johnston, "Long-term effects of magnesium chloride and other concentrated salt solutions on pavement and structural portland cement concrete phase I results," *Transp. Res. Rec.*, no. 1979, pp. 60–68, 2006, doi: 10.3141/1979-10.

[54] J. Monical, C. Villani, Y. Farnam, E. Unal, and W. J. Weiss, "Using low-temperature differential scanning calorimetry to quantify calcium oxychloride formation for cementitious materials in the presence of calcium chloride," *Adv. Civ. Eng. Mater.*, vol. 5, no. 2, pp. 142–156, 2016, doi: 10.1520/ACEM20150024.

[55] Fhwa, "Chemical Deicers and Concrete Pavement: Impacts and Mitigation," no. March, 2018.

[56] W. Kurdowski, "The protective layer and decalcification of C-S-H in the mechanism of chloride corrosion of cement paste," *Cem. Concr. Res.*, vol. 34, no. 9, pp. 1555–1559, 2004, doi: 10.1016/j.cemconres.2004.03.023.

[57] G. Frigione and R. Sersale, “The action of some aggressve solutions on Portland, pozzolanic and blastfurnace slag cement mortars,” *Cem. Concr. Res.*, vol. 19, no. 6, pp. 885–893, 1989, doi: 10.1016/0008-8846(89)90101-4.

[58] “Experimential Deterioration of Highway Concrete By Chloride Salt -1996.”

[59] K. P. Verian, P. Panchmatia, J. Olek, and T. Nantung, “Pavement concrete with air-cooled blast furnace slag and dolomite as coarse aggregates: Effects of deicers and freeze-thaw cycles,” *Transp. Res. Rec.*, vol. 2508, no. 8, pp. 55–64, 2015, doi: 10.3141/2508-07.

[60] J. Weiss, “Concrete Pavement Joint Deterioration : Recent Findings to Reduce the Potential for Damage,” no. June, pp. 1–6, 2015.

[61] J. Duchesne and M. A. Bérubé, “Effect of the cement chemistry and the sample size on ASR expansion of concrete exposed to salt,” *Cem. Concr. Res.*, vol. 33, no. 5, pp. 629–634, 2003, doi: 10.1016/S0008-8846(02)01041-4.

[62] A. Mathematics, “**済無**No Title No Title No Title,” vol. 27, no. 1, pp. 1–23, 2016.

[63] E. S. Sumsion and W. S. Guthrie, “Physical and Chemical Effects of Deicers on Concrete Pavement: Litarature Review,” *UDOT Res.*, no. UT-13.09, pp. 1–42, 2013.

[64] S. Chatterji, “Chemistry of alkali-silica reaction and testing of aggregates,” *Cem. Concr. Compos.*, vol. 27, no. 7–8, pp. 788–795, 2005, doi: 10.1016/j.cemconcomp.2005.03.005.

[65] C. Giebson, K. Seyfarth, and H.-M. Ludwig, “Influence of sodium chloride on ASR in highway pavement concrete,” *15th Int. Conf. Alkali-Aggregate React. Concr.*, p. 10, 2016.

[66] M. Kawamura and K. Takeuchi, “Alkali-silica reaction and pore solution composition in mortars in sea water,” *Cem. Concr. Res.*, vol. 26, no. 12, pp. 1809–1819, 1996, doi: 10.1016/S0008-8846(96)00178-0.

[67] C. Giebson, K. Seyfarth, and J. Stark, “Influence of acetate and formate-based deicers on ASR in airfield concrete pavements,” *Cem. Concr. Res.*, vol. 40, no. 4, pp. 537–545, 2010, doi: 10.1016/j.cemconres.2009.09.009.

[68] M. Kawamura, K. Takeuchi, and A. Sugiyama, “Mechanisms of expansion of mortars containing reactive aggregate in NaCl solution,” *Cem. Concr. Res.*, vol. 24, no. 4, pp. 621–632, 1994, doi: 10.1016/0008-8846(94)90186-4.

[69] and W. C. P. Steven H. Kosmatka, Beatrix Kerkhoff, S. H. Kosmatka, B. Kerkhoff, and W. C. Panarese, *Design and Control Design and Control of*. 2002.

[70] K. P. Verian and A. Behnood, “Effects of deicers on the performance of concrete pavements containing air-cooled blast furnace slag and supplementary cementitious materials,” *Cem. Concr. Compos.*, vol. 90, pp. 27–41, 2018, doi: 10.1016/j.cemconcomp.2018.03.009.

[71] M. L. KOSMATKA, Steven H.; WILSON, *Design and Control of Concrete Mixtures – The Guide to Applications, Methods and Materials.* 2011.

[72] M. C. Santagata and M. Collepardi, “Effect of CMA deicers on concrete properties,” *Cem. Concr. Res.*, vol. 30, no. 9, pp. 1389–1394, 2000, doi: 10.1016/S0008-8846(00)00334-3.

[73] C. Luigi, “M . Collepardi , L . Coppola , C . Pistolesi , ‘ Durability of Concrete Structures Exposed to CaCl2 Based Deicing Salts ,’” no. January 1994, 2014.

[74] GEO, “No TitleВорона,” *Птицы*, vol. 1, no. 2, pp. 12–17, 1988.

[75] M. Fischel, “EVALUATION OF SELECTED DEICERS BASED ON A REVIEW OF THE LITERATURE Marion Fischel COLORADO DEPARTMENT OF TRANSPORTATION,” 2001.

[76] H. U. Sajid, R. Kiran, X. Qi, D. S. Bajwa, and D. Battocchi, “Employing corn derived products to reduce the corrosivity of pavement deicing materials,” *Constr. Build. Mater.*, vol. 263, p. 120662, 2020, doi: 10.1016/j.conbuildmat.2020.120662.

[77] K. Nilssen, A. Klein-Paste, and J. Wåhlin, “The Effect of Additives on the Low Temperature Ice-Melting Capacity of NaCl,” *Transp. Res. Rec.*, vol. 2672, no. 12, pp. 158–166, 2018, doi: 10.1177/0361198118767412.

[78] H. Ullah Sajid, D. L. Naik, and R. Kiran, “Improving the ice-melting capacity of traditional deicers,” *Constr. Build. Mater.*, vol. 271, no. October, 2021, doi: 10.1016/j.conbuildmat.2020.121527.

[79] T. Abbas, D. N. Lavadiya, and R. Kiran, “Exploring the use of polyols, corn, and beet juice for decreasing the freezing point of brine solution for deicing of pavements,” *Sustain.*, vol. 13, no. 11, 2021, doi: 10.3390/su13115765.

[80] R. K. Yellavajjala, D. N. Lavadiya, and H. U. Sajid, *Corn-Based Deicers (Final Report for IHRB Project TR-754*, no. July. 2020. [Online]. Available: https://orcid.org/0000-0002-2370-8592

[81] S. Xianming, M. Laura Fay, Chase Gallaway, Kevin Volkening, C. L. M. Peterson, Tongyan Pan, Andrew Creighton, and and T. A. N. Stephanie Mumma, Yajun Liu, “Evaluation of Alternative Anti-Icing and Deicing Compounds Using Sodium Chloride and Magnesium Chloride as Baseline Deicers - Phase I,” *Color. Dep. Transp. DTD Appl. Res. Innov. Branch.*, no. February, pp. 4,105-142, 2009.

[82] W. A. Nixon, “Economics of Using Calcium Chloride vs. Sodium Chloride for Deicing/Anti-Icing,” no. February, p. 43, 2008.

[83] L. Fay and X. Shi, “Environmental impacts of chemicals for snow and ice control: State of the knowledge,” *Water. Air. Soil Pollut.*, vol. 223, no. 5, pp. 2751–2770, 2012, doi: 10.1007/s11270-011-1064-6.

[84] R. D. Cody, P. G. Spry, A. M. Cody, and G. Gan, “the Role of Magnesium in,” no. November, 1994.

[85] “(Refereed) (Received May 17; in final form November 28.1994),” vol. 25, no. 3, pp. 617–626, 1995.

[86] W. T. Institute, “Field Usage of Alternative Deicers for Snow and Ice Control,” *Transp. Res. Synth.*, vol. 1706, no. September, pp. 1–24, 2017.

[87] S. Sajid and L. Chouinard, “Impulse response test for condition assessment of concrete: A review,” *Constr. Build. Mater.*, vol. 211, pp. 317–328, 2019, doi: 10.1016/j.conbuildmat.2019.03.174.

[88] D. Darwin, J. A. Browning, L. Gong, and S. R. Hughes, “Effects of deicers on concrete deterioration,” *ACI Mater. J.*, vol. 105, no. 6, pp. 622–627, 2008, doi: 10.14359/20204.

[89] H. Egüez Álava, N. De Belie, and G. De Schutter, "Proposed mechanism for the formation of oxychloride crystals during sodium chloride application as a deicer salt in carbonated concrete," *Constr. Build. Mater.*, vol. 109, pp. 188–197, 2016, doi: 10.1016/j.conbuildmat.2016.01.047.

[90] P. Reiterman and M. Keppert, "Effect of various de-icers containing chloride ions on scaling resistance and chloride penetration depth of highway concrete," *Roads Bridg. - Drog. i Most.*, vol. 19, no. 1, pp. 51–64, 2020, doi: 10.7409/rabdim.020.003.

[91] R. Şahin, M. A. Taşdemir, R. Gül, and C. Çelik, "Determination of the optimum conditions for de-icing salt scaling resistance of concrete by visual examination and surface scaling," *Constr. Build. Mater.*, vol. 24, no. 3, pp. 353–360, 2010, doi: 10.1016/j.conbuildmat.2009.08.026.

[92] F. Matalkah and P. Soroushian, "Freeze thaw and deicer salt scaling resistance of concrete prepared with alkali aluminosilicate cement," *Constr. Build. Mater.*, vol. 163, pp. 200–213, 2018, doi: 10.1016/j.conbuildmat.2017.12.119.

[93] "s11527-006-9104-1."

[94] S. Chandra, R. Kumar, S. Kaushik, and S. Kaul, "Thermal performance of a non-air-conditioned building with PCCM thermal storage wall," *Energy Convers. Manag.*, vol. 25, no. 1, pp. 15–20, 1985, doi: 10.1016/0196-8904(85)90064-0.

[95] J. L. Provis and J. S. J. van Deventer, *Geopolymers: Structures, Processing, Properties and Industrial Applications*. Woodhead Publishing, 2009. [Online]. Available: https://books.google.com/books?id=zdpNPgAACAAJ

[96] J. Jain, J. Olek, A. Janusz, and D. Jozwiak-Niedzwiedzka, "Effects of deicing salt solutions on physical properties of pavement concretes," *Transp. Res. Rec.*, no. 2290, pp. 69–75, 2012, doi: 10.3141/2290-09.

[97] K. Shomglin, L. Turanli, H. R. Wenk, P. J. M. Monteiro, and G. Sposito, "The effects of potassium and rubidium hydroxide on the alkali-silica reaction," *Cem. Concr. Res.*, vol. 33, no. 11, pp. 1825–1830, 2003, doi: 10.1016/S0008-8846(03)00204-7.

[98] L. Berntsson and S. Chandra, "Damage of concrete sleepers by calcium chloride," *Cem. Concr. Res.*, vol. 12, no. 1, pp. 87–92, 1982, doi: 10.1016/0008-8846(82)90102-8.

[99] R. G. and M. Pigeon, "Deicer Salt Scaling Resistance of High-Performance Concrete," *ACI Symp. Publ.*, vol. 122, doi: 10.14359/2444.

[100] J. W. Jang, M. G. Hagen, G. M. Engstrom, and I. Iwasaki, "Cl-, SO42-, and PO43- distribution in concrete slabs ponded by corrosion-inhibitor-added deicing salts," *Adv. Cem. Based Mater.*, vol. 8, no. 3–4, pp. 101–107, 1998, doi: 10.1016/S1065-7355(98)00012-1.

[101] Y. Hassan, A. O. Abd El Halim, A. G. Razaqpur, W. Bekheet, and M. H. Farha, "Effects of runway deicers on pavement materials and mixes: Comparison with road salt," *J. Transp. Eng.*, vol. 128, no. 4, pp. 385–391, 2002, doi: 10.1061/(ASCE)0733-947X(2002)128:4(385).

[102] M. A. Bérubé, J. F. Dorion, J. Duchesne, B. Fournier, and D. Vézina, "Laboratory and field investigations of the influence of sodium chloride on alkali-silica reactivity," *Cem.*

Concr. Res., vol. 33, no. 1, pp. 77–84, 2003, doi: 10.1016/S0008-8846(02)00926-2.

[103] P. Rangaraju, K. Sompura, and J. Olek, "Investigation into Potential of Alkali-Acetate-Based Deicers to Cause Alkali-Silica Reaction in Concrete," *Transp. Res. Rec.*, vol. 1979, pp. 69–78, Jan. 2006, doi: 10.3141/1979-11.

[104] G. Skripkiunas, D. Nagrockiene, G. Girskas, M. Vaičiene, and E. Baranauskaite, "The cement type effect on freeze - Thaw and deicing salt resistance of concrete," *Procedia Eng.*, vol. 57, pp. 1045–1051, 2013, doi: 10.1016/j.proeng.2013.04.132.

[105] A. Poursaee, A. Laurent, and C. M. Hansson, "Corrosion of steel bars in OPC mortar exposed to NaCl, MgCl2 and CaCl2: Macro- and micro-cell corrosion perspective," *Cem. Concr. Res.*, vol. 40, no. 3, pp. 426–430, 2010, doi: 10.1016/j.cemconres.2009.09.029.

[106] X. Shi, Y. Liu, M. Mooney, B. Hubbard, L. Fay, and A. Leonard, "Effect of Chloride-based Deicers on Reinforced Concrete Structures," no. July, p. 86, 2010, [Online]. Available: https://rosap.ntl.bts.gov/view/dot/23879

[107] N. Xie, X. Shi, and Y. Zhang, "Impacts of Potassium Acetate and Sodium-Chloride Deicers on Concrete," *J. Mater. Civ. Eng.*, vol. 29, no. 3, pp. 1–10, 2017, doi: 10.1061/(asce)mt.1943-5533.0001754.

[108] B. D. Lee, Y. S. Choi, Y. G. Kim, I. S. Kim, and E. I. Yang, "A comparison study of performance and environmental impacts of chloride-based deicers and eco-label certified deicers in South Korea," *Cold Reg. Sci. Technol.*, vol. 143, no. August, pp. 43–51, 2017, doi: 10.1016/j.coldregions.2017.08.010.

[109] Z. Wu, C. Shi, P. Gao, D. Wang, and Z. Cao, "Effects of Deicing Salts on the Scaling Resistance of Concrete," *J. Mater. Civ. Eng.*, vol. 27, no. 5, pp. 1–11, 2015, doi: 10.1061/(asce)mt.1943-5533.0001106.

[110] H. E. Cutler, K. Wang, V. R. Schaefer, and J. T. Kevern, "Resistance of portland cement pervious concrete to deicing chemicals," *Transp. Res. Rec.*, no. 2164, pp. 98–104, 2010, doi: 10.3141/2164-13.

[111] J. Kim, J. H. Moon, J. W. Shim, J. Sim, H. G. Lee, and G. Zi, "Durability properties of a concrete with waste glass sludge exposed to freeze-and-thaw condition and de-icing salt," *Constr. Build. Mater.*, vol. 66, pp. 398–402, 2014, doi: 10.1016/j.conbuildmat.2014.05.081.

[112] Y. Farnam, H. Todak, R. Spragg, and J. Weiss, "Electrical response of mortar with different degrees of saturation and deicing salt solutions during freezing and thawing," *Cem. Concr. Compos.*, vol. 59, pp. 49–59, 2015, doi: 10.1016/j.cemconcomp.2015.03.003.

[113] H. U. Sajid, R. Kiran, and D. S. Bajwa, "Effect of agro-derived corrosion inhibitors on the properties of Portland cement mortar," *Constr. Build. Mater.*, vol. 310, no. June, p. 125236, 2021, doi: 10.1016/j.conbuildmat.2021.125236.

[114] S. Goñi and A. Guerrero, "Accelerated carbonation of Friedel's salt in calcium aluminate cement paste," *Cem. Concr. Res.*, vol. 33, no. 1, pp. 21–26, 2003, doi: 10.1016/S0008-8846(02)00910-9.

[115] ASTMC109/109M-08, "Standard test method for compressive strength of hydraulic cement mortars (Using 2-in. or cube specimens)," *Annu. B. ASTM Stand.*, pp. 1–10, 2016,

doi: 10.1520/C0109.

[116] N. Hoivik *et al.*, “Long-term performance results of concrete-based modular thermal energy storage system,” *J. Energy Storage*, vol. 24, 2019, doi: 10.1016/j.est.2019.04.009.

[117] A. Goyal, E. Ganjian, H. S. Pouya, and M. Tyrer, “Inhibitor efficiency of migratory corrosion inhibitors to reduce corrosion in reinforced concrete exposed to high chloride environment,” *Constr. Build. Mater.*, vol. 303, no. August, p. 124461, 2021, doi: 10.1016/j.conbuildmat.2021.124461.

[118] Z. Liu, “Frost deterioration in concrete due to deicing salt exposure: mechanism, mitigation and conceptual surface scaling model,” *Dr. Diss.*, 2014.

[119] N. ANNET and J. Naranjo, “No 主観的健康感を中心とした在宅高齢者における 健康関連指標に関する共分散構造分析Title,” *Appl. Microbiol. Biotechnol.*, vol. 85, no. 1, pp. 2071–2079, 2014.

[120] H. Lee, R. D. Cody, a M. Cody, and P. G. Spry, “Effects of Various Deicing Chemicals on Pavement Concrete Deterioration,” *Proc. Mid-Continent Transp. Symp.*, pp. 151–155, 2000.

[121] Y. Lee, S. Lim, and H. Lee, “Chloride Resistance of Portland Cement-Based Mortar Incorporating High Aluminate Cement and Calcium Carbonate.,” *Mater. (Basel, Switzerland)*, vol. 13, no. 2, Jan. 2020, doi: 10.3390/ma13020359.

[122] S. Cheng, Z. Shui, X. Gao, J. Lu, T. Sun, and R. Yu, “Degradation progress of Portland cement mortar under the coupled effects of multiple corrosive ions and drying-wetting cycles,” *Cem. Concr. Compos.*, vol. 111, no. April, p. 103629, 2020, doi: 10.1016/j.cemconcomp.2020.103629.

[123] N. America, “N Ights,” no. November, pp. 46–47, 2014.

[124] D. G. Manning, “Corrosion performance of epoxy-coated reinforcing steel: North American experience,” *Constr. Build. Mater.*, vol. 10, no. 5 SPEC. ISS., pp. 349–365, 1996, doi: 10.1016/0950-0618(95)00028-3.

[125] A. Mathematics, “済無No Title No Title No Title,” no. June, pp. 1–23, 2016.

[126] D. D. L. Chung, “Corrosion Control of Steel-Reinforced Concrete,” vol. 9, no. April, pp. 585–588, 2000.

[127] J. L. Smith and Y. P. Virmani, “Materials and Methods for Corrosion Control of Reinforced and Prestressed Concrete Structures in New Construction,” *Fed. Highw. Adm. U.S. Dep. Transp.*, no. FHWA-RD-00-081, p. 82, 2000, [Online]. Available: https://www.fhwa.dot.gov/publications/research/infrastructure/structures/00081.pdf

[128] H. U. Sajid and R. Kiran, “Improving the wettability of structural steels by employing ionic liquids,” *J. Mol. Liq.*, vol. 324, p. 115137, 2021, doi: 10.1016/j.molliq.2020.115137.

[129] X. F. and D. D. L. C. Jiangyuan Hou, “Improving Both Bond Strength and Corrosion Resistance,” vol. 27, no. 5, pp. 679–684, 1997.

[130] H. U. Sajid and R. Kiran, “Influence of corrosion and surface roughness on wettability of ASTM A36 steels,” *J. Constr. Steel Res.*, vol. 144, pp. 310–326, 2018, doi: 10.1016/j.jcsr.2018.01.023.

[131] M. H. Nazari, M. S. Shihab, L. Cao, E. A. Havens, and X. Shi, “A peony-leaves-derived liquid corrosion inhibitor: Protecting carbon steel from NaCl,” *Green Chem. Lett. Rev.*, vol. 10, no. 4, pp. 359–379, 2017, doi: 10.1080/17518253.2017.1388446.

[132] M. Honarvar Nazari, E. A. Havens, A. Muthumani, and X. Shi, “Effects of Processed Agro-Residues on the Performance of Sodium Chloride Brine Anti-Icer,” *ACS Sustain. Chem. Eng.*, vol. 7, no. 16, pp. 13655–13667, 2019, doi: 10.1021/acssuschemeng.8b06043.

[133] M. H. Nazari and X. Shi, “Developing Renewable Agro-Based Anti-Icers for Sustainable Winter Road Maintenance Operations,” *J. Mater. Civ. Eng.*, vol. 31, no. 12, pp. 1–13, 2019, doi: 10.1061/(asce)mt.1943-5533.0002963.

[134] M. Aliofkhazraei, Ed., “Corrosion Inhibitors, Principles and Recent Applications.” IntechOpen, Rijeka, 2018. doi: 10.5772/intechopen.70101.

[135] N. Krishnan, D. K. Kamde, Z. Doosa Veedu, R. G. Pillai, D. Shah, and R. Velayudham, “Long-term performance and life-cycle-cost benefits of cathodic protection of concrete structures using galvanic anodes,” *J. Build. Eng.*, vol. 42, no. March, p. 102467, 2021, doi: 10.1016/j.jobe.2021.102467.

[136] M. Su, L. Wei, J.-H. Zhu, T. Ueda, G. Guo, and F. Xing, “Combined Impressed Current Cathodic Protection and FRCM Strengthening for Corrosion-Prone Concrete Structures,” *J. Compos. Constr.*, vol. 23, no. 4, pp. 1–11, 2019, doi: 10.1061/(asce)cc.1943-5614.0000949.

[137] C. Zhang and F. Zhang, “Incorporation of silicon fume and fly ash as partial replacement of portland cement in reinforced concrete: Electrochemical study on corrosion behavior of 316lN stainless steel rebar,” *Int. J. Electrochem. Sci.*, vol. 15, pp. 3740–3741, 2020, doi: 10.20964/2020.05.77.

[138] R. G. Duarte, A. S. Castela, R. Neves, L. Freire, and M. F. Montemor, “Corrosion behavior of stainless steel rebars embedded in concrete: An electrochemical impedance spectroscopy study,” *Electrochim. Acta*, vol. 124, pp. 218–224, 2014, doi: 10.1016/j.electacta.2013.11.154.

[139] P. Gu, S. Elliott, J. J. Beaudoin, and B. Arsenault, “Corrosion resistance of stainless steel in chloride contaminated concrete,” *Cem. Concr. Res.*, vol. 26, no. 8, pp. 1151–1156, 1996, doi: 10.1016/0008-8846(96)00110-X.

[140] S. Nandhini and M. Devasena, “Review on Graphene Oxide Composites,” *Int. J. Nanomater. Nanostructures*, vol. 2, no. June 2016, p. 1, 2016, [Online]. Available: www.journalspub.com

[141] Y. Cubides and H. Castaneda, “Corrosion protection mechanisms of carbon nanotube and zinc-rich epoxy primers on carbon steel in simulated concrete pore solutions in the presence of chloride ions,” *Corros. Sci.*, vol. 109, pp. 145–161, 2016, doi: 10.1016/j.corsci.2016.03.023.

[142] L. F. Montoya *et al.*, “Study of anticorrosive coatings based on high and low molecular weight polyphenols extracted from the Pine radiata bark,” *Prog. Org. Coatings*, vol. 127, no. November 2018, pp. 100–109, 2019, doi: 10.1016/j.porgcoat.2018.11.010.

[143] K. Karattu Veedu, T. Peringattu Kalarikkal, N. Jayakumar, and N. K. Gopalan, "Anticorrosive Performance of Mangifera indica L. Leaf Extract-Based Hybrid Coating on Steel," *ACS Omega*, vol. 4, no. 6, pp. 10176–10184, 2019, doi: 10.1021/acsomega.9b00632.

[144] X. Q. Zhang, Y. Feng, Q. Q. Yao, and F. He, "Selection of a new Mycobacterium tuberculosis H37Rv aptamer and its application in the construction of a SWCNT/aptamer/Au-IDE MSPQC H37Rv sensor," *Biosens. Bioelectron.*, vol. 98, no. June, pp. 261–266, 2017, doi: 10.1016/j.bios.2017.05.043.

[145] X. Ren and M. Soucek, "Soya-Based Coatings and Adhesives," in *ACS Symposium Series*, vol. 1178, 2014, pp. 207–254. doi: 10.1021/bk-2014-1178.ch010.

[146] K. Saio, M. Kamiya, and T. Watanabe, "Food Part Processing Effect Soybean Characteristics of Difference Varieties on of Soybean 11S and Components of Tofu-gel 7S Proteins among of Protein Formation By Kyoko SAID , Makoto KAMIYA * and Tokuji WATANABE Food Research Institute , Ministry of Agric," *Agr. Biol. Chem.*, vol. 33, no. 9, pp. 1301–1308, 1969.

[147] N. H. Ullsten, M. Gällstedt, and M. S. Hedenqvist, "Plasticizers for Protein - Based Materials".

[148] N. B. Shaw, F. J. Monahan, E. D. O'Riordan, and M. O'Sullivan, "Physical properties of WPI films plasticized with glycerol, xylitol, or sorbitol," *J. Food Sci.*, vol. 67, no. 1, pp. 164–167, 2002, doi: 10.1111/j.1365-2621.2002.tb11377.x.

[149] X. Mo and X. Sun, "Plasticization of soy protein polymer by polyol-based plasticizers," *JAOCS, J. Am. Oil Chem. Soc.*, vol. 79, no. 2, pp. 197–202, 2002, doi: 10.1007/s11746-002-0458-x.

[150] M. Tanaka, K. Iwata, R. Sanguandeekul, A. Handa, and S. Ishizaki, "Influence of plasticizers on the properties of edible films prepared from fish water-soluble proteins," *Fish. Sci.*, vol. 67, pp. 346–351, Apr. 2001, doi: 10.1046/j.1444-2906.2001.00237.x.

[151] X. Zhang, Y. Zhu, Y. Yu, and J. Song, "Improve performance of soy flour-based adhesive with a lignin-based resin," *Polymers (Basel).*, vol. 9, no. 7, pp. 1–10, 2017, doi: 10.3390/polym9070261.

[152] American Society for Testing & Mater, "Standard test methods for felt," 1987, doi: 10.1520/D0968-22.1.

[153] M. G. A. Vieira, M. A. Da Silva, L. O. Dos Santos, and M. M. Beppu, "Natural-based plasticizers and biopolymer films: A review," *Eur. Polym. J.*, vol. 47, no. 3, pp. 254–263, 2011, doi: 10.1016/j.eurpolymj.2010.12.011.

[154] A. Bacigalupe, A. K. Poliszuk, P. Eisenberg, and M. M. Escobar, "Rheological behavior and bonding performance of an alkaline soy protein suspension," *Int. J. Adhes. Adhes.*, vol. 62, pp. 1–6, 2015, doi: 10.1016/j.ijadhadh.2015.06.004.

[155] N. S. Hettiarachchy, U. Kalapathy, and D. J. Myers, "Alkali-modified soy protein with improved adhesive and hydrophobic properties," *J. Am. Oil Chem. Soc.*, vol. 72, no. 12, pp. 1461–1464, 1995, doi: 10.1007/BF02577838.

[156] Y. Xu, Y. Xu, W. Zhu, W. Zhang, Q. Gao, and J. Li, "Improve the performance of soy

protein-based adhesives by a polyurethane elastomer," *Polymers (Basel).*, vol. 10, no. 9, 2018, doi: 10.3390/polym10091016.

[157] K. Jiang *et al.*, "Improved performance of soy protein adhesive with melamine-urea-formaldehyde prepolymer," *RSC Adv.*, vol. 11, no. 44, pp. 27126–27134, 2021, doi: 10.1039/d1ra00850a.

[158] H. U. Sajid, R. Kiran, and D. S. Bajwa, "Soy-protein and corn-derived polyol based coatings for corrosion mitigation in reinforced concrete," *Constr. Build. Mater.*, vol. 319, Feb. 2022, doi: 10.1016/j.conbuildmat.2021.126056.

[159] S. Afgan, R. A. Khushnood, S. A. Memon, and N. Iqbal, "Development of structural thermal energy storage concrete using paraffin intruded lightweight aggregate with nano-refined modified encapsulation paste layer," *Constr. Build. Mater.*, vol. 228, p. 116768, 2019, doi: 10.1016/j.conbuildmat.2019.116768.

[160] L. B. Zhang *et al.*, "Nano-silica anti-icing coatings for protecting wind-power turbine fan blades," *J. Colloid Interface Sci.*, vol. 630, pp. 1–10, 2023, doi: 10.1016/j.jcis.2022.09.154.

[161] A. M. Madhusudhana, K. N. Shetty Mohana, M. B. Hegde, S. R. Nayak, K. Rajitha, and N. K. Swamy, "Development of Al2O3.ZnO/GO-phenolic formaldehyde amine derivative nanocomposite: A new hybrid anticorrosion coating material for mild steel," *Colloids Surfaces A Physicochem. Eng. Asp.*, vol. 601, no. March, p. 125036, 2020, doi: 10.1016/j.colsurfa.2020.125036.

[162] R. Choudhary, D. Khurana, A. Kumar, and S. Subudhi, "Stability analysis of Al2O3/water nanofluids," *J. Exp. Nanosci.*, vol. 12, no. 1, pp. 140–151, 2017, doi: 10.1080/17458080.2017.1285445.

[163] T. Yousefi, D. Naylor, and M. Z. Saghir, "Refractive index and temperature coefficient of refractive index of Al2O3- and SiO2-water nanofluids," *Int. J. Thermofluids*, vol. 16, no. October, p. 100238, 2022, doi: 10.1016/j.ijft.2022.100238.

[164] C. W. Chang, H. L. Lee, and K. T. Lu, "Manufacture and characteristics of oil-modified refined lacquer for wood coatings," *Coatings*, vol. 9, no. 1, 2019, doi: 10.3390/coatings9010011.

[165] N. Sharma, S. Sharma, S. K. Sharma, R. L. Mahajan, and R. Mehta, "Evaluation of corrosion inhibition capability of graphene modified epoxy coatings on reinforcing bars in concrete," *Constr. Build. Mater.*, vol. 322, no. October 2021, p. 126495, 2022, doi: 10.1016/j.conbuildmat.2022.126495.

[166] E. L. Brookfield, *Brookfield engineering laboratories(ixodometro)*, no. M. 2018.

[167] ASTM D 1005, "Standard Test Method for Measurement of Dry-Film Thickness of Organic Coatings," *Astm*, vol. i, no. Reapproved 2013, pp. 2013–2015, 2015, doi: 10.1520/D1005-95R20.Copyright.

[168] American Society for Testing & Mater, "Standard test methods for felt," pp. 6–10, 1987, doi: 10.1520/D0968-17.1.

[169] S. T. Method, "Standard Test Method for Apparent Shear Strength of Single-Lap-Joint Adhesively Bonded Metal Specimens by Tension Loading (Metal-to-," vol. 01, no.

Reapproved, pp. 1–5, 2019, doi: 10.1520/D1002-10R19.1.2.

[170] O. C. Choi, H. Hadje-Ghaffari, D. Darwin, and S. L. McCabe, “Bond of epoxy-coated reinforcement: bar parameters,” *ACI Mater. J.*, vol. 88, no. 2, pp. 207–217, 1991, doi: 10.14359/2023.

[171] D. L. Naik, A. Sharma, R. R. Chada, R. Kiran, and T. Sirotiak, “Modified pullout test for indirect characterization of natural fiber and cementitious matrix interface properties,” *Constr. Build. Mater.*, vol. 208, pp. 381–393, 2019, doi: 10.1016/j.conbuildmat.2019.03.021.

[172] H. Li, H. Chen, X. Li, and J. G. Sanjayan, “Development of thermal energy storage composites and prevention of PCM leakage,” *Appl. Energy*, vol. 135, pp. 225–233, 2014, doi: 10.1016/j.apenergy.2014.08.091.

[173] A. Dacić and O. Fenyvesi, “Packing density investigation of blended cement pastes incorporating waste perlite and recycled concrete powder,” *Mater. Today Proc.*, no. xxxx, pp. 0–4, 2023, doi: 10.1016/j.matpr.2023.03.561.

[174] I. Mehdipour and K. H. Khayat, “Effect of particle-size distribution and specific surface area of different binder systems on packing density and flow characteristics of cement paste,” *Cem. Concr. Compos.*, vol. 78, pp. 120–131, 2017, doi: 10.1016/j.cemconcomp.2017.01.005.

[175] A. C. 805/C 805M-20, “Standard Test Method for Rebound Number of Hardened Concrete 1,” *Concrete*, vol. 14, pp. 1–3, 2020, doi: 10.1520/C0900-19.2.

[176] C. C. Test, C. Concrete, and L. Concrete, “Standard Specification for Concrete Made by Volumetric Batching and Continuous,” 2009, doi: 10.1520/C0685.

[177] “Understanding Salt Spray Tests.”

[178] ASTM International, “Standard Practice for Operating Salt Spray (FOG) Apparatus.,” *Water*, vol. 03, no. February, pp. 1–15, 2003, doi: 10.1520/B0117.

[179] L. A. Dobrzański, Z. Brytan, M. A. Grande, and M. Rosso, “Corrosion resistance of sintered duplex stainless steels in the salt fog spray test,” *J. Mater. Process. Technol.*, vol. 192–193, pp. 443–448, 2007, doi: 10.1016/j.jmatprotec.2007.04.077.

[180] Astm a 36/a 36M-05, “Standard Specification for Carbon Structural Steel,” *Standards*, vol. 14, pp. 1–4, 2005, doi: 10.1520/A0036.

[181] M. Srivastava, P. Tiwari, S. K. Srivastava, R. Prakash, and G. Ji, “Electrochemical investigation of Irbesartan drug molecules as an inhibitor of mild steel corrosion in 1 M HCl and 0.5 M H2SO4 solutions,” *J. Mol. Liq.*, vol. 236, pp. 184–197, 2017, doi: 10.1016/j.molliq.2017.04.017.

[182] R. I. HOLLAND, “Use of potentiodynamic polarization technique for corrosion testing of dental alloys,” *Eur. J. Oral Sci.*, vol. 99, no. 1, pp. 75–85, 1991, doi: 10.1111/j.1600-0722.1991.tb01026.x.

[183] E. McCafferty, *Introduction to corrosion science*. 2010. doi: 10.1007/978-1-4419-0455-3.

[184] P. R. Roberge, *Handbook of corrosion engineering*, vol. 37, no. 09. 2000. doi: 10.5860/choice.37-5122.

[185] T. Progress, “S ， d S 。 d S,” *Policy*, vol. 26, no. 5, pp. 3–5, 2009, doi: 10.1520/G0059-97R20.2.

[186] S. Steel, R. Alloys, and R. Stock, “Standard Specification for High-Strength Low-Alloy Columbium-Vanadium Structural,” pp. 6–9, 2021, doi: 10.1520/A0572.

[187] C. Halmen, K. Reinschmidt, and D. Trejo, “Corrosion Performance Tests for Reinforcing Steel in Concrete,” *ACI Spring Meet.*, vol. 7, no. 2, 2012.

[188] C. J. Reader and M. Nargiello, “The use of engineered silica to enhance coatings,” *Waterborne Symp.*, pp. 1–9, 2020, [Online]. Available: https://www.paint.org/coatingstech-magazine/articles/the-use-of-engineered-silica-to-enhance-coatings/

[189] M. Harilal, R. P. George, S. K. Albert, and J. Philip, “A new ternary composite steel rebar coating for enhanced corrosion resistance in chloride environment,” *Constr. Build. Mater.*, vol. 320, no. October 2021, p. 126307, 2022, doi: 10.1016/j.conbuildmat.2022.126307.

[190] R. Weiß *et al.*, “A biobased, bioactive, low CO2impact coating for soil improvers,” *Green Chem.*, vol. 23, no. 17, pp. 6501–6514, 2021, doi: 10.1039/d1gc02221k.

[191] L. Cisneros-Zevallos and J. M. Krochta, “Dependence of coating thickness on viscosity of coating solution applied to fruits and vegetables by dipping method,” *J. Food Sci.*, vol. 68, no. 2, pp. 503–510, 2003, doi: 10.1111/j.1365-2621.2003.tb05702.x.

[192] G. Cui, Z. Bi, R. Zhang, J. Liu, X. Yu, and Z. Li, “A comprehensive review on graphene-based anti-corrosive coatings,” *Chem. Eng. J.*, vol. 373, no. 66, pp. 104–121, 2019, doi: 10.1016/j.cej.2019.05.034.

[193] S. Zheng *et al.*, “High abrasion-resistant biobased composite coatings with improved hardness and corrosion resistance performance based on natural lacquer and SiC nanowires,” *Prog. Org. Coatings*, vol. 172, no. July, p. 107082, 2022, doi: 10.1016/j.porgcoat.2022.107082.

[194] D. Zhang and Y. Huang, “Influence of surface roughness and bondline thickness on the bonding performance of epoxy adhesive joints on mild steel substrates,” *Prog. Org. Coatings*, vol. 153, no. December 2020, p. 106135, 2021, doi: 10.1016/j.porgcoat.2021.106135.

[195] T. S. Renuga Devi and S. Gayathri, “FTIR And FT-Raman spectral analysis of Paclitaxel drugs,” *Int. J. Pharm. Sci. Rev. Res.*, vol. 2, no. 2, pp. 106–110, 2010.

[196] A. M. D. F, “FTIR and Photoluminescence of Annealed Silicon Rich Oxide films,” *Superf. y vacío*, vol. 22, no. 1, pp. 11–14, 2009.

[197] Y. Su, J. Wang, and H. Liu, “FTIR Spectroscopic Study on Effects of Temperature and Polymer Composition on the Structural Properties of PEO-PPO-PEO Block Copolymer Micelles,” *Interface*, no. 22, pp. 5370–5374, 2002.

[198] M. Achehboune *et al.*, “Microstructural, FTIR and Raman spectroscopic study of Rare earth doped ZnO nanostructures,” *Mater. Today Proc.*, vol. 53, pp. 319–323, 2021, doi: 10.1016/j.matpr.2021.04.144.

[199] R. Liu *et al.*, “Effects of nano-SiO 2 on the permeability-related properties of cement-

based composites with different water / cement ratios," *J. Mater. Sci.*, 2017, doi: 10.1007/s10853-017-1906-8.

[200] J. a Luna-LopeZ, J. Carrillo-Lopez, M. Aceves-Mijares, a Morales-Sanchez, and C. Falcony, "FTIR and photoluminescence of annealed silicon rich oxide films," *Superf. y Vacio*, vol. 22, no. 1, pp. 11–14, 2009.

[201] V. Piazza *et al.*, "H2 from biofuels and carriers: gas-phase and surface ethanol conversion pathways on Rh/Al2O3 investigated by annular microreactor coupled with Raman and FTIR spectroscopy," *J. Catal.*, vol. 413, pp. 184–200, 2022, doi: 10.1016/j.jcat.2022.06.012.

[202] X. Bao, S. A. Memon, H. Yang, Z. Dong, and H. Cui, "Thermal properties of cement-based composites for geothermal energy applications," *Materials (Basel).*, vol. 10, no. 5, pp. 11–13, 2017, doi: 10.3390/ma10050462.

[203] J. Valli, "A review of adhesion test methods for thin hard coatings," *J. Vac. Sci. Technol. A Vacuum, Surfaces, Film.*, vol. 4, no. 6, pp. 3007–3014, 1986, doi: 10.1116/1.573616.

[204] K. V. Akpanyung and R. T. Loto, "Pitting corrosion evaluation: A review," *J. Phys. Conf. Ser.*, vol. 1378, no. 2, 2019, doi: 10.1088/1742-6596/1378/2/022088.

[205] S. U. Rahman and A. Atta Ogwu, *Corrosion and Mott-Schottky probe of chromium nitride coatings exposed to saline solution for engineering and biomedical applications*. Elsevier Inc., 2020. doi: 10.1016/B978-0-12-819712-7.00013-9.

[206] M. Ben Harb, S. Abubshait, N. Etteyeb, M. Kamoun, and A. Dhouib, "Olive leaf extract as a green corrosion inhibitor of reinforced concrete contaminated with seawater," *Arab. J. Chem.*, vol. 13, no. 3, pp. 4846–4856, 2020, doi: 10.1016/j.arabjc.2020.01.016.

[207] A. Maldonado-Alameda, A. M. Lacasta, J. Giro-Paloma, J. M. Chimenos, L. Haurie, and J. Formosa, "Magnesium phosphate cements formulated with low grade magnesium oxide incorporating phase change materials for thermal energy storage," *Constr. Build. Mater.*, vol. 155, pp. 209–216, 2017, doi: 10.1016/j.conbuildmat.2017.07.227.